In vivo Imaging of Light Induced Intrinsic Optical Signals in the Chicken Retina with a Combined Ultra-High Resolution Optical Coherence Tomography and Electroretinography System

by

Alireza Akhlagh Moayed

A thesis
presented to the University of Waterloo
in fulfillment of the
thesis requirement for the degree of
Doctor of Philosophy
in
Physics

Waterloo, Ontario, Canada, 2012

AUTHOR'S DECLARATION

I hereby declare that I am the sole author of this thesis, except where explicitly noted. This is a true copy of the thesis, including any required final revisions, as accepted by my examiners.

I understand that my thesis may be made electronically available to the public.

Abstract

The main objective of this thesis is to investigate the intrinsic optical signals (IOSs) with an ultra-high resolution optical coherence tomography system (UHROCT). In order to study the retinal IOSs evoked by visible light, an UHROCT and an Electroretinogram (ERG) system was combined. An animal model (chicken retina) based on its retinal avascularity and cone dominance, was selected. Imaging the chicken retina with OCT resulted in high contrast, high resolution (~3µm axial and ~5 µm lateral resolution) 2D and 3D volumetric tomograms, in which all retina layers were clearly distinguishable. Using the combined UHROCT and ERG system to image IOSs from the chicken retina exposed to visible light (7ms green flash) resulted in highly reproducible IOS recordings from all retinal layers for the first time. All inner retinal layers showed an initial increase and subsequently a decrease in the intensity of the backreflected imaging light within the first 100 ms after the onset of the stimulus. Outer segments of the photoreceptors also showed a decrease in the backreflected imaging light within 100 ms after the onset of the flash. All retinal layers showed a strong decrease in the backreflected light within 150 to 175 ms after the onset of the flash. Imaging the pupil dynamics of the chicken with a modified combined UHROCT and ERG system showed that part of the strong negative IOSs observed in all retinal layers resulted from the vignetting of the imaging beam due to the light induced pupil constriction. Thorough analysis of the pupil dynamics acquired with UHROCT showed a time dependent effect of the anesthesia agent on pupil constriction. Further experiments to investigate an anesthesia effects on retinal function showed significant changes in ERG components. Statistical analysis showed that Isoflurane anesthesia severely affects the inner retinal response.

In conclusion, it was hypothesized that the fast IOSs within ~50-100 ms after the onset of the visual stimulus originated from the neuronal tissue in the retina and are related to tissue optical property changes as a result of the electrical signal propagation in the light activated retina. Longer term decreases in backreflected light are likely due to pupil changes.

Acknowledgements

This work was supported in part by research grants from the Natural Sciences and Engineering Research Council of Canada (NSERC) and the Canadian Foundation for Innovation (CFI) and in-kind contributions from Diagnosys LLC.

I would like to thank my supervisor, Dr. Bizheva for her kind support during my project. I would also like to thank my committee members, Dr. Campbell, Dr. Simpson, and Dr. Thompson for all of their support and constructive discussions, and Dr. Miller for accepting to be my external committee member. I would like to thank Dr. Choh for her advice on statistical data processing and the structure and physiology of the chicken retina. I would like to thank Dr. Tim Craft and Dr. Peter Ahnelt for fruitful discussions. I would like to thank Nancy Gibson and Martin Ryan for all their help in animal handling.

I also would like to thank Dr. A. Zam for assistance with creating a ZEMAX model of the chicken eye that was necessary for the optical design of the OCT imaging probe. I am very grateful to K. Dworski and H. van der Heide from the Science Shop for assistance with building custom electrical and mechanical components for the fOCT system. I would like to thank co-op students at Biomedical Imaging Lab, David Lee, Eun Sun Song, Patrick Lee, Saad Shakeel and Daryl Chulho Hyun for assistance with imaging and data processing.

I would like to thank all of my family and friends. Without their support, I could not reach to this point.

Dedication

To Mehdi, Farideh, Davood, and Sepideh. Without you I would not be here.

Table of Contents

List of Figures

List of abbreviations

OCT: Optical Coherence Tomography

UHROCT: Ultra-High Resolution OCT

fOCT: functional OCT

FWHM: Full-Width-at-Half-Maximum

IFT: Inverse Fourier Transform

NA: Numerical Aperture

FD-OCT: Fourier Domain Optical Coherence Tomography

TD-OCT: Time Domain Optical Coherence Tomography

SNR= Signal to Noise Ratio

IOSs: Intrinsic Optical Signals

ERG: Electroretinography

MRI: Magnetic Resonance Imaging

CT scan: Computerized Tomography scan

PET: Positron Emission Tomography

NIR: Near Infrared

SLO: Scanning Laser Ophthalmoscope

NO: Nitric Oxide

AO: Adaptive Optics

NFL: Nerve Fiber Layer

GCL: Ganglion Cell Layer

IPL: Inner Plexiform Layer

INL: Inner Nuclear Layer

OPL: Outer Plexiform

ONL: Outer Nuclear Layer

ELM: External Limiting Membrane

IS: Inner Segment of Photoreceptors

OS: Outer Segment of Photoreceptors

RPE: Retina Pigment Epithelium

COR: Choroid

CSI: Chorio-scleral interface

PR: Photoreceptor

AOSLO: Adaptive Optics Scanning Laser Ophthalmoscope

TTX: Tetrodotoxin

APB: 2-Amino-4-Phosphonobutyric acid

PDA: cis-2,3 piperidine dicarboxylic acid

cGMP: Cyclic guanosine monophosphate

ANOVA: Analysis of variations

SEM: Standard error of mean

SD: Standard deviation

ms: millisecond.

Cd: Candela

s: second

UV: Ultra Violet

IR: Infra Red

Chapter 1
Introduction and overview

1.1 Motivation and Thesis Objectives

Retinal diseases are of the main causes of vision loss in developed countries, which severely affect patients' quality of life and impose considerable cost to society[1]–[3]. Retinal diseases alter the structure and physiology of the retina progressively and their treatment currently starts after such changes are diagnosed [4]–[11]. Imaging methods that provide only a view of the retinal structure, including morphological Optical Coherence Tomography (OCT) imaging, may not be capable of detecting these diseases in their early stages of development. Since the retina is a neuronal tissue, its function could be assessed by measuring the ongoing electrical processes. The electroretinogram (ERG) family of techniques are currently one of the informative methods to assess the retinal function [12]. Yet, ERG is not directly sensitive to non-electrical activities in the retina and its spatial resolution is relatively low. Usually, ERG detects the phases of the diseases when the damage reaches the minimum spatial resolution of the ERG [11]. A more sensitive and higher spatial resolution technique could improve our current knowledge about retinal diseases initiation and progression.

Measuring electrical activity in neuronal tissue is not the only way to evaluate its function. Neuronal cell function also could be assessed by detecting intrinsic optical signals (IOSs) [11], [13]–[21]. IOSs are the result of alteration in the optical properties of the activated neuronal tissue [22]–[24]. These IOSs could originate from all kinds of cellular activities, e.g., electrical activities, ionic flow, cellular shrinkage and swelling which are categorized as fast IOSs and hemodynamic and metabolic activities which are categorized as slow IOSs [11], [25]. Many optical techniques have been used or specifically developed to detect IOSs originating from healthy and diseased retinal models [7], [11], [26], [27]. Since most of these methods do not have sufficiently high axial resolution to be able to distinguish clearly the boundaries between different retinal layers, they could not separate IOSs from all retinal layers. However, each of those studies has provided a piece of the big puzzle which is; how does the retina respond to visual stimuli in health and disease?

In the studies described here, I used a relatively novel optical imaging technique, OCT, which can image the retina non-invasively with high axial resolution, enough for the visualization of the retinal

layers. The high axial resolution, heterodyne detection of weak optical signals and high image acquisition speed makes OCT a suitable candidate for imaging IOSs.

The goal of this project was to develop a combined OCT and ERG system to image the IOSs, specifically fast IOSs, from the chicken retina.

1.2 Chapter Overview

This thesis is organized in a paper-based format. Chapters 4, 5, 6, 7 and appendix A have been published in peer reviewed journals. They are presented here with the original journal format, with some modifications in the method section and results. All of the graphs in the result sections are reproduced based on the improvements in the processing code. For consistency, chapter 8 is also presented in paper-based format. Each chapter contain its own introduction, method, results and conclusion. However, the paper-based nature inevitably results in repetition of some essential ideas and methods. Therefore, the reader's absolution is sincerely appreciated.

The chapters are organized as follows:

In chapter 2, the general concept and definitions about OCT has been introduced. It elaborates on why OCT is a proper system to image IOSs.

Chapter 3 is an extensive review about all efforts made to image IOSs from the retina. Advantages and disadvantages of each method will be discussed. The results of different research groups will be compared with each other. Some of the remaining questions about IOSs are addressed.

As the first step toward imaging IOSs from the chicken retina, the morphological OCT imaging of the chicken retina with designed imaging probe has been discussed in detail in chapter 4.

Chapter 5 is about the combined OCT and ERG system and processing methods resulting in acquiring first IOSs from all retinal layers from the chicken retina. The emphasis of this chapter is on the design of the imaging system.

In chapter 6, the capability of the combined system to obtain fast IOSs from the chicken retina and their comparison with ERG recordings has been discussed.

Chapter 7 is focused on establishing a correlation between the slow IOSs and light induced pupil constriction, by use of a modified design of the combined fOCT+ERG system.

Chapter 8 discusses on the effect of the Isoflurane gas on the ERG recordings.

This thesis ends with a summary and the final discussion in chapter 9.

To show the evolution of the combined OCT and ERG system, the first version of the system is presented in appendix A. The combined system was used to investigate outer retina degeneration in a rat model and has been published as a paper.

Chapter 2
Optical Coherence Tomography (OCT):

2.1 Introduction:

We, humans have five senses to feel and sense our environment. From the beginning of the time we have used these senses to survive and move on. Some of us started to observe these feelings and extract the information coming from our senses and connect them to make a bigger picture of our environment. People started to observe celestial bodies and their movement in the sky, seasonal changes and their effect on the agriculture or hunting seasons, and record these observations. After a while and from these observations, they started to conclude some general laws of nature. This was the beginning of science and the scientific way of understanding nature. During past centuries, people discovered many natural laws and adjusted their scientific views and methods. From observations and recordings with their five senses, they found the limitations to probe nature just using the senses and hence started to extend their senses by inventing tools to overcome these limitations. Centuries have passed and people have invented sophisticated tools to probe nature. Nowadays, instead of using the naked eye to observe macro-cosmos or micro-cosmos we use telescopes and microscopes. By extending our senses, the amount of information we could acquire from our environment has increased exponentially. This revolution has fundamentally influenced all branches of science.

One of the areas of interest which has always been of great importance is health. Therefore, scientists and engineers have invented many techniques and technologies to investigate and study human anatomy and physiology. Among these technologies, medical imaging has a critical role. Studying the morphology of biological tissue has improved our understanding about how it works. There are three main areas in which imaging is required; imaging large volumetric portions of the body (i.e. organs, muscles, and bones), small scale imaging (i.e. cells, intra-cellular organelles and individual molecules), and imaging the intermediate scales, which connects the large and the small [28], [29]. Another important factor to be considered is the ability of the imaging technology for *in vivo* imaging which requires development of non-invasive imaging modalities. In different imaging technologies

different parts of the electromagnetic spectrum are used [28], [29]. In ultrasonic imaging sound waves are employed for imaging.

Optical coherence tomography (OCT) is the only imaging technique which fills the gap between relatively deep image penetration, but low resolution imaging modalities such as Magnetic Resonance Imaging (MRI), Computerized Tomography (CT), Positron Emission Tomography (PET), and ultrasound and high spatial resolution but shallow penetrating imaging systems such as confocal microscopy. OCT provides up to ~2mm of image penetration in biological tissue, combined with resolution in the scale of 0.5µm to 10µm, along with high speed volumetric *in vivo*, non-invasive imaging [28], [29].

In principle, OCT and ultrasound imaging are very similar. In ultrasound imaging, high frequency sound waves propagate through tissue and reflect back from different depths due to differences in the density of the biological tissue. Since the intensity of the backreflected sound waves is related to the density of the tissue and the speed of sound is a known parameter in the tissue, the time delay between backreflected sound waves can be scaled to distance between the locations from which the sound waves have been reflected [28]. In the case of electromagnetic waves or in particular, light, direct measurement of time delay between backreflected waves is impossible since the speed of the light is about 3×10^{8} m/s and the time delay would be in the order of ~ 30 fs (30×10^{-15}s)[29] not detectable by current instruments. Therefore, interferometry is used to measure, with very high sensitivity, the magnitude and echo time delay of back reflected light from the sample. Using an interferometer and a low coherent light source Huang, et. al.[30] were able to acquire the first 2D image (tomogram) of retinal tissue and the optical system was named optical coherence tomography, or in short OCT.

2.2 Principle of operation:

OCT is based on an interferometer system consisting of a reference arm, a sample arm, a low coherence light source, and a detector. Figure 2.1 presents a general schematic of an OCT system.

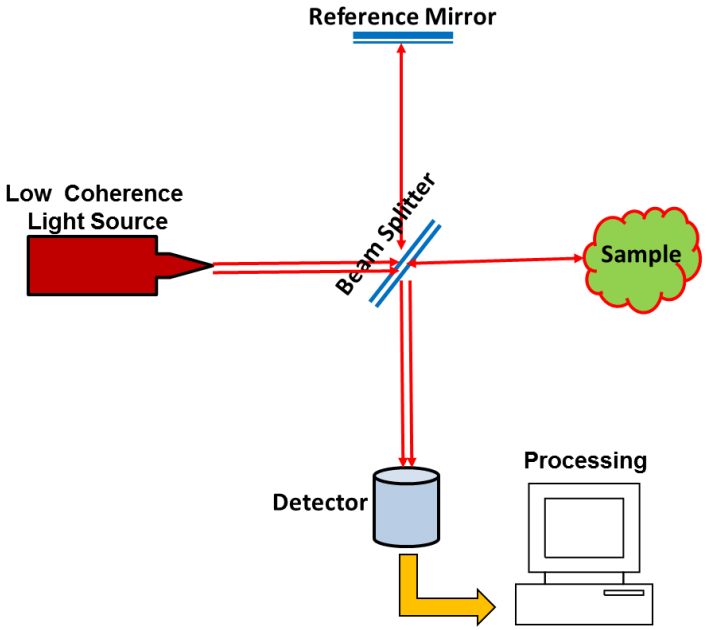

Figure 2.1: The general schematic of an OCT system.

The electromagnetic radiation from a low coherent light source is divided into two parts by a beam splitter. One part of the beam travels in the reference arm of the interferometer towards a mirror and reflects back to the beam splitter. The other part of the beam is directed to the imaged object (sample) and backreflected or scattered from different depths in the sample. The backreflected beams from both the sample and the reference arms are superimposed at the beam splitter, creating an interference pattern that is projected onto and detected by the photodetector. Post processing of the detector signal yields an OCT tomogram.

In practice, photodetectors record the intensity (I) of the incident light, which is proportional to the squared and averaged electric field.

$$I = \langle E^*(t)E(t)\rangle \qquad (2.1)$$

$$I \sim |E_r|^2 + |E_s|^2 + 2E_rE_s\cos(2k\Delta L) \qquad (2.2)$$

Here E_r is the electric field component of the electromagnetic radiation back reflected from the reference arm, E_s is the electric field from back reflected light from the sample arm, k is the wave number, and ΔL is the optical path-length difference between the sample and reference arms of the interferometer. If a coherent light source is used, interference is observed over a wide range of path-

length differences. However, for a low coherent light source (short temporal coherence length), interference is observed only when the path difference between the sample and reference arms match within the coherence length, hence, allowing one to acquire information from a narrow axial interval within the imaged sample (low coherence gating). The coherence length is inversely proportional to the frequency bandwidth of the light and determines the OCT axial resolution. According to equation (2.2) the weak backreflected light from the sample, $E_{s,}$ is multiplied by the strong signal from the reference mirror, $E_{r,}$ leading to heterodyne gain and detectable interference signal.

2.2.1 Axial resolution:

For a Gaussian spectrum, the axial resolution of an OCT system, Δz, is defined as:

$$\Delta z = \frac{2\ln 2}{n\pi}\frac{\lambda_c^{\,2}}{\Delta\lambda} \quad (2.3)$$

Where Δz is the full-width-at-half-maximum (FWHM) of the autocorrelation function, λ_c is the central wavelength of the light source, $\Delta\lambda$ is the FWHM of the power spectrum, and n is the refractive index of the sample [29], [31]. One of the main advantages of OCT over other microscopy methods is that its axial resolution is independent of the optics of the system and only depends on the spectral characteristics of the light source, which means that axial and lateral resolution of the OCT can be adjusted independently. As seen in equation (2.3), the axial resolution is inversely proportional to the bandwidth of the light source and directly proportional to the central wavelength. In other words, the broader the spectral bandwidth of the light source and the shorter the central wavelength, the better is the axial resolution of OCT. In practice, wavelength-dependent tissue optical properties (scattering and absorption), tissue safety considerations, and available light sources impose limitations to the spectral bandwidth and central wavelength used for OCT imaging [29], [31].

2.2.2 Lateral resolution:

The lateral or transverse resolution of an OCT system, as in any other optical microscopes, depends on the imaging beam diameter and optics of the focusing lens and is determined by the diffraction limited spot size of the focused imaging beam which is inversely proportional to the numerical aperture (NA) of the beam. Lateral resolution in OCT for a Gaussian beam and without considering any aberration is defined as:

$$\Delta x = \frac{4\lambda}{n\pi}\frac{f}{d} \propto \frac{1}{NA} \quad (2.4)$$

Here f is the focal length, d is the beam diameter of the optical beam incident on the imaging lens, λ is the wavelength of the light, and n is the refractive index of the sample [29], [31]. Equation (2.4) shows that high lateral resolution requires an imaging lens with a large numerical aperture. The lateral resolution is also related to the depth of field or confocal parameter b $=2Z_R$ which is two times the Rayleigh range:

$$b = 2z_R = \frac{\pi \Delta x^2}{n\lambda} \quad (2.5)$$

this indicates that the finer the lateral resolution, the shorter the depth of field.

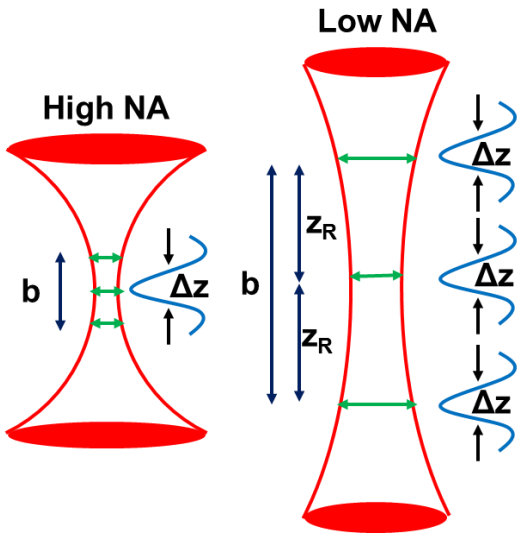

Figure 2.2: relation between depth of field and lateral resolution for high and low NA[28], [29]

In practice, having a longer depth of field is preferred for OCT imaging to maintain a uniform illumination profile throughout the entire axial imaging range. Therefore, a low NA is utilized in most OCT systems so that the whole desired depth of the sample is in focus. If finer lateral resolution is required (i.e. optical coherence microscopy), a high NA is used at the expense of losing depth of field [29], [31].

2.3 Time Domain OCT (TD-OCT):

The first OCT system was built in 1991 by Huang, et. al.[30] and was called Time Domain OCT (TD-OCT). Since the interference occurs only when the path length difference between the sample and the reference arm matches within the coherence length of the light source, TD-OCT system utilizes a scanning mirror in the reference arm to match the path length difference between the two arms for different depths within the sample. A general schematic of such a system is shown in figure 2.3.

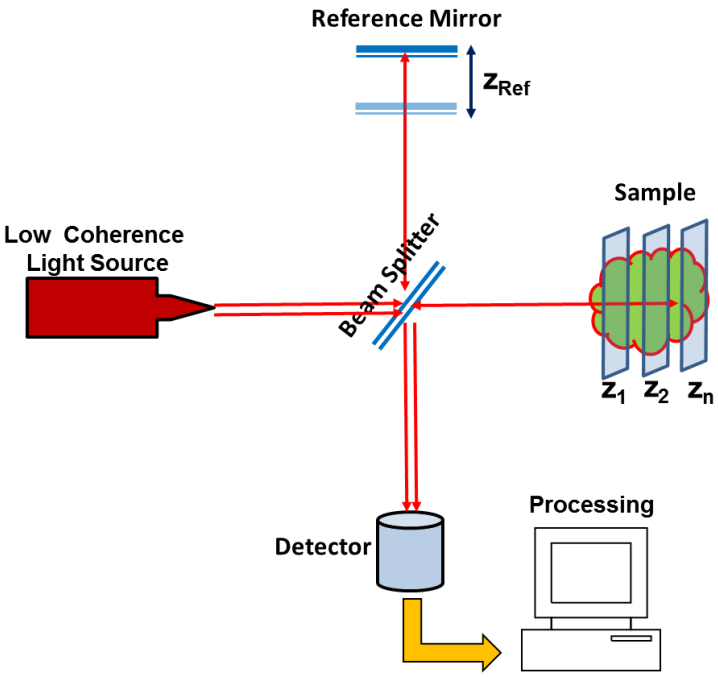

Figure 2.3: A general schematic of a TD-OCT system.

In the case of TD-OCT, equation (2.2) can be written as:

$$I(\tau) = I_0(a_r + \sum_n a_n + 2\sum_n \sqrt{a_r a_n}\,\mathrm{Re}\{\gamma(\tau_n)\} + 2\sum_{m\neq n} \sqrt{a_n a_m}\,\mathrm{Re}\{\gamma_{ss}(\tau_{nm})\}) \quad (2.6)$$

In which a_r and a_n are attenuation coefficients of light in the reference and sample arms respectively, I_0 is the intensity of light before the beam splitter, $\gamma(\tau)$ is the complex degree of coherence related to the autocorrelation function $\Gamma(\tau)$[32] :

$$\gamma(\tau) = \frac{\Gamma(\tau)}{\sqrt{I_0^{ref} I_0^{Sampl}}} = |\gamma(\tau)| \exp(-i\omega t) \quad (2.7)$$

Where the autocorrelation function is:

$$\Gamma(\tau) = \langle E^*(t) E(t+\tau) \rangle \quad (2.8)$$

The first two terms in equation (2.6) are DC terms which is a path length independent offset to the detector current. The third term is the cross correlation term which is the interaction between reflections from each sample reflector with the reference beam and depends on the wave number k and the path length difference between the two arms. The last term is the auto correlation term which is caused by interference among different reflectors in the sample and considered as an imaging artifact [29]. The values τ_{nm} in equation (2.6) are delays of different back reflections from different depths within the imaged sample and do not depend on the position of the reference arm [31]. Movement of the reference mirror in the reference arm introduces a variable τ_r therefore the registered signal takes the form:

$$I(\tau_r) = Const + 2I_0 \sum_n \sqrt{a_r a_n} \, |\gamma(\tau_n)| \cos(\omega \tau_n) \quad (2.9)$$

Similar to the coherence function, the envelope of the normalized coherent function $|\gamma(\tau_n)|$ depends on the spectral shape S(ω) of the light source, which according to the Wiener-Khintchine theorem is related to the Γ(τ) via a Fourier transform:

$$S(\omega) = \frac{1}{2\pi} \int_{-\infty}^{+\infty} \Gamma(\tau) \exp\{i\omega(\tau)\} d\tau \quad (2.10)$$

Shifting the mirror in the reference arm, allows for acquisition of information from different depths within the imaged sample. Reflection from interfaces with different refractive indices causes a delay τ in the observed oscillatory signal which allows for determination of the depth-dependent distribution of the refractive index changes that will be translated into an image. Similar to ultrasound imaging, putting together information acquired from all scanned depths within the sample from one lateral location generates an axial scan called an A-scan [28], [29]. A set of cross sectional A-scans acquired from adjacent locations create a 2D image called a B-scan [28], [29]. A volumetric construct of

several B-scans from the sample volume makes a 3D construct. Figure 2.4 shows the sample A-scan, B-scan, and a 3D construct.

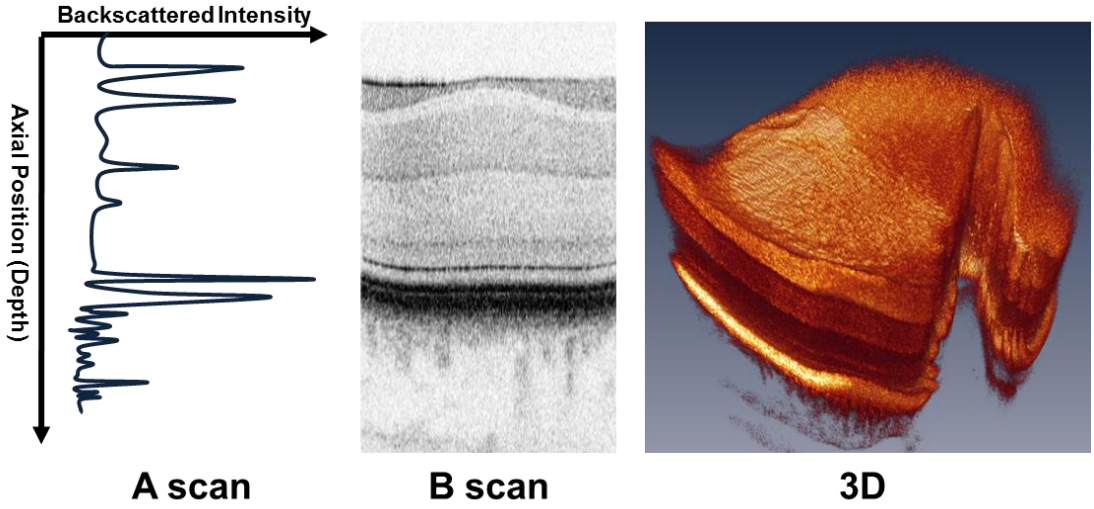

Figure 2.4: samples showing an A-scan, B-scan, and 3D volumetric OCT tomogram.

2.4 Fourier Domain OCT (FD-OCT):

The mechanical motion of the scanning arm in the TD-OCT system limits the imaging speed. Scanning large *in vivo* tissue volumes requires a high speed imaging system. An alternative to the TD-OCT which solved the speed problem, is Fourier domain OCT. In a Fourier domain OCT system, the reference mirror is stationary and the superimposed light reflected from the sample and reference arms is detected as a function of wavelength[33]–[37]. The first FD-OCT system was made by Wojtkowski et al in 2003[10–12]. Figure 2.5 represents a schematic of a typical FD-OCT system. The construction of the image acquired with FD-OCT is based on a simple fact that information about the location of reflective points within the sample is modulated on the frequency of the oscillator signal which is superimposed on the original spectrum of the light source. Hence, information from all depths within the sample (A-scan) is acquired simultaneously.

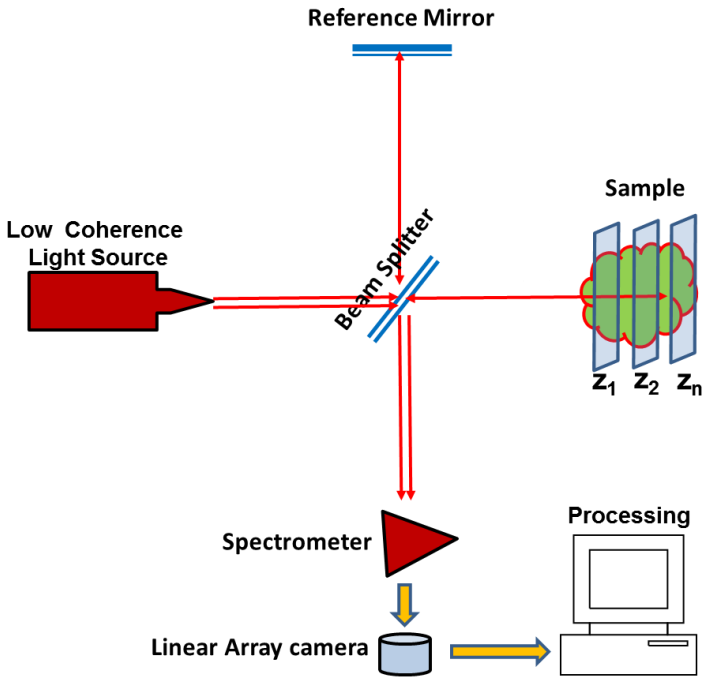

Figure 2.5: representation of the general schematic of FD-OCT.

Equation (2.6) can be written in the Fourier domain as follows:

$$S_{total}(\omega) = S(\omega)\left[a_r + \sum_n a_n + 2\sum_{m \neq n} \sqrt{a_n a_m}\cos(\tau_{nm}\omega) + 2\sum_n \sqrt{a_r a_n}\cos(\tau_n \omega) \right] \quad (2.11)$$

In which a_n is the attenuation coefficient of the backscattered light within the sample. This optical frequency dependent distribution of the signal in equation (2.11) is called a spectral fringe pattern[31]. To obtain the axial structure of the recorded sample, an inverse Fourier transformation is applied to equation (2.11):

$$\tilde{I}(\tau) = IFT^{\omega \to \tau}\{S_{total}(\omega)\} \quad (2.12)$$

$$\tilde{I}(\tau) = \left(a_r + \sum_n a_n \right)\Gamma(\tau) + \sum_n \sqrt{a_r a_n}(\Gamma(\tau) \otimes \delta(\tau \pm \tau_n)) + \sum_{m \neq n} \sqrt{a_n a_m}(\Gamma(\tau) \otimes \delta(\tau \pm \tau_{nm})) \quad (2.13)$$

The first term in equation (2.13) is the DC term, the second term is the cross correlation term from which the axial location of the reflectors within the sample is calculated, and the third term is the autocorrelation term. Similar to equation (2-6) the autocorrelation term is the result of interference of backscattered light within the different layers of the sample. There are also contributions from

reflections within the optics of the system, creating artifacts [29]. All these unwanted interference signals are referred to as coherent noise (Figure 2.6). Since $S_{total}(\omega)$ is a real function, its inverse Fourier transformation, $\tilde{I}(\tau)$, would be a Hermitian symmetric function. Therefore, in constructing the image from one spectral fringe pattern, two symmetrical images (mirror images) are generated, which is shown in figure 2.6.

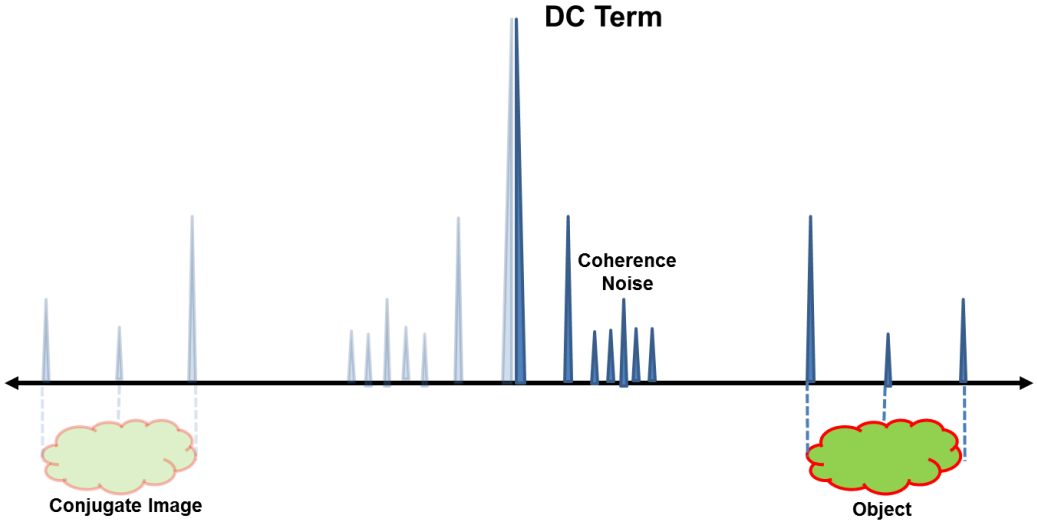

Figure 2.6: Representation of an A-scan of the FDOCT including symmetrical image and coherent noise.

In the TD-OCT systems the coherence noise and the problem of having the mirror images do not exist. Although, the mechanical movement in the sample arm of the TD-OCT limits the imaging speed and stability. In contrast to TD-OCT, FD-OCT is more stable and allows for significant increase in the imaging speed [29], [31]. Another important advantage of FD-OCT over TD-OCT is its improved signal to noise ratio (SNR) [29], [31]. The relation between SNR of FD-OCT and TD-OCT is:

$$SNR_{FD-OCT} = \frac{2\ln 2}{\pi}\frac{Z_{\max}}{\Delta z} SNR_{TD-OCT} \quad (2.14)$$

Here Z_{max} is the optical length corresponding to the maximum axial imaging range (optical length of a single A-scan) and Δz is the axial resolution[38], [39]. In tissue imaging the ratio of Z_{max} to Δz is much higher than one which in practice reaches to 10^3 [31]. Therefore according to equation (2.14) SNR for the FD-OCT system is approximately 25 dB higher than that of the TD-OCT system.

2.5 Ophthalmic OCT imaging:

OCT has found applications in many different areas of medical imaging, but its most early and successful application is in ophthalmology for retinal and corneal imaging. Since the eye is relatively transparent for radiation in the visible and NIR regions of the electromagnetic spectrum, light can penetrate into the eye with minimum attenuation and make it possible to image both the anterior segment[40]–[43] of the eye which includes the cornea, iris, pupil, and crystalline lens, and the posterior segment[29], [31], [43], [44] of the eye which includes the retina, choroid and the sclera. OCT is the only imaging technique that allows for *in vivo*, non-invasive cross sectional imaging of individual layers of the retina. Over the past 20 years, OCT has been applied to imaging both healthy and pathological human and animal retinal structures in 3D and with unprecedented spatial resolution[29], [31], [43], [44]. Furthermore, different functional modalities of OCT were developed and used for non-invasive imaging of dynamic physiological processes in the retina, such as retinal blood flow[45], birefringence[46]–[48], and even visually evoked functional responses[7], [8], [10], [49]–[53], both in healthy and diseased human or animal retinas.

In the next chapter imaging the optophysiology or measuring the evoked intrinsic optical signals (IOSs) within the retina will be discussed.

Chapter 3
Intrinsic Optical Signals (IOSs):

3.1 Introduction:

Assessing the function of biological systems besides their structure results in better understanding of their normal and abnormal states and has the potential for diagnosis in pathological cases. In the history of biology and medical science, many techniques have been introduced for measurement of functional responses to external / internal stimuli in biological tissue, e.g. Electrocardiogram, Electroencephalogram, and functional MRI. In ophthalmology, recording the electrical activity of the retinal cells, evoked by a visual stimulus is called Electroretinography (ERG) and depending on whether the visual stimulus is applied to the entire retina or only to a small area at a time, the ERG method is defined as full field ERG or multifocal ERG. Both methods are sensitive only to electrical changes in the retina cells and have fairly low spatial resolution. Since the retina is considered an extension of the brain and mainly consists of neuronal tissue, most of the attempts to find a way to acquire functional information from other neuronal tissue are applicable here. For instance, the "Optical intrinsic signals (IOSs)" name comes from extensive attempts to find an optical method to monitor the activity of brain neuronal cells[13]–[21]. The use of optical methods for acquisition of visually evoked IOSs from the retina has many advantages over electrical detection techniques. Optical methods are non-invasive (do not require physical contact with biological tissue), sensitive to all types of cellular activity (electrical and metabolic, such as cell swelling, membrane hyper- or de-polarization, changes in the refractive index or optical density of the tissue, etc.), and can provide very high spatial resolution (both axial and lateral), thus allowing for measurement of retinal activity from individual retinal layers.

This chapter provides a brief history and a review of the major optical techniques including optical transmission methods, optical reflectance methods, and OCT, which have been used for acquisition of light induced IOSs from the retina.

3.2 Early Discoveries of the optical changes in neuronal tissue as a result of propagating action potentials

Two major studies, which showed a relation between an action potential propagating through a neuron and changing optical properties of the neuron, were carried out by Cohen et al [22] in 1968 and Stepnoski et al [24] in 1991. Cohen et al used two optical techniques, light scattering and birefringence, to detect rapid structural changes in two types of non-myelinated nerve fibers from squid and crab, resulting from the propagation of action potentials in the nerves. They found a very good match between changes in the membrane potentials of the neurons over time and the changes in the intensity of the scattered light from the neurons. The authors argued that these optical changes were due to the changes in the orientation of the radially positioned molecules within the membrane of the axons during neuronal signaling[22].

In 1991, Stepnoski et al reported intrinsic optical property changes accompanying electrical activity in *Aplysi*a cultured neurons. They used dark-field microscopy imaging to monitor the scattered light from the neuron coming from different angles. They found a linear relationship between changes in the transmembrane potential and changes in the scattered light. From the analysis of the angular distribution of the scattered light, they concluded that radial components of the index of refraction of the membrane increased, while as a result of increase in membrane potential, the tangential component decreased which could be related to the reorientation of dipoles in the membrane during the propagation of the action potential[24].

These discoveries showed that it is possible to image the function of the neurons during their activity. The transparency of the ocular media makes it possible to access the retina non-invasively by the use of light and to acquire *in vivo* IOSs from the retina.

3.3 Acquisition of retinal IOSs in transmission mode:

Light induced IOSs could originate from neuronal activity and also from the corresponding hemodynamics and metabolic changes which potentially could provide important information about the normal or abnormal state of the tissue[54], [55]. These hemodynamic or metabolic related IOSs are relatively slow (~ seconds) and are different from IOSs originated from neuronal activity, which generally are faster (~ milliseconds) and their time course is comparable to electrophysiological

activities [11]. Therefore, fast IOSs in the retina most likely originate from neuronal activity of various types of retinal cells. Since the amplitude of the fast IOSs is relatively small, *in vivo* imaging of IOSs from the light evoked retina is technically challenging mostly because of eye motion[56]. Therefore imaging *ex vivo* samples is free from hemodynamic responses, and eye motion, which results in increase in the signal to noise ratio for detected IOSs[11].

Yao et. al. have recorded fast visually evoked IOSs from isolated frog[11], [57]–[60] and mouse retina[25] using bight-field, dark-field, cross polarization, and flood illumination microscopes[11], [57]–[60], combined with different high-resolution high speed CCD[57]–[59] and CMOS[11], [25], [59], [60] cameras. This research group used visual stimuli of different duration (ranging from 10 ms to 500 ms) and intensities, in order to investigate the dependence of the visually evoked retinal IOSs on these factors. One general observation from these studies was that IOSs measured from the photoreceptor, inner nuclear, and the ganglion cell layers initiated simultaneously and as early as ~ 5 ms after the stimulus onset and peaked within 50-200 ms after the stimulus onset in healthy frog retinas[11]. In studies with wild type and rod degenerated mutant mice, there was a delay in the time course of the initiation of the IOSs signals in mutant types, as compared to control age matched animals with healthy retinas[25].

There were both increases and decreases in the intensity of the transient light in all retinal layers at the cellular level but on average, in the photoreceptor layer the intensity of the signal in comparison to the background decreased which was defined as negative polarity for IOSs in the photoreceptor layer and increased in the inner retina layers, which was defined as positive polarity for IOSs of the inner retina. Another interesting observation in these studies showed that in the photoreceptor layer, at the center of the stimulated area, the polarity of the signal was negative on average, while the signal from the immediate surroundings of the stimulated area was on average positive. Furthermore, the polarity sign was reversed in the inner retina layers, which was positive at the center of the stimulated area and negative at the surrounding[11]. The magnitude of the observed IOSs varied within a few percent and depended on the imaging method, duration of the stimulus and the signal to noise ratio of the imaging system[11]. The magnitude of the observed IOSs of their photoreceptor layer in the wild type mice was in general larger than measured in mutant mice, which suggests that the photoreceptor layer did not have a normal response to the visual stimuli. According to the literature, Yao et al suggested that

these IOSs changes are related to the cell swelling and shrinking[11], water and ionic flow[11], [61]–[63], and the release of certain proteins[64] during the neural activity, in response to the visual light stimulation of the retina.

3.4 Acquisition of retinal IOSs in reflection mode:

Light induced IOSs can be imaged *in vivo* in reflection mode. Therefore, a number of imaging techniques have been developed and utilised to investigate the effect of the visual stimulation on the back reflected imaging light from the retina.

Delint et al used fundus reflection densitometry to measure the spectral reflectance changes (450-740 nm) of the healthy human fovea (*in vivo*) during light and dark adaptations over a period of 66 minutes[65]. They also examined the directional properties of the fundus reflections and spatial distribution of the reflectance changes using a scanning laser ophthalmoscope (SLO). From these observations, it was concluded that there are two mechanisms that govern the reflectance changes in the visually stimulated fovea. The first mechanism was related to relatively rapid changes in the absorption of the cone pigments. The second mechanism, which occurs much more slowly (~ minutes), was related to alterations in the index of the refraction between the interphotoreceptor matrix and the photoreceptors. A number of *ex vivo* studies, that were carried out ex-vivo in frog, chicken, and cat retinas suggest that the visual stimulation may result in changes in the composition of the interphotoreceptor matrix[66]–[68]. Also any change in the dimensions or refractive index of the photoreceptors might influence the waveguiding properties of retinal cones, which could modulate the fundus reflection[69]–[78].

An extensive review[79] was written by Riva et al based on experiments carried out by their other research groups on *in vivo* imaging of retina and optic nerve IOSs resulting from long duration exposure (from at least 40 seconds to several minutes) of the macula and optic nerve head to visible flickering light. These studies were carried out both in animals and human subjects. Most of these studies were carried out with an ocular fundus reflectometer and the imaging beam was in the visible range of the light spectrum. The combination of these measurements with other modalities, such as optic nerve laser Doppler flowmetry, retinal laser Doppler velocimetry, retinal scanning laser Doppler flowmetry, the blue field simulation technique, laser-targeted angiography, pulsed Doppler sonography, and retinal functional magnetic resonance imaging has provided better understanding of

the physiological processes which were activated as a result of visual stimulation in the retina. Based on the observations, the authors concluded that visual stimulation of the retina and the optic nerve head modulated the retinal blood flow and oxygenation. Furthermore, based on these studies, it was suggested that there is a neurovascular coupling between activated neuronal tissue and the blood flow in the retina and optic nerve head, with nitric oxide (NO) and potassium ions acting as the mediators for this coupling.

Using a high speed flood-illuminating retina camera equipped with adaptive optics (AO), Jonnal et al [80] investigated *in vivo* visually evoked reflectance changes in individual photoreceptors in healthy human subjects. This study utilized long coherence and short coherence NIR light, in comparison to the physical length of the human cone for imaging visible light evoked IOSs in individual cones. Furthermore, the intensity and duration of the visual stimulation was also varied. It was observed that change in the reflectance of the photoreceptors depended on the presence or absence of visible light stimulation and without this stimulation there was no change in back reflected NIR imaging light. Both increases and decreases in the photoreceptors reflectance were observed in the stimulated area. The initiation of IOSs happened 5-10 ms after the onset of high intensity stimulation and lasted about 300-400 ms. The duration of IOSs was independent from the intensity of the flash. The occurrence of observed IOSs from the same number of cones was significantly higher using long coherence in comparison to using short coherence light in the imaging system. Based on these observations, Jonnal et al hypothesized that the observed changes in the back reflected light from individual photoreceptors as a result of visible light stimulation, was due to the interference between reflections corresponding to different depths within the photoreceptor, a process called scintillation [80]. Furthermore, Jonnal et al. hypothesized that scintillation most likely results from stimulus induced changes in the scattering properties of the photoreceptors, that may correspond to physiological processes such as protein phosphodiesterase, swelling of the photoreceptors due to rapid influx and efflux of water caused by stimulus-evoked osmotic gradients, and change in refractive index of the photoreceptors due to biochemical processes accompanying phototransduction. It also established that the optical changes causing scintillation might not be linear, which would suggest that scintillation was not directly caused by changes in the concentration of chemical factors such as activated opsin and G-protein or phosphodiesterase, which starts to change linearly with light

stimulation[81]. Short exponential changes of photopigment concentrations which took under one millisecond and long photopigment regeneration processes which took minutes to happen, were ruled out as the likely cause of scintillation[82]. Jonnal et al concluded that the nonlinear processes such as change in the concentration of Cyclic guanosine monophosphate (cGMP) , hyperpolarization, any changes in the properties of outer segment (OS) membrane, or any changes in the physical size of the OS due to cell swelling were the most probable causes for scintillation in the light evoked photoreceptors [80].

Following Jonnal et al 's experiment[80], Rha et al used high speed AO camera and short coherent length light source for *in vivo* imaging of the light evoked IOSs from human photoreceptors[83]. The authors showed that more than 80% of the cones in a given stimulated retina area were activated and the patterns of their activation could be classified into four categories in terms of their polarity. These four categories of activated cones from the largest to the smallest number of cones in each category were, negative polarity (decrease in the backreflected light), oscillating polarity, non-changing polarity, and positive polarity (increase in the backreflected light). From this observation, it was concluded that back reflected light from most of the cones was decreased or oscillated in polarity. However, there were cones with no change in the back reflected light as well as some showing increased back reflection.

Grieve and Roorda used an adaptive optics scanning laser ophthalmoscope (AOSLO) with NIR light for imaging and red light for light stimulation to image *in vivo* IOSs in human retinas[56]. The high lateral resolution of the AOSLO system allowed them to monitor the response of single cone photoreceptors to visual stimuli over time. Different patterns, durations, and intensity of the visual stimulus were used in different imaging conditions (dark vs. light adaptation) in this study, to determine the parameters that result in the strongest measured IOSs. They found out that higher luminance stimuli and dark adapted subjects had more consistent results. The duration of stimuli was about 2 to 3 seconds and caused positive IOSs that peaked (max 5% increase in the backreflected light with averaging over multiple photoreceptors) within 2 to 3 seconds and decreased to baseline within 2 to 10 seconds with respect to the stimulus onset. They concluded that the origin of these positive IOSs was in cone photoreceptors. The time course of observed IOSs in these experiments was long enough to rule out the role of ion flux, cell swelling and shrinking, membrane

hyperpolarization, and structural changes in the OS layer as possible causes of light evoked IOSs in the photoreceptors. It was hypothesized by the authors that observed IOSs in this experiment might be caused by changes in scattering of the cones due to the physiological processes as a result of visual stimuli.

Using a modified fundus camera, Daniel Ts'o et al intensively studied the visible light evoked IOSs in cats, monkeys, and human subjects[27]. NIR light was used for imaging while a three second green flash with different patterns and intensities was used for stimulation. The light induced IOSs in these studies were mostly negative in the stimulated area, accompanied by a positive signal with a similar time course in the area adjacent to the stimulated patch. Both signals had less than one percent change from the background. Stimulation of the retina with a solid green strip induced a greater response than the checkered counter-flickering bar[27], [84]. This result ruled out the role of cells with center-surround receptive field (GCL) as the likely origin for the observed IOSs. In addition, pharmacologic dissection with a sodium channel blocker tetrodotoxin (TTX), which suppresses the action potentials in the retina and primarily in the GCL, and also 2-amino-4-phosphonobutyric acid (APB) and cis-2,3 piperidine dicarboxylic acid (PDA), which blocked the ON and OFF bipolar/photoreceptor synapses, did not show any change in IOSs which indicated an outer retinal anatomic origin of the observed signals[27], [85]. Studies on glaucomatous cats also did not produce any change in the observed IOS in comparison to normal cats[27], [86]. The authors concluded that the anatomical origin of the observed IOSs in their experiments was most likely in the outer retinal layers. From the studies on the imaging of the IOSs with different visible wavelengths of the light, it was concluded that the biophysical mechanism of the observed functional change was not dominated by oximetry (oxy/deoxyhemoglobin absorption ratio) [27], [84]. The use of blood contrast agents showed that the mechanism for the observed IOS was dominated by changes in the total hemoglobin or blood volume [27], [84]. The authors could not identify any mechanisms for the observed positive signal. However, they hypothesized that blood stealing by the activated retina from adjacent retina could be the cause for the observed positive IOSs[27], [84].

Tsunoda and colleagues conducted a series of experiments to identify the source of the observed IOSs in the monkey's retina as a result of visible light stimulation[5], [26], [87], [88]. They used a modified digital fundus camera to image the retina and stimulated the entire posterior pole of the retina with a 1

ms white flash. Five series of experiments were designed to find the anatomical origins of IOSs. In the first experiment, IOSs and ERG evoked by the same flash were recorded under different stimulus conditions (different flash intensities, dark and light adapted conditions)[26], [87]. The second experiment was carried to find out the role of the inner retinal layers in observed IOSs and focused on measuring IOSs from the optic disk and the visual cortex simultaneously with different wavelengths of light (yellow, red, and infrared)[26], [88].The third experiment aimed to find out the role of blood oxygenation in observed slow IOSs by use of laser Doppler flowmetry, to measure the changes in the retinal blood flow simultaneously with a fundus camera to measure the time course of IOSs by same visual stimulus [5], [26]. The fourth experiment, aimed to investigate the role of blood flow changes in the retina on the observed IOSs [5], [26]. The fifth experiment was designed to find out the contribution of the neuronal activities in the inner retina in the observed IOSs by the use of neuronal inhibitor drugs [5], [26]. They found that IOSs measured from the foveal region, the optic disk, and the posterior retina had different characteristics, although all of them were negative in polarity[26], [87]. The IOSs from the foveal region were relatively fast (peaked in <100ms) and had the largest magnitudes (~1%). The signals from the optic disks were relatively slow (peaked in ~5 seconds) with magnitudes less than ~0.5 %. The posterior retina had signals of combined fast and slow components [26], [87]. From the analysis of the time course and characteristics of the ERG recordings and IOSs during different imaging conditions and with different stimulus light intensities, it was hypothesized that the IOSs in the foveal region most likely originated from cone photoreceptors and the fast component of the posterior retina dominated by responses from cone photoreceptors and some from inner retina. These fast IOSs were not related to changes in blood flow or blood oxygenation level and were rooted in structural changes in outer segment disks, membrane hyperpolarization, cell swelling, and changes in the composition of the interphotoreceptor matrix. From the results of the experiments 3, 4, and 5, it was hypothesized that the slow IOSs observed at the optic disk and the posterior retina were independent from the changes in the blood oxygenation level and derived mainly from the blood flow increase in vessels and capillaries and triggered by GCL and the rest of inner retina. The authors also found that local stimulation of the retina in addition of having a local decrease in the back reflected light (local negative IOSs) in the stimulated region, also had positive IOSs in the adjacent not-stimulated areas which they could not explain the source of such positive

signals. They hypothesized that the IOSs should originate from all retinal layers and probably with different intensity, polarity, and time courses.

Using a flood-illumination imager[89] and confocal microscopy[90], [91], Yao et al conducted a series of experiments to image the IOSs from *ex vivo* [89], [90]and *in vivo* frog retina[90]. In these experiments, they extracted IOSs from back reflected light from the photoreceptor layer in the retina. The IOSs from intact *ex vivo* frog eye tightly correlated with ON and OFF edges of the 1 second white light stimulus. The fast IOSs initiated less than ~10 ms after the onset of the visual stimulus and reached to their maximum magnitude within 100 ms after the onset of the flash. Both positive and negative polarity IOSs were observed in the light evoked area. However early responses were dominated by positive IOSs and later responses were dominated by negative IOSs. Imaging the photoreceptor layer of the *ex vivo* excised frog retina with confocal microscopy showed similar characteristics of positive and negative IOSs in the stimulated retinal area. Using flickering stimulus light showed that IOSs from photoreceptor layer could track at least 2 Hz visible light flicker. In vivo confocal imaging of the frog retina, evoked by 10 ms green flash, showed both positive and negative IOSs. Fast IOSs initiated ~10 ms and peaked within 300 ms after the onset of the stimulus. From the analysis of the results of these experiments, the authors concluded that the fast IOSs (in the photoreceptor layer) were directly related to early phototransduction procedure in the photoreceptors, while slow IOSs stemmed from later phototransduction procedure and metabolic dynamics, e.g. retinoid metabolism.

3.5 Imaging IOSs with OCT:

Results from studies on imaging retinal IOSs with optical systems other than OCT suggest that IOSs most likely originate from different retinal layers and develop simultaneously, may have different polarities, develop over a relatively short period of time (~100ms) and have a relatively low magnitude (typically < 10% fractional change). To be able to study the origin and different polarity of the IOSs, it is necessary that the optical instrument have a sufficiently high axial resolution to resolve individual retinal layers, along with the capability of very fast 2D or 3D image acquisition, to sustain sufficiently high time resolution to map out all peaks and valleys in the measured retinal IOSs. Furthermore, because the magnitude of IOSs is very small and *in vivo* measurements are subject to biological noise (physiological and metabolic processes, as well as eye movement), the higher the

SNR of the imaging system, the better the chance for successful and reproducible measurement of the IOSs.

Optical coherence tomography allows for volumetric imaging of the retina with axial resolution (~2μm to 10μm), sufficiently high to resolve clearly individual retinal layers and sub-layers. Furthermore, recent developments in laser and camera technologies have increased the OCT image acquisition speed to the range from 100, 000 to > 2,000,000 A-scans/s, thus providing sufficiently high temporal resolution for measurement of visually evoked IOSs[92]–[94]. Last, but not least, because of the heterodyne detection, OCT allows for higher system SNR as compared to other optical methods such as confocal microscopy or adaptive optics (AO). From this prospective, OCT might be a useful imaging modality for *in vivo*, non-invasive studies of visually evoked retinal IOSs both in animal models and human studies.

The idea of using OCT to measure light induced IOS in the retina was first proposed by Dr. Bizheva and colleagues at the OSA BIOMED 2004 meeting [95].

The first proof-of-principle experiments were conducted with a TD-OCT system (λ=1250 nm, $\Delta\lambda$=150 nm, Δz=3.5 μm, Δx=10 μm, SNR=100dB, P=2mW, Δt=4.5 ms) in isolated rabbit retinas [10]. In that study, the retina was stimulated with 200 ms long white single flashes with different intensities, and inhibitor drugs were used to interrupt specific retinal cell responses, such as the photoreceptor and bipolar cells. Results from those studies showed slow decrease in the reflectivity of the inner segment (IS) and slow increase in reflectivity in outer segment (OS) of the photoreceptor layer in the intact light stimulated retina. The magnitude of observed IOSs was significantly higher than the back ground noise, non-stimulated retina, and functionally suppressed retina IOSs which indicated that the IOSs resulted from the visible light stimulation of the retina. Increasing the stimulus intensity resulted in increasing the magnitude of IOSs. Preliminary results showed an increase in reflectivity of IPL, although the IOSs from IPL were not as reproducible as signals from IS and OS. The authors hypothesized that the observed slow IOSs in the photoreceptor OS layer were most likely caused by ion shifts involved rather than rapid hyperpolarization of the photoreceptor membrane, while changes in the IS were most likely due to altered metabolic activity of the mitochondria, associated with the visible light stimulus[10]. The authors further hypothesized, that the slow varying

IOSs observed from the IPL is most likely related to swelling / de-swelling processes in the Mueller cells.

Dr. Yao et al used a modified TD-OCT (λ=793 nm, $\Delta\lambda$=15 nm, Δz=19 μm) to image the IOSs from an activated excised frog retina. They observed a positive change in back reflected light in the GCL and a negative change in back reflected light in the photoreceptor layer. They hypothesized that the negative response in the photoreceptor layer was due to the physiological processes during phototransduction[49].

For imaging visible light stimulated rat retina[50] and human subjects[7], Srinivasan et al used FD-OCT system to image *in vivo* IOSs. Rat *in vivo* imaging was done with a FD-OCT system in which λ=890 nm, $\Delta\lambda$=145 nm, Δz=2.8 μm, Δx=10 μm, SNR=95dB, P=620μW, and the imaging speed was 24000 axial scans per seconds[50]. The retina was stimulated with a 1.3 s long white flash in dark and light adapted conditions. They found a slow increase in the reflectivity of the photoreceptor layer both in dark and light adapted conditions. The only difference in the IOSs acquired in dark and light adapted condition was that the magnitude of the IOSs in dark adapted condition was higher than light adapted condition but the time course of both IOSs were same. The authors concluded that the observed signal was originated in structural changes in the OS due to phototransduction [50].

Human *in vivo* imaging of the IOSs was done with a FD-OCT system in which λ=800-1020 nm, $\Delta\lambda$=150 nm, Δz=3.3 μm, Δx=10 μm, SNR=92dB, P=750μW, and the imaging speed was 50000 axial scans per seconds [7]. The foveal region, parafovea and periphery of the fovea were imaged (localized stimulation and imaging) in dark and light adapted conditions in this study. After an extensive statistical analysis of the results, a slow positive signal was detected from IS/OS junction which believed to be from cone photoreceptors. Under the light condition, this positive signal was absent. In addition, the observed positive signal from IS/OS junction was not detected at the periphery where the cone density is lower than the foveal region. The authors concluded that detecting the positive IOSs may depend on the location and size of the entrance and the exit pupils during the imaging. A negative signal was also observed from the perifovea and the periphery of the retina, and the authors hypothesized that it originated from the rod photoreceptors. These negative IOSs had slow time courses and they could be related to photomechanical changes in the photoreceptors, but their mechanism is currently unknown [7].

Using a FD-OCT (λ=1050 nm, $\Delta\lambda$=70 nm, Δz=7 μm, Δx=20 μm) with imaging speed of 47,000 axial scans per seconds, Tumlinson et.al., conducted a series of *in vivo* experiments to image the light induced IOSs from the human retina[8]. They used a 50 minutes duration high intensity light to bleach all photoreceptors in the retina and imaged an area in which the rods were dominant. After intensive post processing and applying a noise reduction technique, they showed a slow increase in the reflectance of the IS/OS junction which decayed over 30 minutes after the onset of stimulation. The results of these experiments were not conclusive enough to hypothesize the origin of the observed signals [8].

Schmoll et al later imaged *in vivo* IOSs from the light stimulated human retina with FD-OCT (λ=830 nm, $\Delta\lambda$=45 nm, Δz=6.7 μm, SNR=98 dB), with imaging speed of 17,000 axial scans per seconds[9]. They stimulated the retina with a flickering green-red flash with different stimulus time and frequency. They found that the optimum duration and frequency (to obtain reproducible IOSs) for the stimulus was 250 ms and 5 Hz respectively. A clear reflectivity decrease in the OS of the retina in the superior of the fovea for both ON and OFF set after the flash was observed [9].

Using a commercially available OCT system (λ=870 nm, Δz=3.9 μm), with imaging speed of 40,000 axial scans per seconds, Theelen and colleagues monitored the light induced IOSs from healthy and damaged retina in human subjects[96]. They used a single white flash of 200 ms duration to stimulate the retina and bleach 95% of the cones and 40 % of the rods. Decrease in the reflectivity of the NFL, IS, and peripheral OS and increased in the reflectivity of OS in the fovea, were observed in healthy subjects while in the damaged retina subjects, the polarity and magnitude of the IOSs varied over and between the imaged areas. The authors concluded that the observed reflectivity increase in the fovea could be related to the cones' activity during phototransduction, while the reflectivity decrease in the peripheral region could be linked to the rods' activity. The authors further hypothesized that the reflectivity decrease in the IS could be related to alterations of the intra cellular ion concentration, while the reflectivity decrease in the NFL might be related to changes in the intra cellular tubules in the NFL [96].

In summary, over the past decade, many research groups have attempted to image light induced IOSs in the human and animal retinas with varying degree of success and reproducibility. Those studies were carried out with a variety of different imaging instruments (dark field, bright filed, NIR or

confocal microscopy, fundus cameras, AO and AS-SLO , as well as OCT systems); in different retinal tissues – human and animal (frog, rabbit, rat, mouse, monkey); with different sample preparations (ex-vivo vs. in-vivo); with different visual stimulus parameters: color (mono and polychromatic), duration (between 5ms and several seconds), intensity (from weak to strong enough to saturate photoreceptors), single flash vs. pulse train, local vs. global retinal illumination, as well as use of spatially invariant stimuli vs. flickering grid or checkered pattern. Despite the extensive variability in the study designs, there are some general trends that can be observed across the reviewed studies:

1. In majority of the cases, IOSs were recorded only from the photoreceptor layer, with only a few studies have reported IOSs from some inner retinal layers.
2. None of the research groups were able to record IOSs simultaneously from all retinal layers.
3. The observed IOSs can be classified into two major groups based on their time course of appearance and development: fast IOS (initiate and peak within ~100 ms from the stimulus onset, which loosely corresponds to the time course of single flash ERG traces); and slow IOS (initiate and peak during the time period from 100 ms to several seconds after the onset of the visual stimulus). In general it is concluded that slow signals are related to hemodynamic and metabolic processes originated from neurovascular couplings in the inner retina and fast IOSs are linked to true neuronal responses originated from phototransduction processes in the outer retina.
4. IOSs of different polarities, positive (increased reflectivity as compared to baseline) and negative (decreased reflectivity) were observed both within individual and across different retinal layers.

Currently there is a debate on the origin of the polarity of IOSs. Other than OCT, optical imaging methods based on reflection and transmission of light do not have sufficient axial resolution for *in vivo* imaging to dissect the individual retinal layers. Therefore, the observed signals from these methods are the combination of at least two retinal layers. For instance, OCT studies have shown that the IOSs from IS and OS of photoreceptors have opposite polarities. Therefore their combined

signals, depend on their magnitude, could be resulted in positive, negative, oscillating, and neutral signals in different experiments and from different locations.

In addition, different imaging parameters, stimulation protocols, and imaging samples (*in vivo* vs. *ex vivo*, animal vs. human subjects), make it difficult to compare the results presented by different groups. For example, rats are rod dominated and IOSs reported from them with OCT imaging were positive. However, there are other reports showing that the IOSs imaged with OCT from the cones are positive and IOSs from rods are negative. One reason for achieving such diversity in the polarity and the time course of the observed IOSs is that there is no standard procedure for imaging and stimulation of the retina. Although, there have been many efforts to image the IOSs, there are many questions remain to be answered. What is the biophysical origin of the positive and negative signals? How can IOSs from photoreceptors have both polarities? What is the best stimulation protocol to stimulate retina for imaging IOSs? Do other retina layers other than photoreceptors and the NFL have light evoked IOSs?

Because of biological noise and motion artifacts, *in vivo* imaging of IOSs is very challenging. The magnitudes of the IOSs are fairly small and by considering hemodynamic IOSs and biological noise, imaging the fast neuronal IOSs is even more challenging. The vascular network in the mammalian inner retina is one the sources of biological noise, including hemodynamic responses and shadowing effect of blood vessels, for imaging fast IOSs. Therefore, in order to investigate the origins of the IOSs, specifically fast IOSs, and IOSs from other retina layers, choosing a proper imaging sample is very important. However, for clinical applications, presence of the retinal vasculature should be taken into account. Therefore, *in vivo* imaging of the fast IOSs requires developing novel imaging modalities and post processing algorithms to overcome the limitations posed by inner retinal vascular network.

Since the only imaging technique to image the IOSs from the retina with high enough SNR and speed to detect small and fast IOSs is OCT, a high speed ultra-high resolution FD-OCT has been utilized to image the fast IOSs in this project. In the following chapter the characteristics of the OCT system is described.

As a first step in finding the origins of the fast IOSs and acquiring IOSs from all retinal layers, based on having avascular inner retina and cone dominated outer retina, chicken was selected as an animal

model for this project. Preliminary *in vivo* OCT imaging of the chicken retina showed lower motion artifacts in the resultant images than rat or human subjects which was ideal to study fast IOSs. Therefore, in order to study the chicken retina structure for functional imaging, *in vivo* imaging of the morphology of the chicken retina was carried out, which is described in detail in the chapter 4. In the following chapters (5 and 6), the functional imaging of the fast IOSs is presented.

Chapter 4

In vivo volumetric imaging of chicken retina with ultra-high resolution spectral domain optical coherence tomography

4.1 Overview

The chicken retina is an established animal model for myopia and light-associated growth studies. It has a unique morphology: it is afoveate and avascular – oxygen and nutrition to the inner retina is delivered by a vascular tissue (pecten) that protrudes into the vitreous. Here we present, to the best of our knowledge, the first *in vivo*, volumetric high resolution images of the chicken retina. Images were acquired with an ultrahigh resolution optical coherence tomography (UHROCT) system with 3.5 μm axial resolution in the retina, at the rate of 47,000 A-scans/s. Spatial variations in the thickness of the nerve fiber and ganglion cell layers were mapped by segmenting and measuring the layer thickness with a semi-automatic segmentation algorithm. Volumetric visualization of the morphology and morphometric analysis of the chicken retina could aid significantly studies with chicken retinal models of ophthalmic diseases.

4.2 . Introduction

The chicken is a widely used animal for studies of ocular development and eye growth. It has been, and continues to be, the first model used in studies examining the factors and mechanisms mediating refractive error development[97]–[99]. Chickens are diurnal, and their retinas contain cones (65%, [100], [101]) and rods, however, the chicken eye has several structures or adaptations that differ from their mammalian counterparts. For example, chickens are afoveate, having instead, an area centralis [102] and their retinas are devoid of blood vessels; the pecten, a sheet of vascular tissue that protrudes into the vitreous chamber, supplies the internal milieu of the eye with oxygen and nutrients [103]. Recently, *in vivo* images of photoreceptors in the chicken retina with adaptive optics laser scanning ophthalmoscope (AO-SLO) were reported [104]–[106], suggesting that optical imaging techniques

could prove an excellent research tool for longitudinal studies of chicken models of ophthalmic diseases. Although the AO-SLO technique offers high lateral resolution in the living retina (~ 3 μm in human retina [107]), the axial imaging resolution is limited by the optics of the eye and the imaging beam (~ 40 μm in human retina [108]).

Optical coherence tomography (OCT) is a non-invasive imaging modality based on detection of partially coherent light, that can provide depth-resolved, cellular level resolution imaging of the structural composition of biological tissue at depths of 1-2 mm below the surface [30], [109]. Pioneer cross-sectional images of healthy chicken retina were first acquired with a slow scanning, Time-Domain OCT system [110]. However, significant development in OCT technology over the past decade has led to ~10× improvement in the OCT axial resolution and more than 100× improvement in the OCT image acquisition rate. While *in vivo* ultra-high resolution OCT (UHROCT) images of the avian retina in birds of prey were recently reported [111], birds of prey have a different retinal morphology compared to the various species of chicken that are typically used in studies of myopia or retinal degeneration.

Here we present preliminary results from a morphometric study of the healthy chicken retina, conducted with a research grade UHROCT system. Volumetric images of a healthy chicken retina were acquired *in vivo* and a custom segmentation algorithm was used to measure spatial variations of the individual retinal layers. As a first step in assessing UHROCT as a modality for imaging chicken retinal morphology, UHROCT images and traditional histological micrographs of the same retina were compared.

4.3 . Methods

4.3.1 Imaging system description

A high speed, spectral domain UHROCT system (Fig.4.1) operating at ~1060 nm was used for *in vivo* imaging of the chicken retina. Details about the imaging system design and performance for *in vivo* imaging of the human and rat were published previously [112], [113]. Briefly, the UHROCT system is based on a spectral domain design. The system core is a fiberoptic Michelson-Morley interferometer, interfaced to a broad bandwidth superluminescent diode (SLD)-based light source (Superlum Ltd., $\lambda c = 1020$ nm, $\Delta\lambda = 110$ nm, $P_{out} = 10$ mW). The SLD spectral output was a custom-

shaped to provide higher power at ~980nm, where water absorption has a local maximum. Considering the average axial length of 13 day old chicken eye (~8mm; [114]), the spectral shaping resulted in 3.5 µm UHROCT axial resolution in the chicken retina. An imaging probe (Fig. 4.1) composed of an achromat doublet collimator (Edmund Optics, L_1, f_1 = 12 mm), a pair of galvanometric scanners (Cambridge Technologies) and a pair of achromat doublet lenses (Edmund Optics, L_2, f_2 = 60 mm and L_3, f_3 = 30 mm) was designed and built for imaging of the chicken retina. The diameter of the imaging beam was ~1.25 mm at the cornea, resulting in lateral imaging resolution in the chicken retina of about 4.8 µm at 1020 nm. The OCT lateral resolution at the chicken retina surface was estimated by creating a ZEMAX model of the OCT imaging probe and the chicken eye and considering both the monochromatic and polychromatic aberrations. However, in this model, aspheric surfaces or the gradient of refractive index of the crystalline lens, which would affect the monochromatic and chromatic aberrations, were not considered. Information about the refractive indexes, thickness and curvature of the chicken eye cornea, lens and vitreous were obtained from the available literature [114]. The diffraction limited lateral resolution of the chicken eye for a two weeks old chicken was estimated to be about 2.75 µm at 1020 nm which was close to the value reported in the literature [115].

The OCT interference signal was detected with a custom, high performance spectrometer (P&P Optica Inc.), interfaced to a 1024 pixel linear array InGaAs camera (SUI, Goodrich Corp.) with a data transfer rate of 47 kHz. The UHROCT system provided ~99 dB SNR for 1.7 mW power of the imaging beam. The maximum permissible exposure intensity of the incident imaging beam at the cornea for the wavelength region used here is about 2 mw for 10 s continues exposure for human [113]. The larger numerical aperture of the chicken eye results in a smaller imaging spot size on the retina and a higher energy density which suggests the need for more conservative measures. However, the high imaging speed (21 µs/A-scan) limits the tissue exposure to about 5 s for a total 1 mm^2 (1000 A-scans x 256 B-scans) for the narrow scan and 9 mm^2 for wider scan on the retina. Dispersion within the imaging system, due to the optical and fiberoptic components, was compensated for by the use of a tunable dispersion compensation unit composed of a pair of BK7 prisms (Edmund Optics), connected to each other with an optical gel (Thorlabs) and attached to a pair of miniature manual translation stages (Edmund Optics).

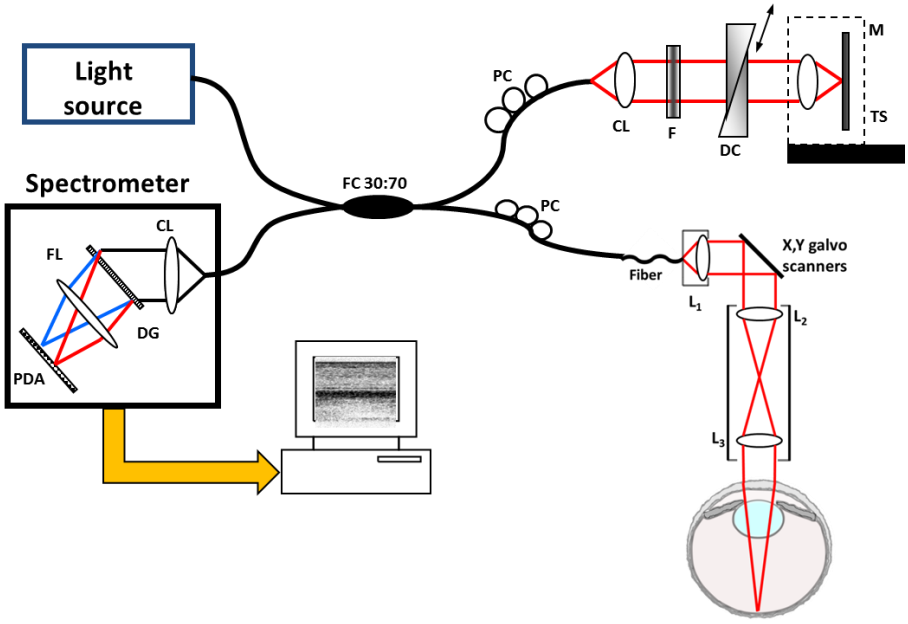

Fig. 4.1: Schematic of the UHROCT system used to image the morphology of the chicken retina. Key: CL, collimating lens; DC, dispersion compensation unit; DG, diffraction grating; F, neutral density filter; FC, fiber coupler; FL, focusing lens; L1 – L3, lenses in the eye imaging probe; M, mirror; PDA, photodiode array; PC, polarization controllers; TS, translation stage.

Dispersion arising from the optics of the chicken eye was compensated for numerically with an algorithm based on a previously published method [116]. Multiple 3D image stacks with dimensions 1000 × 512 × 256 (A-scans x Pixels x B-scans) were acquired from the chicken retina at wide (~20º) and narrow (~7º) scanning angles. The OCT image acquisition code is based on LabView (National Instruments). Retinal 2D tomograms were generated from the raw data and processed with Matlab (Mathworks). The imaging data was rendered in 3D using Amira software (Visage Imaging Inc.). A semi-automatic segmentation algorithm, developed in our research group [117] was used for segmentation and thickness measurement of selected retinal layers.

4.3.2 Animals

A 13 days old White Leghorn (Gallus gallus domesticus) chicken was used in the study. The imaging procedure was approved by the University of Waterloo Animal Ethics Committee. The chicken was anesthetized with 1% isoflurane and placed on a custom-designed holder that keeps the

animal stationary during the imaging session and allows for easy alignment of the eye with respect to the imaging probe. The imaging procedure was carried out in semi-dark environment to achieve natural pupil dilation and pupil diameter was measured to be larger than 2.5 mm throughout the entire imaging procedure. Constant pupil size was confirmed by the absence of obstructions and vignetting that would have occurred had the imaging beam been larger. A retractor was used to keep the eyelid open during the imaging procedure and artificial tear drops were administered frequently to keep the cornea well hydrated and transparent.

4.3.3 Histology

Following the UHROCT imaging session, the chicken was decapitated and the eyes were immediately enucleated. Incisions were made at the ora serrata and the anterior segment and vitreous were removed. The remaining eyecup was fixed in freshly prepared 4% (w/v) para-formaldehyde with 3% (w/v) sucrose in 0.1 M Sorensen's buffer (pH 7.5; SB) for 20 min. Eyecups were then rinsed in 0.1 M SB (3 x 10 minutes) before being cryoprotected (30% (w/v) sucrose in SB, overnight). The next day, the eyes were embedded in Optimal Cutting Temperature embedding medium and then were frozen, before being sectioned in a cryostat onto clean glass slides. Sections were 12 µm or 18 µm thick and were allowed to air-dry prior to staining with hemotoxylin and eosin (H & E). Coverslips were mounted onto the slides using Permount and images of the sections were captured with a light microscope and colour camera (Carl Zeiss).

4.4 Results and Discussion

Figure 4.2 shows representative UHROCT images of the chicken retina at locations away from (A) and near the optical nerve head (C), and corresponding H&E stained histological cross-sections of the same regions (Fig. 4.2B and 4.2D, respectively). Scale bars provided in all images allow for determination of the size and spatial separation of morphological features in the chicken retina. All retinal layers are clearly visualised in the UHROCT tomograms and match well with the retinal layers as observed in the histological cross-sections (Fig. 4.2B, and 4.2D). The ganglion cell layer (GCL) is clearly visible in the UHROCT images as a bright band located immediately below the dark, highly scattering nerve finer layer (NFL). The NFL thickness varies with location in the retina and is thickest at the optic nerve head (ONH). The chicken retina has a fairly thin outer nuclear layer

compared to mammalian retinas, which is clear from the images in Fig. 4.2. The external limiting membrane appears on the UHROCT tomograms as a very distinct dark gray line above the low scattering photoreceptor layer.

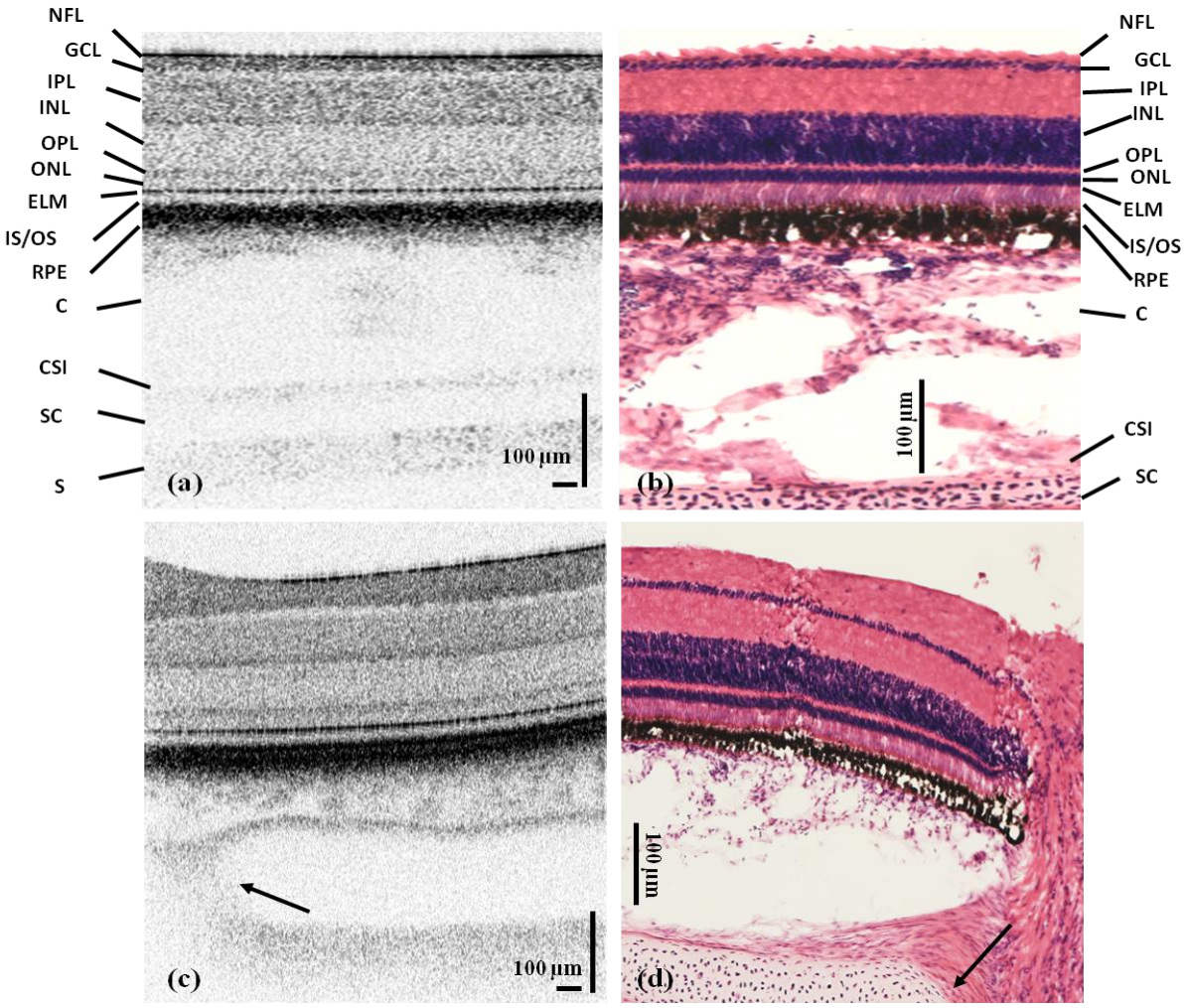

Fig.4.2 Representative UHROCT tomograms of the chicken retina acquired from locations away (A) and near (C) the ONH, compared with H&E stained histology (B and D). Individual retinal layers observed in the UHROCT tomograms match well with corresponding layers in the histological cross-sections. The black arrows in Fig. 4.2C and 4.2D mark the termination of the cartilaginous sclera layer near the optical nerve head. Taken from [118] with permission.

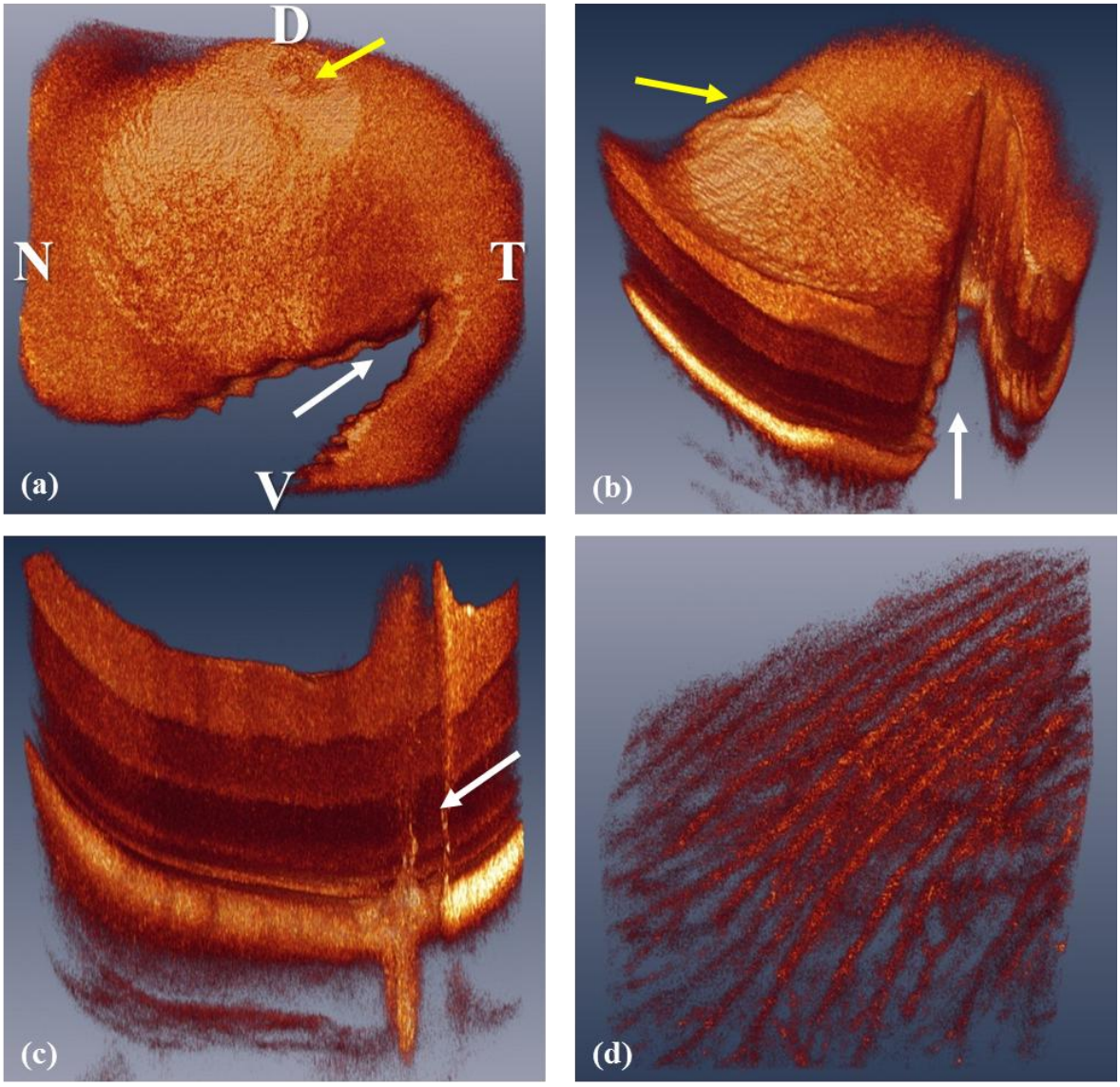

Fig.4.3 Selected frames from rendered volumetric image stacks of the chicken retina acquired at wide (A, B and C) and narrow (D) scanning angles. Different views of the pecten layer are presented in A, B and C and marked with white arrows. The orientation of the 3D tomogram in A is shown by labels nasal (N), temporal (T), dorsal (D), and ventral (V) [115], [119]–[121]. An area in the retina with significantly thinner NFL is marked with yellow arrows in A and B. A view of the choroidal vasculature is shown in D (. Taken from [118] with permission.

The chorio-scleral interface (CSI) is clearly visible on both UHROCT images. The chicken sclera contains a fairly thick cartilaginous layer (SC), separating the choroid from the fibrous sclera (S). The cartilaginous sclera is composed of cells with a large cytoplasm to nucleus ratio, thus rendering the cartilage almost transparent to infrared light. Termination of the cartilage is clearly observed near the

ONH (Fig. 4.2C and 4.2D, black arrows). The apparent difference in the choroidal thickness observed between the UHROCT and histological cross-sections is most likely a post-mortem artefact due to the choroid moving away from the retina during the cryo-sectioning.

Figure 4.3 shows rendered volumetric stacks from different locations in the chicken retina acquired at wide (A, B and C) and narrow (D) scanning angles. These volumes are comprised of 256 B-scans (1000 x 512), corresponding to ~3 mm x 3 mm (wide angle) and ~1mm x 1 mm (narrow scanning angle) area on the tissue surface. The volumetric images presented in Fig. 4.3A, 4.3B and 4.3C, were acquired from a location in the retina close to the pecten (white arrows). Since the pecten is a highly vascular tissue, light absorption and scattering within the blood vessel in the pecten produces a shadowing effect in the UHROCT tomograms. The folds of the pecten can be observed clearly on the *en face* (Fig. 4.3A and 4.3B) and cross-sectional image (Fig. 4.3C). The volumetric images in Fig. 4.3A and 4.3B also show an area at the retinal surface with significantly thinner NFL. This area, located about 2 mm away from the ONH, appears darker, more transparent and round in shape (Fig. 4.3A and 4.3B, yellow arrows), and is tentatively speculated to represent the area centralis of the chicken retina. The ONH and pecten is located at the nasal and ventral section of the chicken retina and area centralis is about the center of the chicken retina [115], [119]–[121]. Further examination of other retinal layers in this area is required for confirmation of this hypothesis. Fig. 4.3D shows a view of the chicken retina choroidal vasculature.

Figure 4.4 shows representative B-scans that were used to generate the volumetric image presented in Fig. 4.3A. The image in Fig. 4.4A shows a cross-sectional view of the pecten (black arrow). This image also shows thickening of the NFL, thinning of the choroid and termination of the sclera cartilage near the ONH.

The images shown in Fig. 4.4B, 4.4C and 4.4D show progressive thinning of the NFL and thickening of both the GCL and the choroid in one location in the retina.

Morphometric analysis of the chicken retina could be very helpful in various chicken models of retinal diseases. Here a semi-automatic segmentation algorithm developed by our research group [117] to segment and measure the thickness of individual layers in the retina, was used. Although NFL and GCL thicknesses are presented in this paper (Fig. 4.5) to highlight the usefulness of UHROCT with optic nerve-associated disease models [122], [123], the algorithm allows for

segmentation of all layers of the retina. An original cross-sectional UHROCT tomogram of the chicken retina is shown in Fig.4.5A.

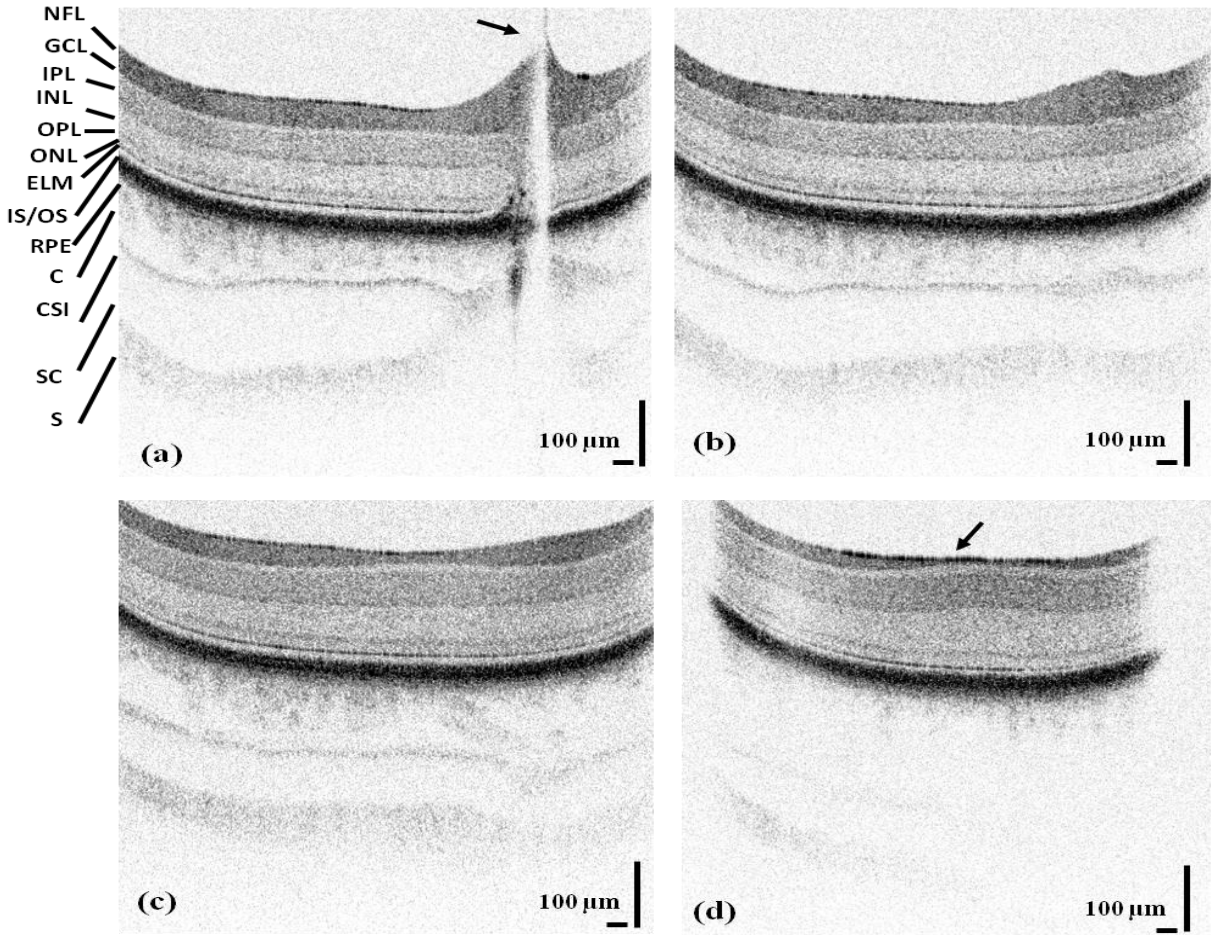

Fig.4.4: Selected B-scans from the volumetric data set presented in Fig. 4.3A. Thickening of the NFL, thinning of the choroid and termination of the sclera cartilage are observed close to the pecten in the vicinity of the ONH (A). Progressive thinning of the NFL and thickening of the GCL and the choroid at a certain area in the retina are shown in B, C and D (black arrow). Image dimensions are 1000 x 512 (A-scans x pixels). Taken from [118] with permission.

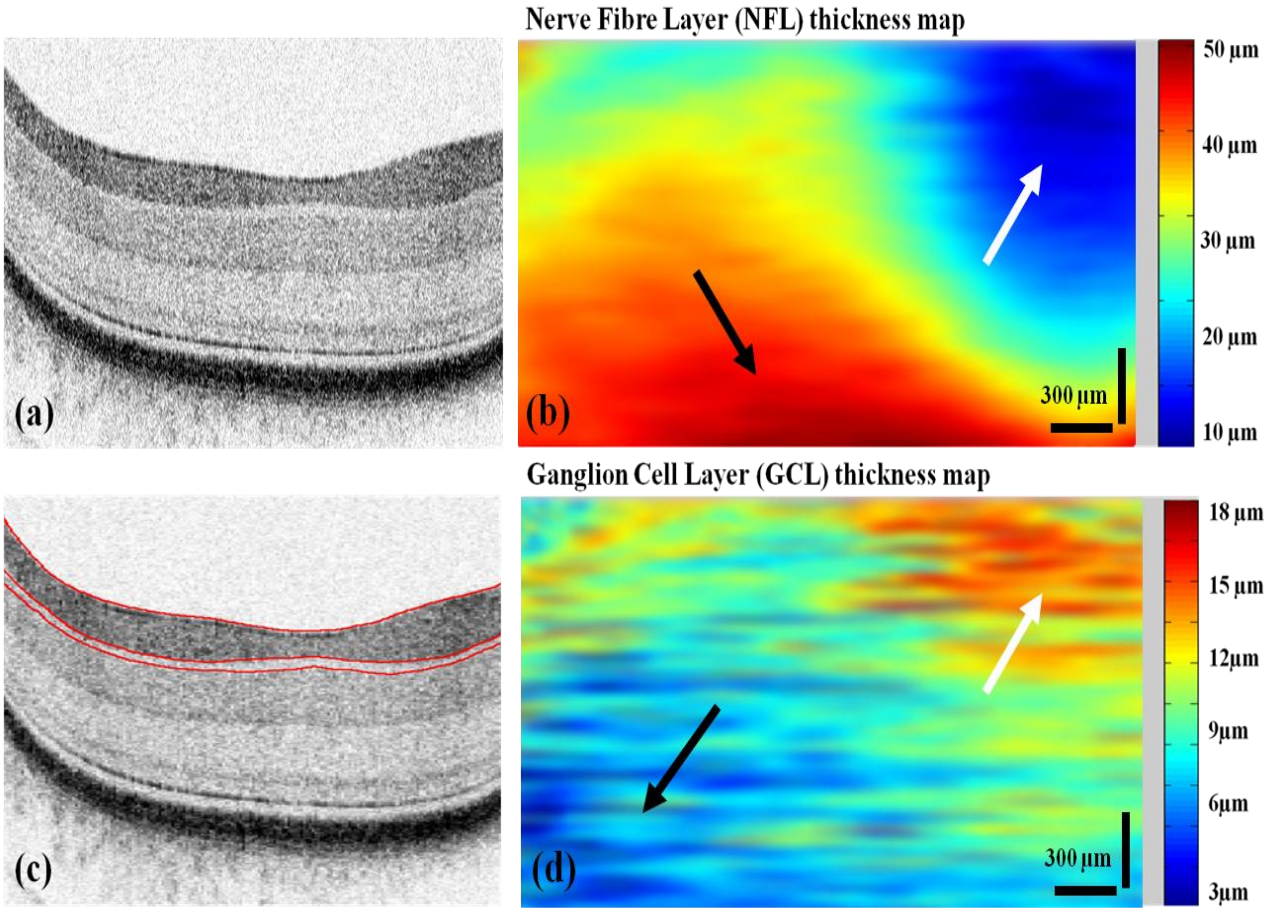

Fig.4.5: Original UHROCT cross-section of the chicken retina (A); the same image with segmented NFL and GCL (C, red lines); thickness maps of the NFL (B) and the GCL (D). Black arrows mark locations close to the pecten and the ONH, while white arrows mark a location with significantly thinner NFL. Taken from [118] with permission.

The same image with selected and segmented NFL and GCL is shown in Fig. 4.4C (red lines). *En face* thickness maps of the NFL and the GCL are shown in Fig. 4.5B and 4.5D, respectively. A Gaussian blur algorithm (10 pixels) was used to smooth the jagged appearance of the thickness maps, which is related to the axial OCT resolution and the limited number of B-scans (256) in the 3D imaging stack of the retina, covering a square area of ~3 mm x 3 mm. In the NFL thickness map (Fig. 4.5B), the area closer to the ONH and the pecten is significantly (~50 µm) thicker (black arrow), while an area located ~2 mm away has a thickness of ~10 µm to 15 µm (white arrow). Similar areas at approximately the same locations are observed in the GCL thickness map (Fig. 4.5D). In this case, the area near the ONH and the pecten has a non-existent GCL, while the area marked with the white arrow has a GCL of ~ 15 µm average thicknesses. No significant spatial variation in the thickness of

the remaining retinal layers was observed in the healthy chicken imaged in this study. It is expected that such thickness changes can occur in some retinal degenerative diseases, which will be the focus of future studies.

4.5 Conclusions

A research grade UHROCT system was used to acquire *in vivo* volumetric images of the healthy chicken retina and to quantify the spatial variation of the thickness of individual retinal layers. The UHROCT cross-sectional images showed excellent comparison with histological images. The volumetric UHROCT tomograms revealed quantifiable thickness changes to the various retina layers depending on location, including a region in which the nerve fibre layer was thinner, and the ganglion cell layer, thicker, than the surrounding area. Confirmation that this area is equivalent to the area centralis is necessary and if proven true, would give us an opportunity to add to the limited data sets that currently exist for this area.

Chapter 5

In vivo imaging of intrinsic optical signals in chicken retina with functional optical coherence tomography

5.1 Overview

Light-evoked intrinsic optical signals (IOS) were measured non-invasively and for the first time *in vivo* from layers of the chicken retina with a combined functional optical coherence tomography (fOCT) and electroretinography (ERG) system. IOS traces were recorded from a small volume in the retina with 3.5 µm axial resolution and 7ms time resolution. IOSs acquired from different layers of the chicken retina clearly showed a change in the intensity of the backreflected imaging beam as a result of a visible light stimuli.

5.2 Introduction:

Intrinsic optical signal (IOS) imaging utilizes optical techniques such as diffuse reflectance, confocal microscopy and optical coherence tomography to measure small changes in the optical properties of biological tissue that result from natural or externally induced alterations in the tissue physiology. IOS imaging was first developed for non-contact probing of neuronal function in isolated neurons [24] and brain slices [124], and was later extended to in vivo studies of the brain cortex [125] and the retina [87]. Compared to other optical techniques, functional optical coherence tomography (fOCT) of the retina has some advantages, as it provides a) 3D imaging with ~3 µm axial resolution, sufficient for the visualization of all individual retinal layers, b) micro-second level line scan rate, that allows averaging of IOSs from retinal volumes while keeping the fOCT time resolution below 10 ms/volume, necessary for the recording of fast physiological processes in the retina and c) sensitivity of ~100 dB, necessary for recording of small magnitude IOSs. Light-induced IOSs were first recorded with fOCT *ex vivo* from frog [49] and rabbit [10] retinas. Recently, IOSs were measured *in vivo* with fOCT from the photoreceptor outer segments (OS) in rat [50] and human retina [7]–[9]. Although these results are very promising, they failed to show reproducible IOS traces in other retinal

layers, unlike the latest results obtained from *ex vivo* retinal studies in frog [60] that show reproducible IOS recordings from the inner and outer nuclear (INL, ONL), inner and outer plexiform (IPL, OPL), and nerve fiber layers (NFL).

In this chapter, to the best of our knowledge, the first fOCT recordings of IOSs from most of the retinal layers acquired *in vivo* from visually stimulated chicken retina is presented.

5.3 Methods:

5.3.1 Imaging system description

A fOCT system (Fig.5.1) operating in the 1060 nm spectral region (Chapter 5) was used for this study. The spectral range of the system was selected to be outside the spectral response of retinal cone and rod photoreceptors to avoid accidental visual stimulation from the optical imaging beam. The fOCT system provided ~3.5 µm axial resolution in the chicken retina, line rate of 22 µs A-scan/s and SNR of ~99 dB for 1.3 mW power of the imaging beam at the cornea. The retina imaging probe is comprised of 3 achromat doublet lenses (Fig.5.1, L_1, f_1 = 12 mm, L_2, f_2 = 60 mm and L_3, f_3 = 60 mm and L3, Edmund Optics) and a pair of galvanometric scanners (Cambridge Technologies), and is designed to project a collimated, 2.5 mm diameter imaging beam at the chicken cornea, resulting in ~5 µm lateral resolution in the retina. A visual stimulator (Fig.5.1) was designed to generate a Maxwellian view spot of ~3.14 mm^2 at the chicken retinal surface with almost homogeneous illumination. The stimulator is composed of 4 LEDs (blue, green, red and white), arranged on a manually rotating wheel (Fig.5.1 inset), that allows one selected (color) LED to be used at a time. The wheel is connected to the console of a commercial ERG system (Diagnosys LLC), which allows for precise control of the light stimulus intensity, duration and timing. The operation of the ERG system is synchronized with the data acquisition of the fOCT system. An image of the LED is formed at the pupil plane of the chicken eye by the use of two achromat doublet lenses (Fig.5.1, L_4, f_4 = 88.9 mm and L_5, f_5 = 50.8 mm Edmund Optics).

The visual stimulator was integrated with the retinal imaging probe via a 90/10 pellicle beam splitter, to minimize walk-off and spectral changes in the imaging beam. The luminance of the visual stimulation beam was measured in free space with a colorimeter (PR-650 SpectraScan. This design of the visual stimulator allows for a) formation of a light stimulus spot on the retina surface with nearly

homogeneous intensity, b) potential separation of IOSs arising from cones and rods by utilizing their different spectral responses and c) preservation of the relative position between the imaging and visual stimulus spots on the retina during eye motion.

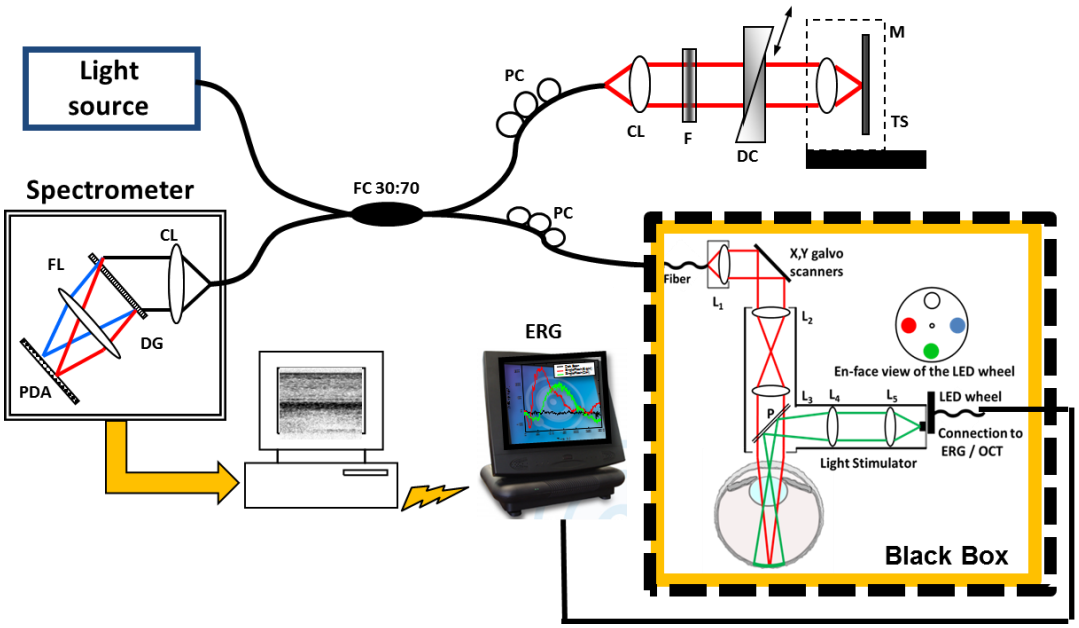

Fig.5.1. Schematic of the fUHR-OCT system and the integrated multicolor visual stimulator. Key: CL, collimating lens; DC, dispersion compensation unit; DG, diffraction grating; ERG, electroretinography system; F, neutral density filter; FC, fiber coupler; FL, focusing lens; L1 – L3, lenses in the eye imaging probe; L4 and L5, lenses in the visual stimulation; LED, light emitting diodes; M, mirror; P, pellicle; PDA, photodiode array; PC, polarization controllers; TS, translation stage. Taken from [126] with permission.

5.3.2 Animals

Three, 13 days old White Leghorn (Gallus gallus domesticus) chickens were used in this study. The chicken retina was chosen because it is cone dominated and void of intra-retinal vasculature that could create shadows and potentially interfere with the IOS measurements from different retinal layers. The imaging procedure was approved by the University of Waterloo animal ethics committee. Chickens were dark adapted for 2 hours in a lightproof container and then anesthetized with 2% isoflurane. Subsequently, the animals were placed in a custom-designed holder that keeps the animal and head stationary during the imaging session and to allow for easy alignment of the eye with respect to the imaging beam. The imaging procedure was carried out in a dark Faraday cage, placed

in a dark room to ensure that the animals were not accidentally exposed to ambient light. A lid retractor was used to immobilize the lid of the chicken eye and artificial eye drops (Refresh tear drops) were administered frequently to prevent the cornea from drying out. Pupils were dilated naturally in dark environment and no mydriatics were used for additional pupil dilation.

5.3.3 Imaging Procedure

Both structural and functional images were acquired from the area centralis on the retina [115], which has a high concentration of cone photoreceptors [102], [115], [121] . The imaging sequence consisted of several steps: a) acquisition of 5 morphological B-scans (1000 A-scans each) and b) fOCT recordings in dark environment and with single flash stimulation. Fig. 5.2A shows a representative morphological tomogram, where most of the retinal layers can be clearly resolved. The red rectangle in Fig. 5.2A shows the dimension of the scanned strip of the retina from where light-evoked IOSs were recorded.

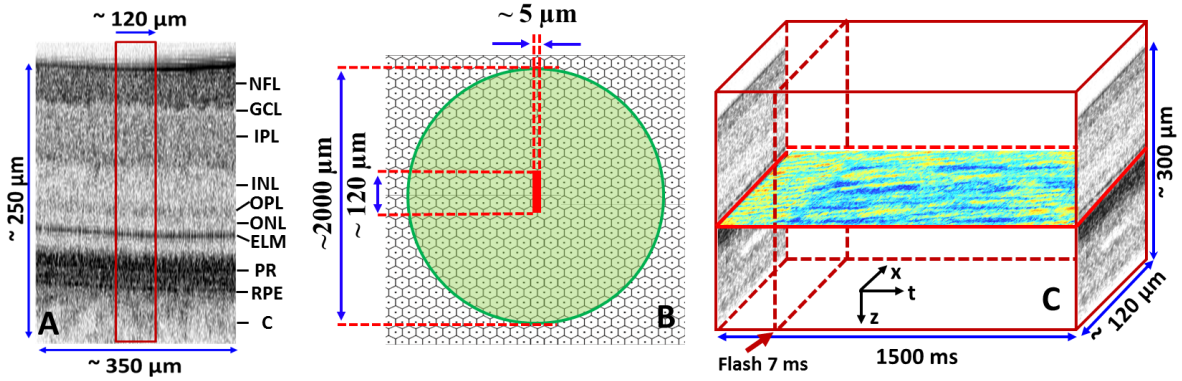

Fig. 5.2. Morphological image of the chicken retina (A). Schematic of the photoreceptor mosaic (B). The green circle marks the location of the visual stimulus spot and the red solid line marks the region from which fOCT recordings were acquired (not to scale). Arrangement of the B-scans in the 3D stack of fOCT images (C). The red arrow marks the onset of the light flash. The colored *en-face* image shows en-face view of the IOS at the photoreceptor layer. Taken from [126] with permission.

Fig. 5.2B shows a schematic of the photoreceptor mosaic, where the green circle marks the area illuminated by the visual stimulus and the solid red line marks the location and dimensions of a strip (B-scan) of the retinal mosaic that was repeatedly scanned during the fOCT recordings and from which changes in the IOS were measured. According to Kisilak et.al.[106], [115] the average linear spacing between cone photoreceptors in a 14 days old chicken is ~ 8.6 µm. Therefore the number of cones in the stimulated area would be ~ 42,500 and the number of cones in the scanned area (area ~ 600 μm^2) would be ~ 8.

Each fOCT recording contained two successive subsets of tomograms, acquired approximately from the same location in the retina over a time period of 1.5 seconds, depended on the anesthesia level and chicken's head orientation, chicken's eye underwent small motions, which would be corrected in post processing. The first subset, a "dark scan", was recorded in complete darkness and used as a reference. During the second subset, a single green color flash of 7 ms duration and ~1.9 Cd/cm^2 intensity entering the pupil was applied 500 ms after the start of the data acquisition. Both the dark and "single flash" scans were composed of 225 B-scans (pixel size x×z ≈ 5μm×1.56μm), 250 A-scans (80/20 duty cycle) each, acquired by scanning repeatedly a strip of the retina with dimensions ~5 μm x 120 μm (Fig. 5.2B, solid red line). fOCT recordings were acquired only from the right eye of the birds and repeated 10 times with ~3 minute pauses between consecutive functional recordings to allow for photoreceptor recovery. Considering the human cone response to a bright stimuli [127], only about up to 30 % of the cones were bleached as a result of the visible light stimuli in this study and would recover after up to 3 minutes [128]. Since the stimulation time was very short (7ms), the number of bleached cones would be much smaller than 30% [127].

5.3.4 Processing Method

The fOCT B-scans were aligned in 3D stacks as shown in Fig. 5.2C and processed with ImageJ (StackReg plugin) to correct for motion artifacts arising from involuntary eye motion, heart or breathing rate. Successive B-scans were cross-correlated to compensate for linear shifts in x and z direction (along the imaged strip and the retinal depth respectively) and for rotational misalignment. Up to 1/3 of the volume of each 3D image stack was removed in the x direction from the two ends of the imaged strip, during the alignment procedure. The involuntary eye motion could add large variations to the result, since it could relocate the scanning beam to a different location. Such relocations were detectable during the alignment procedure and the corresponding data sets were discarded. Recording a b-scan took about 7 ms and no eye movement was observed during this period in the collected data. However, there were eye movements in the total recording time (1500 ms) which could be found during the alignment. The alignment process allowed for aligning the consecutive b-scans and producing an aligned data cube. In this process the date that did not show movements bigger than 20 μm (resulted in cutting 1/6 of the b-scans from both sides) was kept and the data which showed bigger movements was discarded. The aligned images then were manually

segmented to extract the intensity values from individual layers. The segmentation method used here was different from what was used in chapter 4. Since the latter was impractical due to being very time and labour consuming for the functional data. The IOSs were calculated for each layer of the retina from the 3D image matrix as:

$$LayerAverage(t) = LA(t) = \frac{1}{M \times N} \sum_{x}^{M} \sum_{z}^{N} I(x,z,t) \qquad (5.1)$$

$$IOS_{\mathrm{Re}tinaLayer}(t) = \frac{LA(t)}{\frac{1}{T}\sum_{t=0}^{T} LA(t)} - 1 \qquad (5.2)$$

Here I(x,z,t) is the intensity of a pixel with lateral position x, located at depth z in the retina and evaluated at time t, after the start of the data acquisition, M is for the width of the scanned strip, N is the number of pixels for the depth of the retinal layer, and T is the pre-stimulus time of each "dark" or "single flash" scan. To determine the light-induced IOSs originating from each retinal layer, the B-scans in the 3D stack were segmented and averaged in the x direction over the width of the scanned strip and also averaged over the z direction over the thickness of each retinal layer in Eq. 5.1 and the IOS calculated from Eq. 5.2 by subtracting and dividing each averaged intensity from the average of the averaged intensity over pre-stimulus time.

Due to size, contrast and speckle noise issues, the ganglion cell layer (GCL) could not be segmented with high confidence from the NFL, therefore IOS were calculated from the combined NFL and GCL. For the same reasons, the responses of the OS and the retinal pigmented epithelium (RPE) were also combined. Future development of more precise automatic layer segmentation algorithms may allow for separation of the functional responses observed in individual, thin retinal layers.

5.4 Results and Discussion

IOSs calculated for different retinal layers and averaged (Mean±SD) over 5 fOCT measurements from one chicken are presented in figure 5.3. The green strips mark the onset and duration of the light stimulus flash. The black lines in Fig.5.3A-H correspond to "dark scan" IOS traces, evaluated for different retinal layers, which show variations across different measurements. The red lines represent "single flash" IOSs for different retinal layers. The variation of the calculated IOSs around the mean value could be partially related to the relocation of the imaging beam between different

measurements. The IOS traces measured from the NFL+GCL (Fig.5.3A) show an increase of the reflectivity, reaching a maximum (~3%) at 30 ms after the flash onset, followed by a negative response (~6%), peaking at 64 ms after the stimulus onset. A similar behaviour was observed from the rest of the inner retina (Fig.5.3A-C) up to the external limiting membrane (ELM) with slightly varying timing of the negative peaks (from 64 ms to 74 ms). It is interesting to notice that the timing of the positive peak in the inner retina does not vary in different layers, which is discussed later in chapter 9. The IOS from IS was very similar to IOSs from the inner retina (Fig.5.3F). It had a positive peak (~40 ms, 2.5%) and a negative peak (64ms, ~3.6%). The IOS trace from the ELM (Fig.5.3E) showed no positive peak, though the negative peak was present (~6% at 74 ms from the flash onset). Similarly, the IOSs from the photoreceptor OS+RPE layer (Fig.5.3G) showed no positive peak, but very strong negative peak (~15% at 74 ms from the flash onset). Secondary positive peaks were observed in the IOS traces from all retinal layers. These peaks occurred at ~87 ms after the light flash onset for all other layers. All "single flash" IOS traces in Fig. 5.3A-H showed strong negative responses for time beyond ~100 ms after the stimulus onset, and peaked at ~150 ms to 175 ms after the flash onset, with subsequent slow return to a level below the baseline. The IOS trace for choroid (COR) layer was very noisy for both dark and flash scans which could be related to the choroidal blood flow (Fig.5.3H).

IOSs calculated for different retinal layers and averaged (Mean±SEM) over at least 10 fOCT measurements from three different chicken are presented in the figure 5.4. The general trend of the averaged IOSs on three chickens for different retina layers is similar to the IOSs for one chicken. There was a slight difference between timing and values of peaks of the observed IOSs that will be discussed in chapter 8.

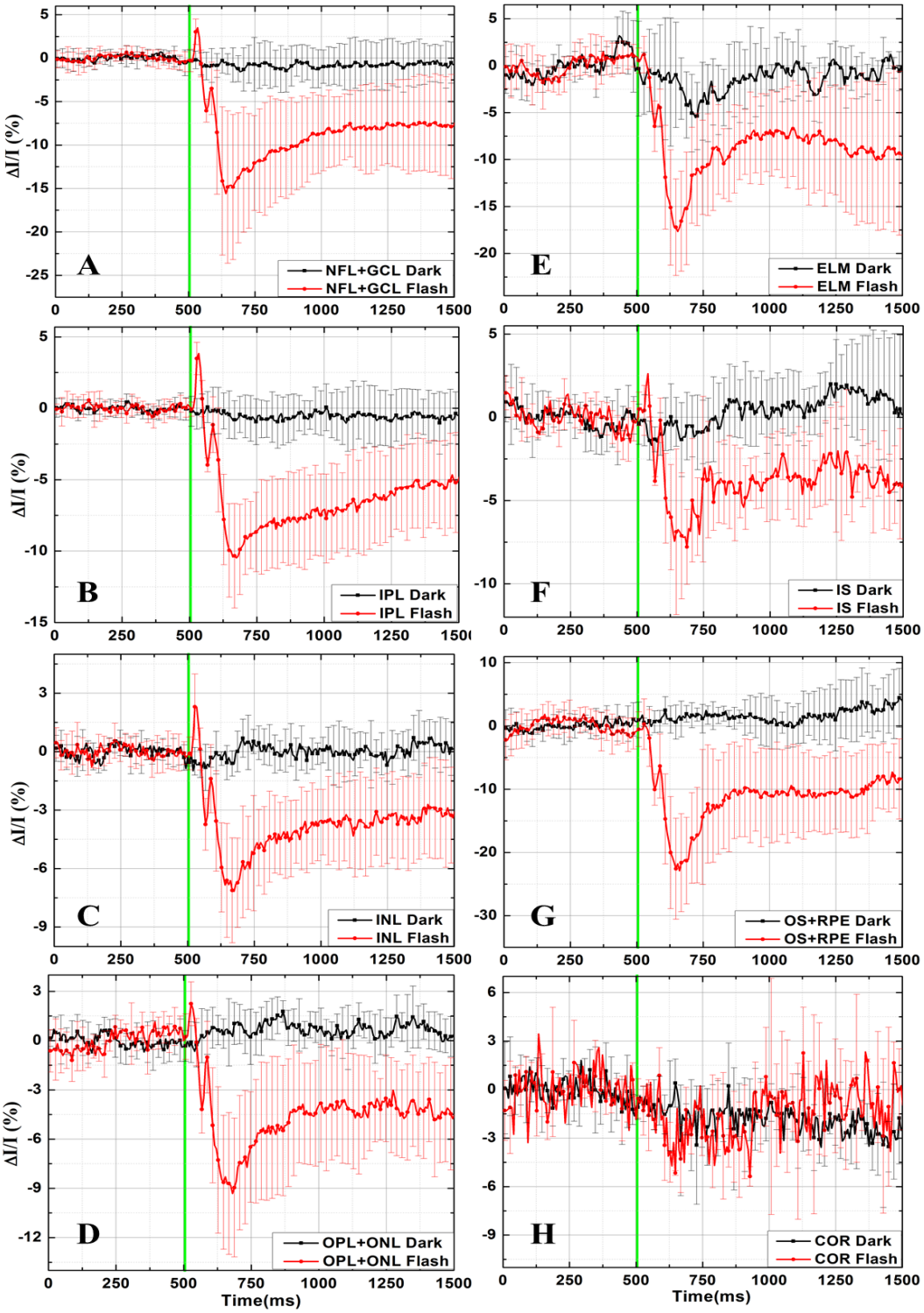

Fig. 5.3: IOSs from different layers of the retina recorded from one chicken (Mean±SD), acquired with fOCT recordings (A-H). The green strip marks the onset and duration of the light stimulus flash. Black lines in 3A-3H represent the "dark scan" IOS, while red lines show the "single flash" IOS.

The IOS traces measured from the NFL+GCL reached to a maximum (~5%) at 34 ms after the flash onset, followed by a negative response (~8%), peaking at 67 ms after the stimulus onset (Fig.5.4A). Like the IOSs recorded from a single chicken, a similar behaviour was observed from the rest of the inner retina up to the external limiting membrane (ELM). Similar to the results obtained from one chicken, the timing of the positive peaks in the inner retina is within the same range in different layers. The IOS from IS (Fig.5.4F) had a positive peak (~40 ms, 4%) and a negative peak (67ms, ~3%). The IOS trace from the ELM (Fig.5.4E) showed no positive peak and the negative peak was present (~6% at 74 ms from the flash onset).

The IOSs from the photoreceptor OS+RPE layer (Fig.5.4G) showed no positive peak, and the value of the strong negative peak was ~10% at 74 ms after the flash onset. Secondary positive peaks occurred at ~87 ms after the light flash onset for all other layers, but not for the choroid (Fig.5.4H). All "single flash" IOS traces in Fig. 5.4A-H showed large negative responses similar to the data from one chicken. This behavior is most likely due to vignetting of the imaging beam due to pupil constriction following the stimulus flash and will be discussed in details in next chapters.

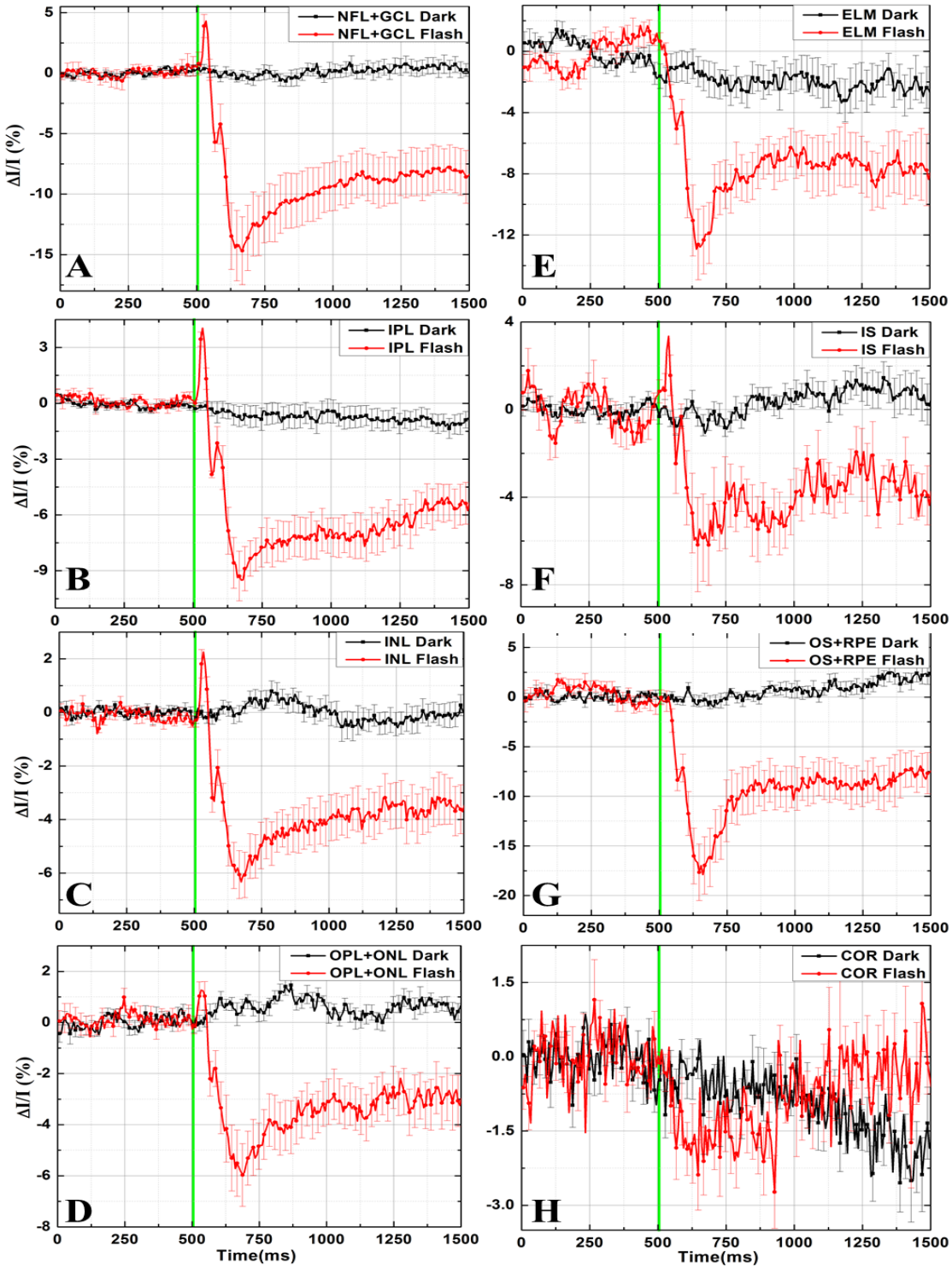

Fig. 5.4: IOSs from different layers of retina from three chickens (Mean±SEM), acquired with fOCT recordings (A-H) represent the "dark scan" IOS, while red lines show the "single flash" IOS. Reproduced from [126] with permission.

5.5 Conclusion

In summary, reproducible, stimulus-induced IOSs were recorded *in vivo* for the first time from all major retinal layers of the chicken retina. Extensive future studies are required to determine the exact physiological origins of the observed IOSs and their correlation with the stimulus characteristics.

Chapter 6

Correlation of visually-evoked intrinsic optical signals and electroretinograms recorded from chicken retina with a combined functional optical coherence tomography and electroretinography system

6.1 Overview

Visible light-evoked, fast Intrinsic Optical Signals (IOSs) were recorded for the first time *in vivo* from retina layers of healthy chicken, using a combined functional optical coherence tomography (fOCT) and electroretinography (ERG) system. The fast IOSs were observed to develop within ~50 ms from the onset of the visual stimulus. The comparison between visible light-evoked IOSs and ERG traces showed clear correspondence between them. The ability to measure visible light -evoked fast IOSs non-invasively and *in vivo* from different retinal layers could improve significantly the understanding of the complex communication between different retinal cell types in healthy and diseased retinas.

6.2 Introduction

The retina is a highly organized neural tissue, where retinal neurons and other cells form a well-defined layered structure. Understanding the communication between retinal cells in healthy and diseased retinas and correlating retinal structure with function has been the goal of many studies. Electroretinography (ERG) method is used in clinical evaluation of retinal function [12] and records the electrical activity of visible light stimulated retinas. Because ERG records an integrated response from all retinal layers to external stimulation, direct correlation between the cellular retinal structure and function is not trivial.

Since the optical reflectivity of neural tissue changes with external stimulation [124], [125], various optical techniques, such as fundus reflectance, near infrared microscopy, confocal microscopy and

adaptive optics, have been utilized to measure visually-evoked intrinsic optical signals (IOSs) in the retina [54], [56], [59], [80], [83], [129], [130]. Fast IOSs, developing within ~50 ms from the stimulus on-set, were measured from individual retinal layers *ex vivo* [59] using near infrared microscopy, however, there are no published records of similar recordings *in vivo*. Optical coherence tomography (OCT) is an imaging technique that allows for non-invasive, *in vivo*, high resolution imaging of the layered structure of the retina [44]. Functional OCT (fOCT) was recently introduced as a novel technique for non-invasive probing of retinal function from individual retinal layers in *ex vivo* retinal preparations [10], [49], *in vivo* animal models [50], and healthy human subjects [7]–[9]. Here, to the best of our knowledge, the first *in vivo* recordings of fast, visible light-evoked IOSs from retinal layers measured with a fOCT are presented.

6.3 Methods

6.3.1 Imaging System

For this study a combined fOCT+ERG system was utilized, which was introduced in the previous chapter. Briefly, the fOCT system is based on spectral domain OCT technology and is designed to operate in the 1060 nm wavelength range. This spectral region was chosen to insure no visual stimulation of the retinal photoreceptors by the imaging beam. The fOCT system provides ~3.5 µm axial and ~ 5 µm lateral resolutions in the chicken retina, a line rate of 22 µs and SNR of ~95 dB for 1.3 mW power of the imaging beam at the cornea. The fOCT system's data acquisition was synchronized with a commercial ERG system (Diagnosys LLC). To measure the electrical activity of the retina, a silver ERG electrode in the shape of a loop (d = 6mm) was employed on the chicken's cornea, while ground and reference electrodes were inserted under the back of the head's skin. The time resolution of the REG system was 1 ms. A custom designed visual stimulator, integrated with the optical imaging probe and described in detail in the previous chapter, was used to project a ~2 mm diameter spot on the retinal surface with pre-selected colour, duration and intensity of the visual stimulus.

6.3.2 Animals

Three 13 days old White Leghorn (Gallus domesticus) chickens were used in this study. The chicken retina was selected as an animal model because it is cone dominated [100], [101] and void of intra-retinal vasculature that could create shadows and potentially interfere with the IOSs measurements from different retinal layers. The imaging procedure was approved by the University of Waterloo animal ethics committee. Chickens were dark adapted for 2 hours in a lightproof box and then anesthetized with 2% isoflurane. The animals were then placed in a custom holder to restrain head motion during the imaging procedure and allow for easy alignment of the eye with respect to the imaging beam. The imaging procedure was carried out in a dark Faraday cage, placed in a dark room to prevent accidental ambient light exposure and minimise electromagnetic noise. A lid retractor was used to immobilize the lid of the chicken eye and eye drops (Refresh tear drops) were administered frequently to hydrate the cornea.

6.3.3 Imaging Procedure

Both structural and functional images were acquired from the chicken retina. Fig. 6.1A shows a representative morphological tomogram, where all retinal layers are clearly resolved. The red dashed line marks a region in the retina from which visually evoked IOSs were measured. Functional OCT data were recorded by repeatedly scanning a ~120 µm long strip of the retina located in the center of the visual stimulus spot. The width of the strip, determined by the diameter of the imaging beam, was estimated to be ~5 µm at the focal plane of the imaging beam. Each fOCT image (B-scan, Fig. 6.1B), corresponds to a single sweep over the retinal strip, consists of 250 A-scans, required ~7 ms of acquisition time (80/20 duty cycle) and represents one data point in the extracted, averaged (Mean±SEM) IOSs traces, a representative of which is shown in Fig. 6.1C. Each fOCT recording consisted of 225 B-scans for a total acquisition time of ~1.5 s. Two types of fOCT recordings were acquired approximately from the same location in the retina in sequence: a baseline (“dark scan”), recorded in complete darkness and used as a reference, and a “single flash” recording, where a single green color flash of 7 ms duration and ~1.9 Cd/cm^2 intensity at the cornea surface was applied 500 ms after the start of the data acquisition. The fOCT recordings were repeated up to 10 times in the right eye of each bird, with 3-minute long pauses between consecutive fOCT recordings to allow for

photoreceptor recovery. The bleaching and recovery of cone photoreceptors were discussed in the previous chapter.

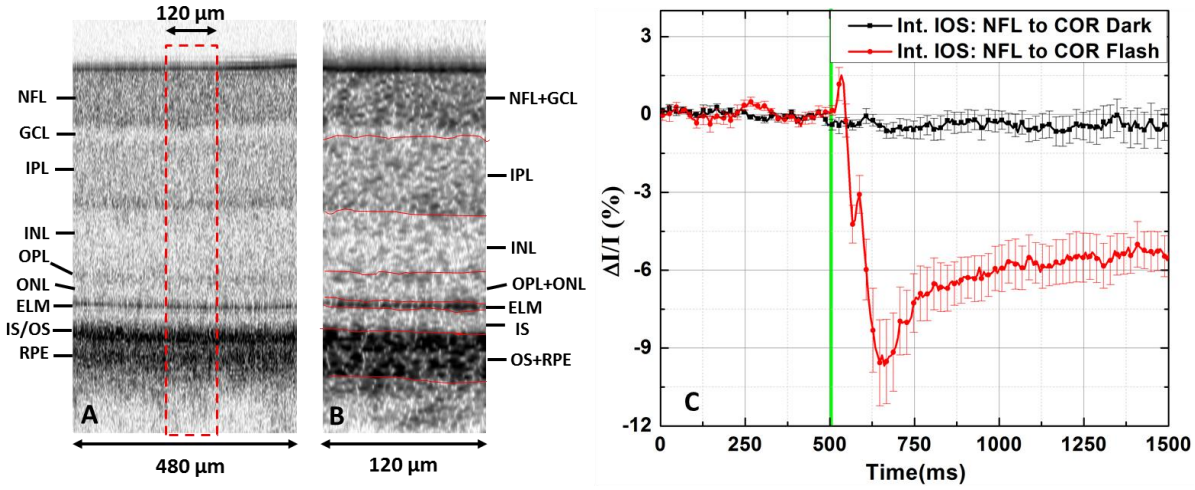

Figure 6.1: Morphological image of the chicken retina (A) with selected region for IOSs recordings (red line). Segmented fOCT tomogram (B). Representative, averaged (Mean±SEM) depth-integrated IOSs traces (C) corresponding to "single flash" (red line) and "dark" scans (black line), averaged across 10 recordings from three chickens. The green line marks the timing and duration of the visual stimulus. Reproduced from [131] with permission.

6.3.4 Image Processing

The fOCT B-scans were aligned in 3D stacks and processed with ImageJ (Stackreg) to correct for motion artefacts arising from involuntary eye motion and heart rate (detail in Chapter 5). Successive B-scans were cross-correlated to compensate for linear shifts in x and z direction (along the imaged strip and the retinal depth respectively) and for rotational misalignment. Up to 1/3 of the volume of each 3D image stack was removed in x direction, from the two ends of the imaged strip, during the alignment procedure because of eye motion artefacts. To determine the visually-evoked IOSs originating from each retinal layer, the fOCT B-scans were segmented manually (red lines in Fig. 6.1B) and the data was averaged in the z direction over the thickness of each segmented layer and in the x direction over the length of the B-scan (length of the imaged strip of the retina). The IOSs were calculated for each layer of the retina by averaging the intensity of each pixel over time for the first 500 ms (pre-stimulus) and subtracting the average from the entire fOCT recording. The differential intensity data was then normalized by the pre-stimulus average intensity to calculate the fractional changes in the tissue optical reflectivity. Due to its small size, low contrast and high speckle noise

tissues, the ganglion cell layer (GCL) could not be segmented with high confidence from the nerve fiber layer (NFL), therefore IOSs were calculated from the combined NFL and GCL. For the same reasons, the photoreceptor outer segments (OS) and retinal pigmented epithelium (RPE), as well as the outer plexiform (OPL) and the outer nuclear layers (ONL) were also combined. Future development of more precise automatic layer segmentation algorithms may allow for separation of the functional responses observed in individual, thin retinal layers. Representative IOSs traces are shown in Fig. 6.1C, where the black line corresponds to a "dark scan" and the red line to a "single flash" recording. The IOSs in Fig. 6.1C are statistical averages (Mean±SEM) of 10 "dark" and 10 "single flash" fOCT recordings from three chickens and represent the integrated retinal response to the visual stimulus from the NFL to the COR. The thin green line marks the light flash on-set and duration.

6.4 Results and Discussions

Representative IOS traces measured from individual segmented retinal layers are shown in Fig. 6.2. The black line corresponds to a "dark scan". The thin vertical green strip at 500 ms marks the onset and duration of the light stimulus flash. The grey area in Fig. 6.2 marks a 150 ms time period of interest that is magnified in Fig. 6.3 for easy comparison and analysis of the IOS data. The IOSs recordings from all retinal layers showed fast increase and/or decrease of the tissue reflectivity within ~80 ms from the visual stimulus onset (fast IOSs, grey area in Fig. 6.2) and slow variation of the optical changes for the rest of the recording (slow IOSs). For comparison, no reflectivity changes were observed from retinal layers during a "dark scan" and in a "single flash" scan during the first 100ms after the stimulus onset. This suggests that the IOS measured from all retinal layers in "single flash" fOCT recordings are evoked by the visible light stimulus. The IOS traces from all retinal layers show a sharp decrease in the reflectivity at time t = 600ms from the start of the fOCT recording and a slow recovery to a new baseline at time t = 1000ms. Very similar behaviour was observed in the choroid IOS trace, which suggests that this effect may not be a true visible light-evoked functional retinal response. Considering that the diameter of the fOCT imaging beam is 2.5 mm at the cornea, and the diameter of the naturally dark dilated chicken pupil was between 3 and 3.5 mm, it is possible that the observed slow changes in the retinal layer reflectivity are due to vignetting of the imaging

beam resulting from stimulus-induced pupil constriction and subsequent dilation which is discussed in chapter 7.

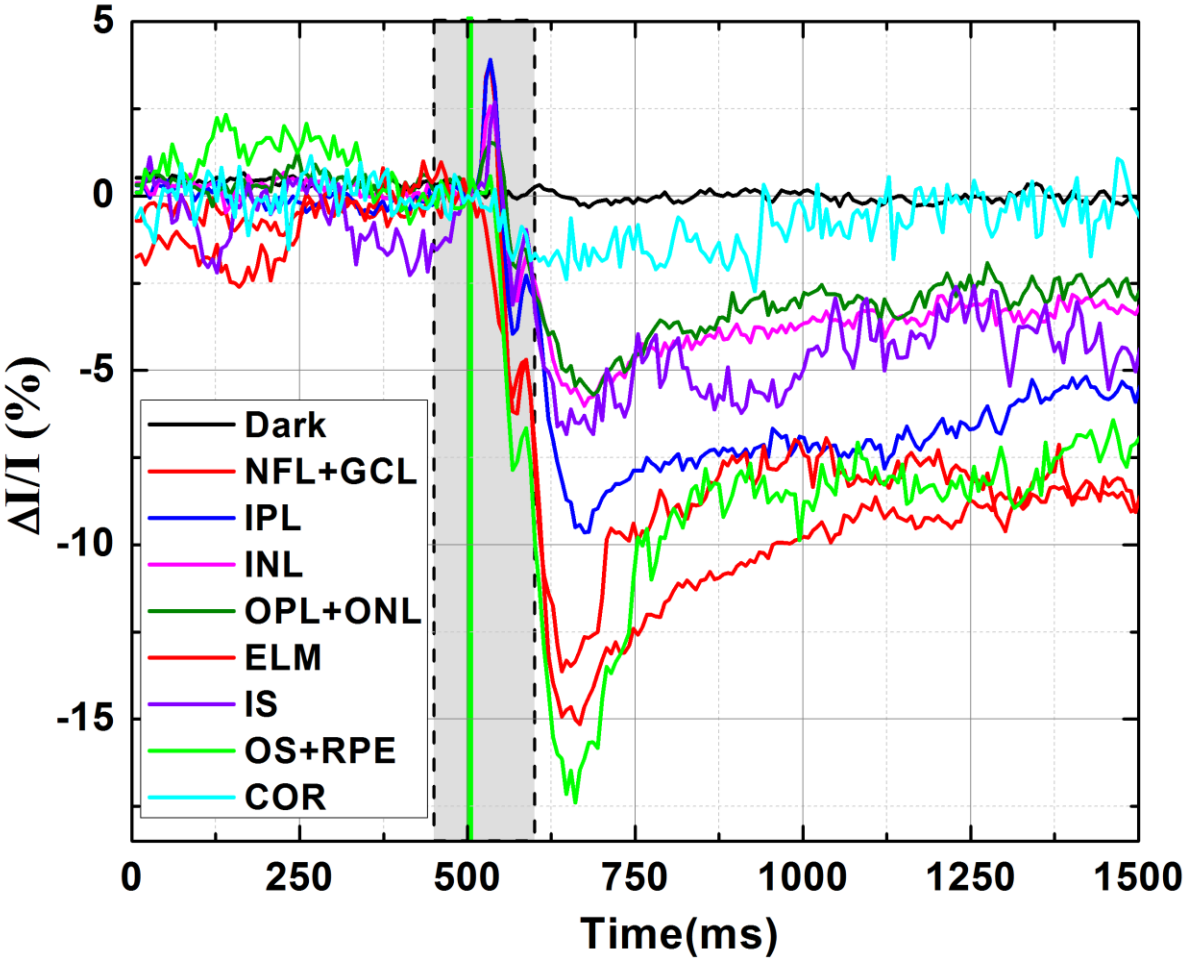

Figure 6.2: Representative averaged IOSs recorded from all segmented retinal layers. The grey area marks ~100ms region over which the fast, visually-evoked IOSs develop in all retinal layers. The green line marks the timing and duration of the visual stimulus. Reproduced from [131] with permission.

According to previously published research [132]–[134], visually-evoked pupil constriction in chicken begins ~100 ms after the stimulus onset and occurs more rapidly than the subsequent dilation. The pupil dynamics timing and behaviour described by Barbur [134] matches well with the changes observed in the slow IOSs from all retinal layers for the time period t = 600 ms to ~1000 ms from the start of the fOCT recording. However, the slow IOSs measured from the retinal layers are most likely a convolution of stimulus-induced changes in the tissue reflectivity associated with post-

flash recovery processes, which can last up to a few 100 ms after the stimulus on-set [12], and pupil induced vignetting of the fOCT imaging beam.

Figure 6.3 shows a magnified view of the grey area in Fig. 6.2 and presents a comparison between the fast IOSs (mean of 10 "single flash" recordings) and the simultaneously recorded ERG traces. Fig. 6.3A shows that the a-wave (the negative peak of the ERG trace) appears at ~15 ms after the visual stimulus onset, which matches well with previous ERG studies in the living chicken retina and indicates normal photoreceptor function [132], [133]. The a-wave in the ERG trace shows the electrical activity of the photoreceptors as result of visible light stimulus [12]. The corresponding IOSs measured from the inner retinal layers, from the NFL to the ONL, show very small (~1.5% to 4%) positive changes and peak between 32 ms and 35 ms post flash onset, which appear to match with the timing of the maximum magnitude of the b-wave (the positive peak in the ERG recording), which shows the electrical activity of the inner retina. Furthermore, these IOSs show a subsequent decrease in the reflectivity, which with minima between 67 ms and 74 ms after the stimulus on-set for the individual inner retina layers. The timing of the negative peaks in the IOSs match well with the end of the b-wave in the ERG recording. The OS+RPE trace shows a sharp decrease in the tissue reflectivity between 34 ms and ~67 ms after the stimulus on-set. This behaviour is followed by a fast increase in the reflectivity, which peaks at 87 ms after the stimulus on-set. The timing of the negative peak in the OS+RPE IOS appears to coincide with the end of the b-wave and the negative peak in the IOSs recorded from the inner retina layers. Figure 6.3B shows a comparison between the integrated IOSs recorded from the NFL to COR layers and the ERG trace which clearly shows the correspondence between the positive peak of the IOS with the maximum of the b-wave and the negative peak of the IOS with the end of the b-wave in the ERG trace.

Considering the fact that the ERG trace is an integrated electrical response of different retinal cells comprising the retinal layers, it is likely that the difference between the timing of the positive and negative peaks in the IOSs from various retinal layers and the a-and b-waves in the ERG trace is due to combination of the electrical responses that occur simultaneously in different retinal layers.

For example, the slow PIII response in the ERG recording is masked by the simultaneous positive electrical activity in the inner retina arising from the bipolar and Müller cells, thus defining the timing and magnitude of the a- and b-wave peaks[12]. In contrast, fOCT measures the individual optical

responses from the various retinal layers that correspond to physiological processes such as cell membrane de- or hyper polarization, cell swelling or de-swelling resulting from ion exchange and water in- and out flux between the intra- and extra-cellular matrix, metabolic activity, etc. Although these physiological processes develop in parallel over time, fOCT is able to resolve the spatial location in the retina (in depth) where these processes occur.

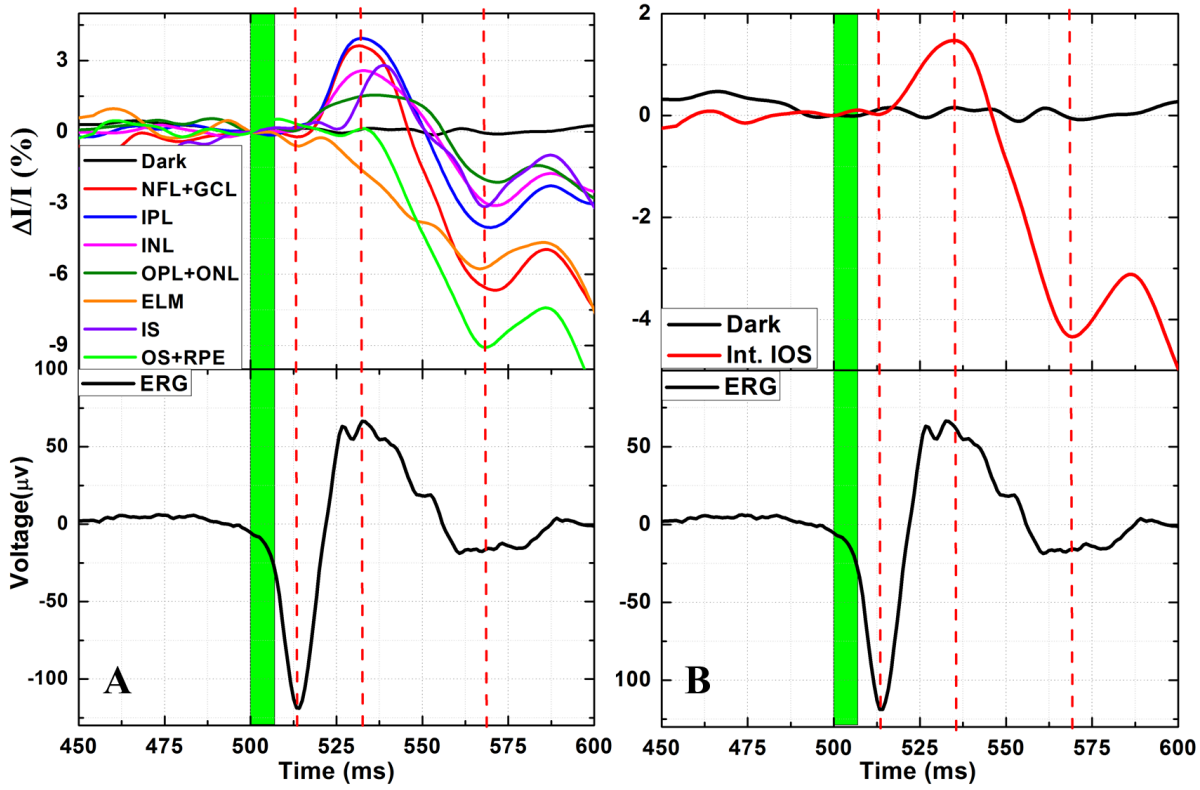

Figure 6.3: Comparison of the visually-evoked IOSs (mean of 10 measurements from three chickens, top row) and ERG traces (mean of 9 measurements from 3 chickens, bottom row). Individual IOSs recorded from all segmented layers (A), integrated IOSs from the NFL to the COR (B). The time scale corresponds to the grey area marked in Fig. 6.2. The green line marks the onset and duration of the visual stimulus. Reproduced from [131] with permission.

Figure 6.4 demonstrates the mean and standard deviation (Mean±SD, three chickens, and total 10 data points for each layer) of the amplitudes and latencies of the major IOS peaks presented in Fig. 6.3A. The timing of the negative and positive peaks of the fast IOSs recorded from different retina layers was consistently within 5% of the values measured from the recordings presented in Fig.6.2 and Fig.6.4. However, the IOS magnitude varied significantly (> 25% for some retinal layers) for recordings acquired from the individual chickens used in this study. This variability could be attributed to a number of between animal factors such as the health status of each bird and its reaction

to the anesthesia, the optical clarity of the eye, which is strongly depended on the previous two factors, etc. In addition, eye movements combined with the small numbers of cones illuminated are among the factors contributing to within animal variability. Future, more extensive studies are needed to establish the exact causes of the variability of the IOS magnitude.

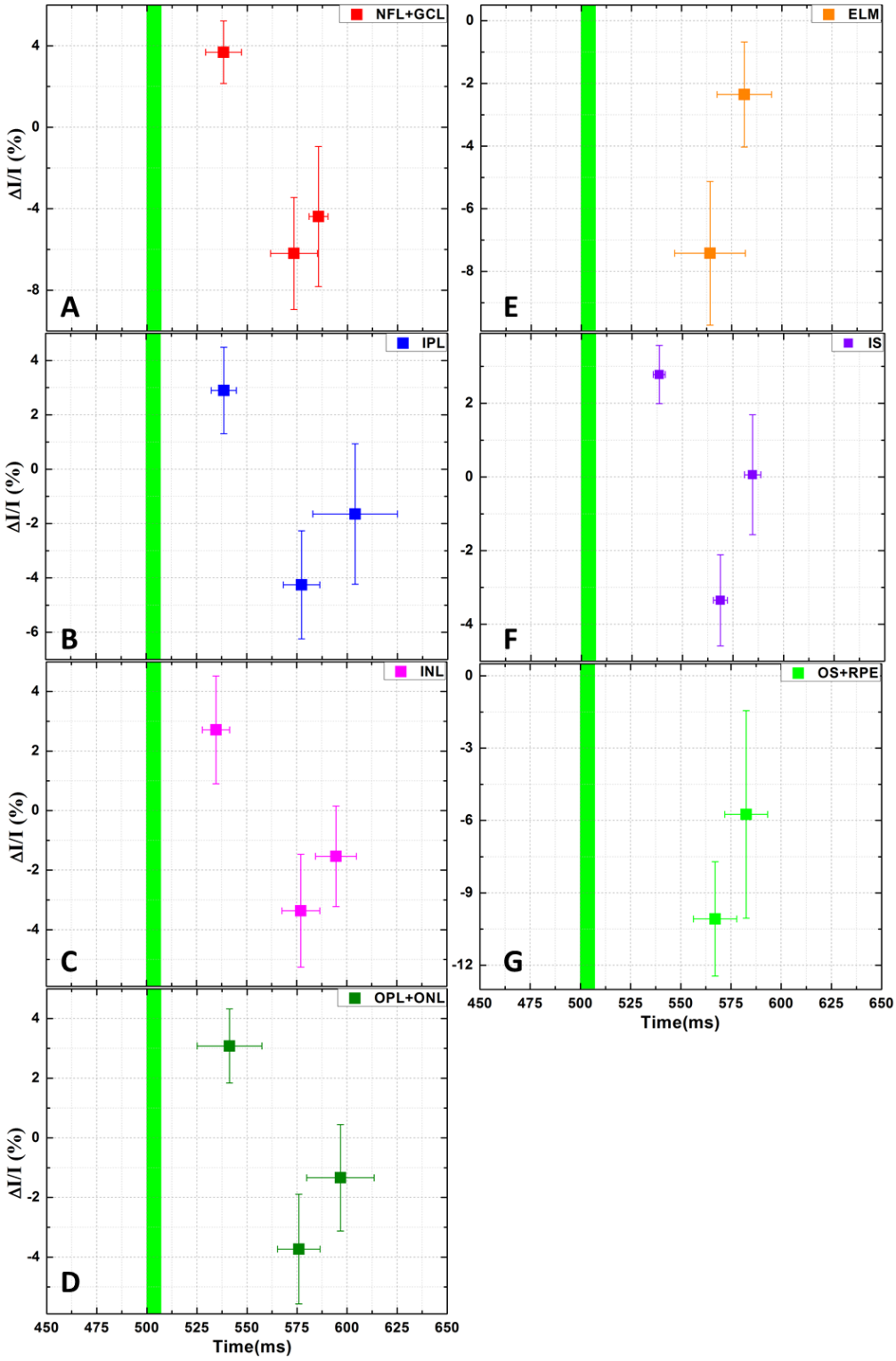

Fig. 6.4: The statistics (Mean±SD) of the major peaks of the fast IOSs from different retinal layers.

To evaluate the spatio-temporal variation of the visually-evoked IOSs measured from individual retinal layers, xy cross-sections from the 3D image stack were selected. Figure 6.5 shows the spatio-temporal profiles obtained from the all retinal layers (Fig 6.5 A, B, E, F, I, J, M ,N), and the corresponding IOS traces (Fig. 6.5 C, D, G, H, K, L, O, P) for those layers obtained by averaging the pixel intensity from the spatio-temporal images over the length of the imaged strip (vertical axis in figures Fig 6.5 A, B, E, F, I, J, M, N). The pale gray rectangles in Fig. 6.5 C, D, G, H, K, L, O, P mark the 150ms region of interest, similar to the one discussed in Fig. 6.2. Although the spatio-temporal profiles show significant variation with time and lateral spatial location in the retina, they also show clear negative and positive responses within ~100ms from the application of the visible light stimulus, that become distinct peaks in the average traces. Considering the very small size of the retinal volume that was sampled in this study (~5µ x 120µm x retinal thickness), and the typical size of retinal cells, it is difficult to determine a clear relationship between the observed spatio-temporal profiles of the IOSs measured from individual retina layers and visually evoked physiological processes that occur in those layers. Future advances of fOCT technology, that can enable faster scanning of larger retinal volumes, while preserving the high temporal resolution, would allow for the exploration of such a relationship.

The fOCT results presented here appear to correlate well with results from previously published studies. For example, a fast, visually-evoked increase in the tissue reflectivity of the GCL and the inner nuclear layer (INL), as well as a simultaneous decrease in the photoreceptor layer reflectivity was reported by Yao [59] for *ex vivo* studies of the leopard frog. The timing of the positive and negative peaks for these retinal layers appears very similar to the results presented in this thesis. Differences in the magnitude of the measured IOSs can be attributed to differences in the imaging techniques (NIR microscopy used by Yao vs. fOCT used in our study), as well as the animal models (frog vs. chicken retina) and the measurement conditions (*ex vivo* vs. *in vivo*). The negative IOS measured from the OS+RPE layers in our studies also appears to correlate very well with a decrease in human cone reflectivity measured from the outer segments of individual retinal cones *in vivo* with adaptive optics [83]. Since other published *in vivo* animal [50] and human fOCT studies [7], [8] reported slow IOSs measured with time resolution > 100ms, they cannot be compared directly with the fast retinal IOSs measured in our study.

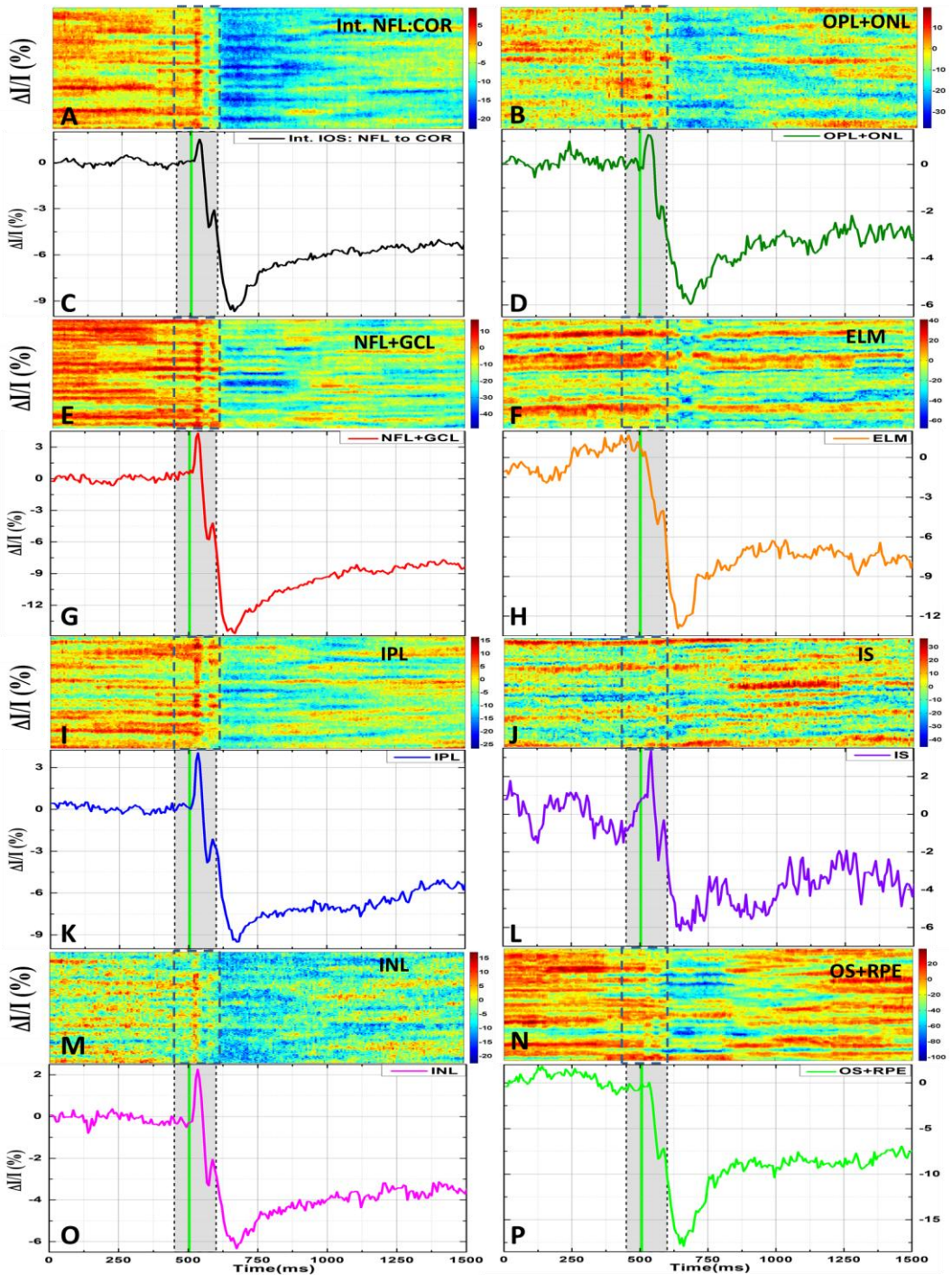

Figure 6.5: Spatio-temporal profiles of the IOSs measured from the all retinal layers, and corresponding IOS trace averages for these layers. Reproduced from [131] with permission.

Considering the complex physiology of the living retina, further thorough studies are required to investigate the physiological origins of the retinal visually-evoked IOSs. The imaging procedure and apparatus presented here could be adapted in the future for non-invasive functional imaging of the human retina. A significant obstacle in such studies would be the proper management of eye motion related imaging artefacts that could mask the small magnitude IOSs in some retinal layers (discussed in chapter 9).

6.5 Conclusion

In summary, visually-evoked fast IOSs were recorded non-invasively and *in vivo* from layers of the chicken retina with a combined fOCT+ERG system. The IOS showed clear correspondence with the ERG traces. The ability to record visually-evoked signals from individual cell layers in the retina non-invasively and *in vivo* could improve the understanding of how retinal cells communicate with each other and respond to external stimuli in healthy and diseased retinas.

Chapter 7

Stimulus Specific Pupil Dynamics Measured in Birds (*Gallus Gallus Domesticus*) *in vivo* with Ultrahigh Resolution Optical Coherence Tomography

7.1 Overview

Purpose: To demonstrate the ability of high speed, ultra-high resolution optical coherence tomography (UHR-OCT) to measure and characterize *in vivo* visual stimulus specific pupil dynamics in birds and its correlation with measured IOSs.

Methods: Ten two-week old White Leghorn (*Gallus gallus domesticus*) chickens were imaged in this study. The chickens were dark adapted for one hour and anesthetized with 2% isoflurane prior to the imaging procedure. Blue, green, and red single flash visual stimuli of 7ms duration were used to evoke pupillary responses. UHR-OCT cross-sectional images of the pupil were acquired prior, during and for several seconds after the visual stimuli onset. Images were processed with a novel custom automatic algorithm, designed to determine the pupil diameter changes over time.

Results: Pupil constriction begins with the onset of the visible light stimuli, however, maximum pupil constriction occurs ~150 ms later. No statistically significant variation in the timing of the maximum pupil constriction was observed for stimuli of different color. However, significant variation was observed in the maximum pupil size constriction, between red -green and red -blue stimuli, but not between blue-green stimuli. Furthermore, the magnitude of the maximum pupil constriction decreased monotonically with time under isoflurane anesthesia.

Conclusion: For the first time measurement of visually evoked pupil dynamics in animals using high speed UHR-OCT is demonstrated. Results suggest dependence of the pupil dynamics on

the color of the visual stimulus, and adverse effects of isoflurane anesthesia on the visually evoked pupillary responses in chicken. Time courses of the maximum pupil constriction and the large slow negative peak in IOSs are same.

7.2 Introduction

Optical coherence tomography is a well-established optical method for non-invasive, cellular level resolution imaging of biological tissue [29]. Over the past decade, ultra high resolution optical coherence tomography (UHR-OCT) has been used for fast, volumetric, morphological imaging the healthy and diseased retina [31], [44] and cornea [42]. In addition to imaging the structure, UHR-OCT is able to image blood perfusion [135] and quantify blood flow [45], provide information about the bi-refringent properties [46]–[48] and even measure visually evoked physiological responses in ocular tissues [7]–[10], [49]–[51], [53], [126], [131].

In previous chapters, *in vivo* imaging of visually evoked physiological changes in all layers of the chicken retina has been demonstrated by use of modified, functional UHR-OCT system. Since chicken has skeletal intraocular muscles that are not affected by commonly-used (smooth muscle) mydriatics, only dark-induced natural pupil dilation was used in those experiments. (Vecuronium bromide, a skeletal muscle mydriatics, clouds the cornea significantly enough to prevent imaging of the chicken retina with UHR-OCT). Because stimulus-induced pupil constriction may have partially obstructed the optical imaging beam during those experiments, it is possible that the data we recorded are the convolution of visually evoked retinal and pupillary responses. Therefore, in order to investigate the effect of the pupil constriction on the measured IOSs from the retina we need to measure the pupillary response under the same imaging conditions.

A number of studies were conducted to investigate visually evoked pupillary responses in avian species in general [134], [136]–[139]. Results from these studies suggest that the maximum pupil constriction occurs on the time scale of hundreds of milliseconds after the stimulus onset and is dependent not only on the color, duration and intensity of the visual stimulus, but also on the background illumination and the use or absence of anesthesia.

In this study, the same functional UHR-OCT system, visual stimulator, and modified imaging probe used to image the chicken iris. The animal handling and imaging procedures remained the same as

the functional retina studies (Chapters 5 and 6). Here, the first *in vivo* measurements of visually evoked pupillary dynamics in domestic chicken acquired with UHR-OCT technology are presented.

7.3 Material and Methods

7.3.1 The imaging system

Briefly, a high speed (92,000 A-scans/sec), spectral domain UHR-OCT system (Fig. 7.1), operating in the 1060 nm wavelength region was used in this study. The choice of imaging in the near infrared (NIR) wavelength region was made to prevent any pupillary response triggered by the imaging beam. Details about the design and technical specification of the imaging system were introduced in previous chapters. The UHR-OCT system provided 11 µs time resolution per A-scan and SNR of ~97dB for 1.8 mW power of the imaging beam incident on the cornea (Fig.7.1). The original imaging probe designed for retinal imaging, consisted of 3 NIR achromat doublet lenses (L_1, f_1 = 12 mm, L2, f_2 = 60 mm, L3, f_3 = 60 mm, Edmund Optics) and a pair of galvanometric scanners (Cambridge Technologies). However for this study, one of the lenses was removed to allow for focusing the UHR-OCT imaging beam at the pupil plane and imaging the chicken iris with high spatial resolution (3.5 µm axial and ~ 30µm lateral resolution). The eye imaging probe was integrated with a custom multi-colour visual stimulator, designed to project an image of the stimulus LED at the pupil plane and generate a Maxwellian view spot of ~3.14 mm^2 at the chicken retina surface (Chapter 5). Thus, the imaging and the visual stimulator beams are coaxially aligned, so that an image of the stimulator LED is formed in the center of the OCT imaging field. The visual stimulator was interfaced to a commercial electroretinography (ERG) system (Diagnosys LLC), which allowed for user-defined selection of the colour, duration and intensity of the visual stimulus. In this study, visual stimuli of blue (455 nm, ~5 Cd/cm^2/sec, corresponding to 1.66 $\times 10^{16}$ photons/cm^2/sec), green (530 nm, 218 Cd/cm^2/sec, corresponding to 8.4×10^{17} photons/cm^2/sec) or red (647 nm, 293 Cd/cm^2/sec corresponding to 1.35 $\times 10^{18}$ photons/cm^2/sec) colours, and 7 ms duration were used. The luminance of the visual stimulation beam was measured in free space with a colorimeter (PR-650 SpectraScan).

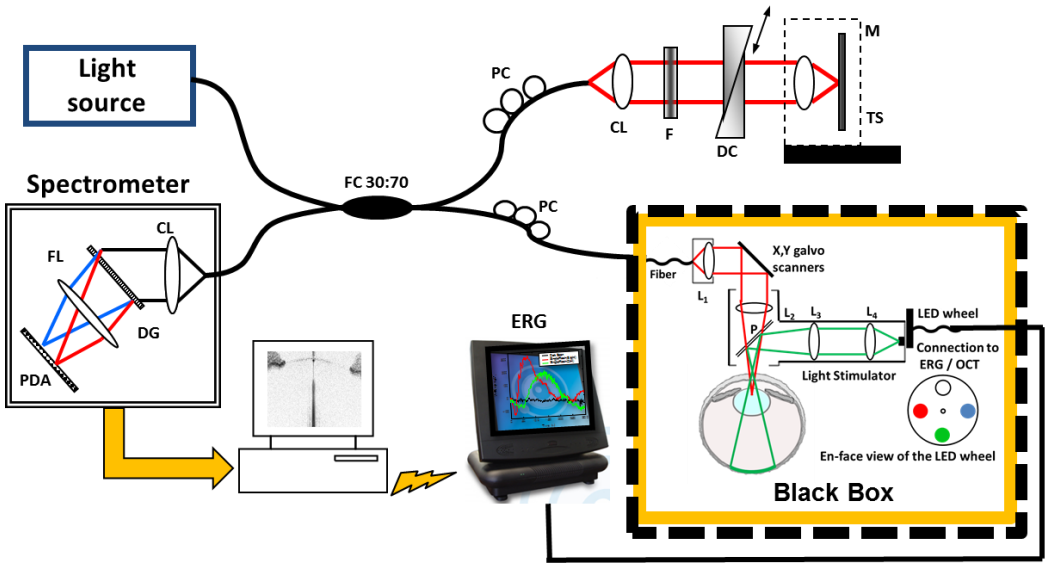

Fig. 7.1 Schematic of the combined functional UHR-OCT and ERG system with modified imaging probe for imaging the pupil dynamics in chicken: CL collimating lenses, (DC) dispersion compensation unit, (NDF) neutral-density filters, (M) mirror, (PC) polarization controllers, superluminescent diode, and (TS) translation stage. The spectrometer consists of a collimating lens (CL), a volumetric diffraction grating (DG), a focusing lens (FL), and a high speed InGaAs camera. Taken from [140] with permission.

7.3.2 The animal preparation

Ten two weeks old White Leghorn (*Gallus domesticus*) chickens were used for this study (4 chickens for blue flash stimulation and 3 chickens for green and red flash stimulation each). The imaging was conducted in the Biomedical Imaging Lab at the University of Waterloo, with approval from the University of Waterloo animal ethics committee and in compliance with the ARVO statement for ethical use of animals in ophthalmic and vision research. Chickens were dark adapted for 1 hour prior to the imaging procedure to induce natural pupil dilation, and then anesthetized with ~2 % isoflurane. The amount of isoflurane anesthesia varied slightly from animal to animal, though it remained unchanged for the duration of each imaging experiment in individual animals. The animals were then placed in a custom animal holder that restricts the head and body motion during the imaging procedure and allows for easy alignment of the eye with respect to the imaging beam. The anesthesia and preparation of the birds for imaging was carried out in a dark room under faint red illumination, while the imaging procedure was carried out in a custom-built dark box, to prevent accidental ambient light exposure of the retina. A lid retractor was used to restrict the motion of the

outer eyelid and eye drops (Refresh tear drops) were administered frequently to hydrate the cornea in order to keep it optically transparent.

7.3.3 The data acquisition and processing

The eye imaging probe was positioned so that the UHR-OCT imaging beam is focused at the pupil plane of the chicken eye, where an image of the visual stimulator LED is formed. The UHR-OCT imaging beam was also aligned so that it is approximately perpendicular to the apex of the cornea. Images were acquired at the maximum camera speed (92,000 A-scans/s) and the alignment of the imaging probe was frequently checked and adjusted when necessary, to ensure that the UHR-OCT cross-sectional images were acquired along the pupil diameter plane. To measure the visually evoked pupil diameter changes, a series of functional UHR-OCT recordings were acquired from the chicken iris and pupil, each recording consisting of 720 B-scans (2D cross-sectional images of the iris). Each B-scan consisted of 512 A-scans and corresponded to acquisition time of ~6.7ms. The total time for each functional UHR-OCT recording, was ~5 seconds. The first 74 B-scans of each functional UHR-OCT recording were acquired in darkness followed by a 7ms flash of the chosen colour. The rest of the recording was completed in darkness.

UHR-OCT images were generated from the raw data using a custom Matlab (Mathworks) code. A novel algorithm was developed to identify the pupil edges from the UHR-OCT images, track their movement over time and calculate the pupil diameter from the spatial coordinates of the pupil edges. The algorithm is based on the following steps: 1) noise-compensated reconstruction for generation of speckle-suppressed UHR-OCT images; 2) Identification and tracking of the pupil edges in successive UHR-OCT image frames, by use of region-based maximum likelihood tracking strategy; and 3) calculation of the pupil diameter from the spatial coordinates of the pupil edges and tracking the pupil size changes over time. The new algorithm was also implemented in Matlab.

For statistical analysis, a one way ANOVA was used to test the preference difference of the minimum amplitude and its latency among three colors (R, G, and B; $p < 0.05$). Holm-Bonferroni post-hoc test was used for pair comparison. The p values were corrected according to the Holm-Bonferroni correction criteria based on the number of pairs (3).

7.4 Results and Discussion

Figure 7.2A shows a representative B-scan from the chicken pupil with the edges of the pupil outlined by the highly reflective tissue of the iris. The black vertical line in the center of the image marked with the black arrow is caused by the strong specular reflection of the imaging beam from the surface of the corneal apex. A faint reflection of the chicken lens surface is also visible on the image (red arrow). Figure 7.2B shows the same image with marked edges of the pupil, where the pupil diameter is marked with a red arrow.

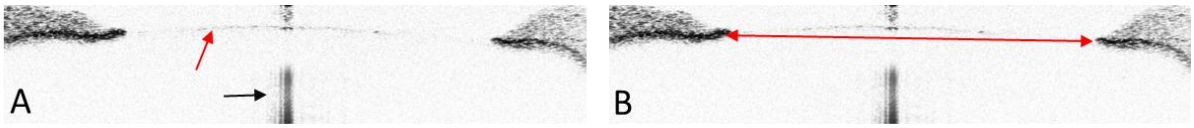

Figure 7.2: A representative cross-sectional UHR-OCT image of the chicken iris and pupil. Red arrow marks the reflective surface of the eye lens, while the black arrow marks the imaging artefact generated by the strong back-refection of the imaging beam off the corneal apex (A). The same tomogram with a red arrow pointing at the pupil edges as determined automatically by the novel pupil edge detection algorithm (B). Taken from [140] with permission.

For each bird, a minimum of 5 recordings of the change in the pupil size as a function of time were recorded for a particular colour. Statistical results (Mean±SEM) obtained from multiple recordings acquired from individual birds are shown in Figures 7.3A-C for 7 ms for blue (12 measurements), green (8 measurements) and red (5 measurements) visual stimuli respectively. Data shown in the graphs were normalized relative to the initial pupil diameter and then averaged over multiple recordings from the same chicken. No standardization was applied with respect to maximum pupillary response for stimuli with different colours. In general, the pupillary responses between multiple flashes of the same colour were relatively consistent for the constriction phase, but dilation of the pupil showed slightly more variability with time.

Figures 7.3D-F show individual pupillary responses of the birds to blue, green and red light stimuli, respectively, without normalization of the maximum pupil constriction. For all wavelengths used, maximum pupil constriction amplitudes average to ~10% of the pupil (range: ~4% to ~16%) and occurs ~160 ms (range: 100 to 225 ms) after the stimulus onset. Pupillary dilation dynamics subsequent to the constriction follows two general trends, one where the pupil dilates fairly fast and reaches a steady state (plateau) ~1 second post stimulus, although it may or may not return to the pre-

stimulus size, or one where the pupillary dilation occurs much more slowly, and pupils do not recover their original sizes until well after ~4.5 seconds post-stimulus.

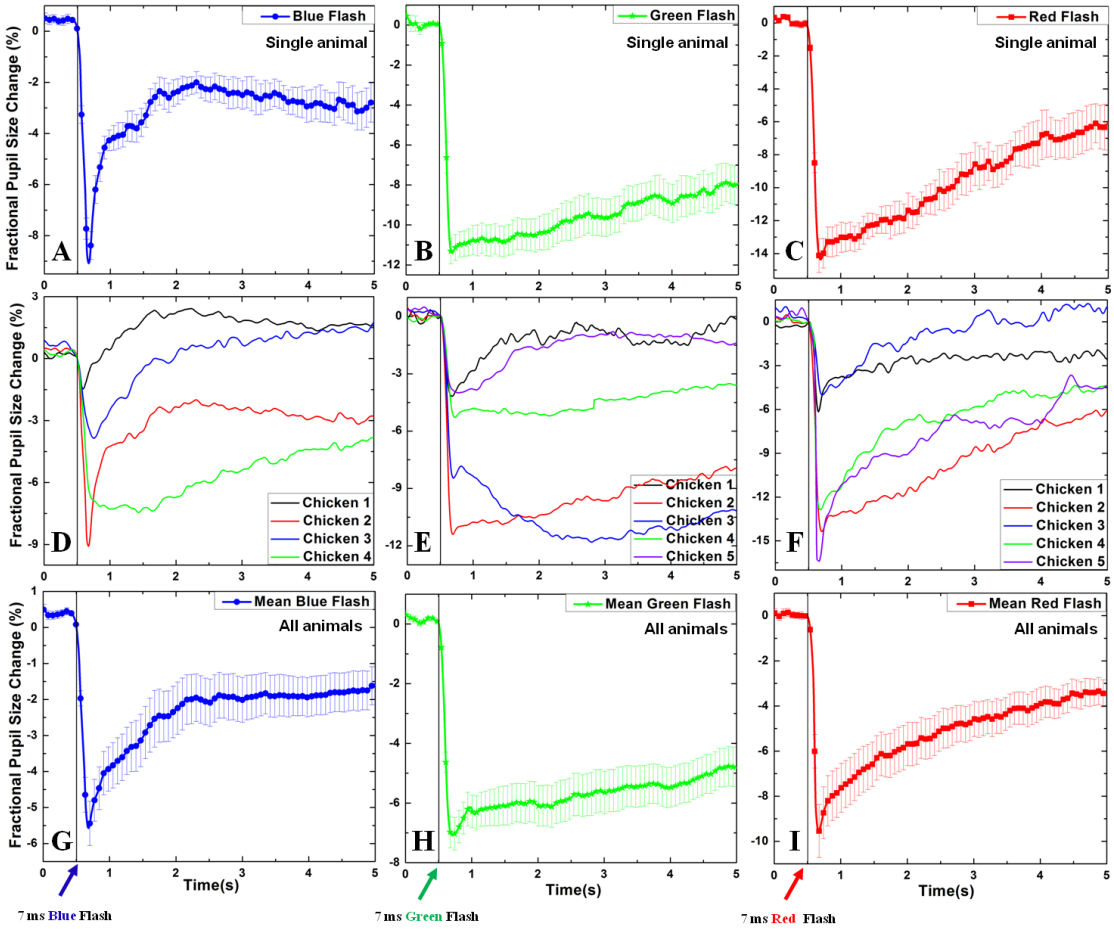

Figure 7.3: Mean and SEM of the fractional pupil size changes as a function of time for multiple recordings obtained from individual animals for blue (A), green (B) and red (C) stimuli of the same duration. Comparison of mean pupil dynamics recordings acquired from different animals for the three colors of the visual stimulus (D, E and F). Mean and SEM of the fractional pupil size changes as a function of time for all chickens for the three colors of the visual stimulus (G, H and I). Taken from [140] with permission.

The curves for the average red (Fig 7.3I), blue (Fig 7.3G) and green flashes (Fig 7.3H) are slightly different shapes. However an overlay of the responses (Fig 7.4A), shows that the differences between the curves following the minimum constriction are of the same order as their SEM's.

The dilation responses for all colours appear to be at least biphasic, showing an initial quicker dilation, followed by a slower return to initial pupil size (Figure 7.4A; summary of Figs G-I). The responses from individual birds (Figs 7.3D-F) appear to confirm that two phases of pupillary dilation exist for almost all the tested birds. On the assumption that at least two of the phases are "real", the

slope of the initial linear phase (S1 on the Fig. 7.4A) was calculated and is presented in Fig 7.4C. Although the statistical significance was not tested, the initial fast dilation rate is greatest for the red and smallest for the green stimulus. The second pupillary dilation phase was fitted by the best functions for each colour of the visual stimulus (Fig. 7.4A).

The amplitudes of pupillary constriction are significantly different depending on the colour of the stimulus used ($F(2,93)=6.2$, $p=0.003$), with amplitudes in response to a red flash significantly greater than for the blue ($p=0.002$) and green ($p=0.02$) flashes. The amplitudes for the blue and green flashes were not different ($p=0.254$). The latencies of the maximum constrictions were not different depending on colour ($p=0.297$). As shown in Fig. 7.4A and C that red flashes result in maximal constriction (Mean ± SEM: 9.5% ± 1.1% change in pupil diameter), while blue and green flashes elicit minimal constriction (5.5% ± 0.6% and 7% ± 0.5%, respectively). The maximum pupil constriction and its latency were calculated from ~95 pupil dynamics recordings acquired from 10 chickens with the blue, green and red color stimuli in Fig. 7.4B, where the yellow vertical line marks the timing and duration of the visual stimulus.

The large variability of the pupil responses to the same color, intensity and duration of the visual stimuli observed across different animals in the study suggested that anesthesia may have some effect on the pupillary dynamics.

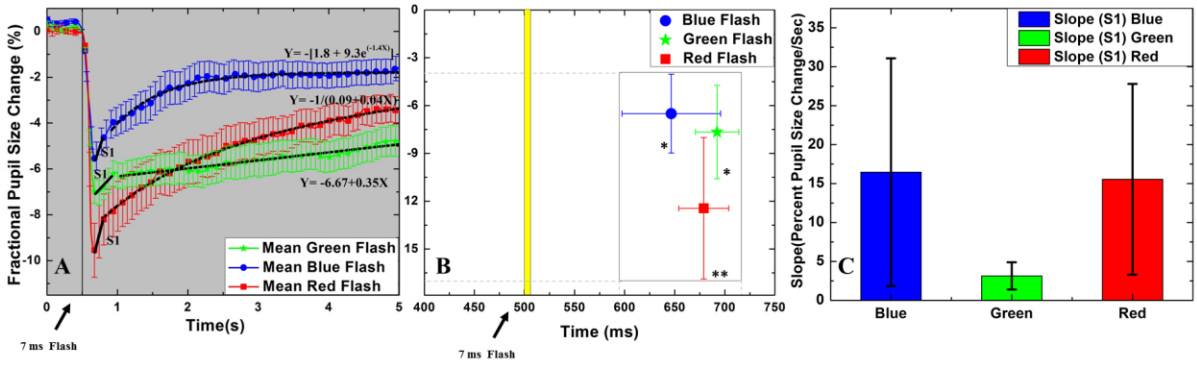

Figure 7.4: Average recordings (Mean±SEM) of the fractional pupil size change as a function of time for all chickens for blue, green, and red color flashes and their fitted functions (A). Statistical summary (Mean±SD) from ~95 pupil dynamics recordings from 10 chicken for the maximum pupil constriction and its latency with respect to the onset of the visual stimulus for the blue, green and red color stimuli. ** shows the significant different between amplitudes of red and both green and blue, * shows that the amplitudes of red and blue are not different (B). Average slopes (Mean±SD) of the first phase of dilation (S1) for all three colors(C). Taken from [140] with permission.

Analysis of the pupillary responses from chickens of the same age and gender to light stimuli of the same color, intensity and duration at different times from onset of the same levels of isoflurane

anesthesia revealed a decrease in the pupillary constriction magnitude with prolonged exposure to isoflurane anesthesia (Figure 7.5). These results show that visually-evoked pupillary constriction begins almost simultaneously with the stimulus onset. The latency responses for peak pupillary constriction were about 3x slower than those observed by Barbur *et al* [134], however there are many differences in the paradigms between our studies, including, but not limited to, stimulus duration (7ms vs 500ms), intensity and projection of the stimulus (spatial frequency and focal plane), age of the chicken and pupil size at the start of the experiment. Moreover, our chickens were raised in artificial light, while those of Barbur's group [134] were raised in natural sunlight, which could have an effect on the spectral sensitivity of the chick as well as other effect on pupil dynamics.

While our method provides a novel way for monitoring and characterization of pupillary dynamics, it should be acknowledged that it is sensitive to noise and variability. Irideal constriction amplitudes were clearly affected by the amount and duration of anesthesia and this method is also sensitive to eye motion; although animals were anesthetized and the head motion was restricted, translation and rotation of the chicken eyeball during the imaging procedure induced some uncertainty in the measurement of the pupil diameter, which may partially account for some of the variability that was observed in my data (Figure 7.3G-I).

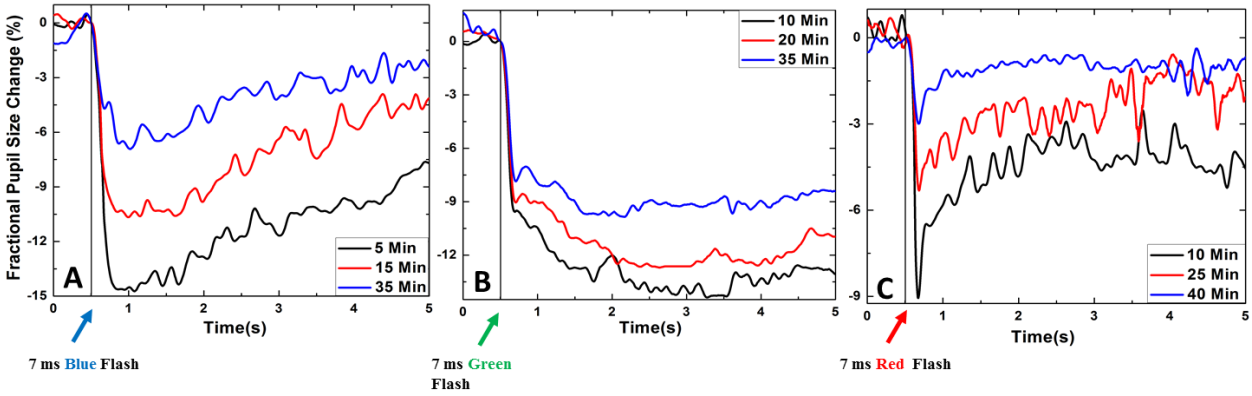

Figure 7.5: The effect of isoflurane anesthesia measured for three different colors at different times relative to the onset of the anesthesia from individual chickens. Taken from [140] with permission.

Due to the integrated design of the OCT imaging probe and the visual stimulator, necessary to provide stability by coaxial alignment of the imaging and stimulus beams, only one eye could be measured and data for consensual pupillary responses were not available. Potentially, a second visual stimulator can be interfaced to the OCT+ERG system to allow for measurement of contralateral

pupillary responses but building a binocular system comes with other challenges, including but not limited to, alignment of and keeping the position of the stimulus LED image in the center of the pupil and at the pupil plane in the presence of eye motions.

Until now, three mechanisms have been identified to explain the visible light exposed pupil response dynamics. Pupil response could be initiated by 1) rod and cone photoreceptors in the outer retina [141], 2) melanopsin-containing intrinsically photosensitive retinal ganglion cells (ipRGCs) in the inner retina [139] , and 3) intrinsically photosensitive iris [137], [142].

Despite the variability mentioned above, I was able to detect wavelength-dependent differences, with the pupillary constriction amplitudes to red stimulation significantly greater than either of the other two colours. At least some of the differences must be related to the relative intensities of the flashes used, with the red flash having the highest intensity and the blue the lowest.

However, it should also be noted that other investigators have found that red flashes of light are behaviorally preferred [143], induce stronger pupillary constriction amplitudes [134] and ERG signals [144].

Presumably, the different coloured flashes were detected by the visible spectrum-sensitive cones, of which chickens possess three, long wavelength-sensitive (red) cones, medium wavelength-sensitive (green) cones, and short wavelength-sensitive (blue) cones. Chickens are tetrachromats, that possess ultraviolet (UV)-sensitive cones, and the spectral sensitivities of the chicken cones are further complicated by the presence of 6 types of oil droplet filters, which, in general, act to fine-tune the spectral sensitivity of the cone in which they are embedded [145]. Several investigators reported relatively similar peak-wavelength sensitivities of the four single cones, with slight variations primarily dependent upon whether peak sensitivities were measured using electrophysiological or psychophysical means and whether oil droplet filtering has been taken into account. The sensitivities range from 562 – 602 nm, 507 – 540 nm, 455 – 475 nm and 413 – 420 nm, for the longest to shortest wavelength-sensitive cones, respectively [144]–[149].

In the chicken, melanopsin-containing intrinsically photosensitive retinal ganglion cells (ipRGCs) are localized to two regions in the retina, the retinal ganglion layer and the outer regions of the inner nuclear layer [150], [151]. As noted for ipRGCs in other species, the chick ipRGC sensitivities are maximal in the blue range, with an absorption maximum at 468 nm and the range of response

maxima between 402 - 473 nm [152]. In humans, blue light-induced pupillary constriction is more stable [153] and is greater in amplitude [141], [154] than that for red light when matched for photopic luminance. Blue light-exposed ipRGCs mediate circadian rhythms and pupillary light reflexes in GUCY1* chickens, a blind breed of birds that do not have functional rods or cones [139]. It is likely that ipRGCs contributed to the blue flash response in our study, but because of the disparity in the light flash intensities, their contribution remains unknown.

In addition, it has been shown that avian iris contains cryptochrome which is sensitive to shorter wavelengths of the visible light (λ_{max}<400 nm) and control the local pupillary light reflex [137], [142]. However, since our illumination was a Maxwellian illumination and the focal point of the stimulus was at the center of the pupil, it is less likely that the stimulus beam could affect the iris. Although, any minor internal reflection of the stimulus which reflects back to the eye from the probe or any sudden movement of the eye during the imaging which could relocate the focal point of the stimulus beam to the iris, could influence the iris. Because of the disparity in the light flash intensities and the uncertainty in the role of iris in pupil response in our experiments, the contribution of the local pupillary light reflex of the iris to pupil dynamics is unknown.

With the possible exception of one bird (Fig 7.3E), our short (7 ms) flash was not of sufficient duration to allow for a sustained contracture of the iris muscles, resulting in a biphasic dilation of almost all pupils immediately following pupillary constriction (Figs 7.3 and 7.4A). The mechanism underlying the biphasic dilation response is not known, however we postulate that the initial fast rate of dilation may reflect a relaxation of the iris sphincter muscles, while the slower rate may be attributable to dilator contraction that is initially masked by the action of the sphincter muscles; it has been shown that the time course for dilator muscles that have been stimulated via the nerves connected to them is longer, and can persist after the end of the stimulation pulse [155]. Alternatively, the fast and slower dilation rates may be only related to the sphincter muscle. Pilar and colleagues [155] also show that chicken iris muscles can exhibit both skeletal (fast twitch) and smooth muscle (tetanic contractions) properties; the fast and slow dilation responses may reflect the cessation of these sphincter muscle behaviors. Additional studies are necessary to clearly define the physiological mechanisms underlying the irideal muscles and pupillary behaviors, as observed in our experiments.

7.5 IOS vs. Pupil Constriction

In chapters five and six, it was demonstrated that the light induced IOSs acquired with OCT from the chicken retina, as a result of 7 ms green visual stimuli, showed a significant decrease in the back reflected light from all retinal layers after ~100 ms onset of the flash. According to the previous studies [134] on the pupil response to visual stimulation, it was hypothesized that the large negative signal observed in all retinal layers was a combination of the light induced IOSs and the effect of the pupil constriction on the imaging beam entering into the chicken's eye.

The IOS from all retinal layers in Fig. 7.6 is plotted along the averaged fractional pupil size change, which is normalized to the minimum peak in IOSs in each layer. From comparing the results of the chicken pupil response and IOSs to the visual stimuli (7ms green flash), it is clear that the time course of the strong negative peak in IOSs after ~100ms onset of the flash is comparable to the time course of the maximum pupil contraction to visual stimulation. According to Fig.7.6 for the green flash, the pupil size reaches to its maximum constriction between ~ 150 to 210 ms after the onset of the flash. Therefore, a part of the negativity of the IOSs after ~ 100 ms after the onset of the flash, acquired from the chicken retina, might be due to the vignetting effect of the pupil constriction on the imaging beam. Considering the fully dilated pupil size in the two weeks old chicken (about 3.5 mm in diameter), the 8% decrease in the pupil area (~4 % decrease in diameter) at ~100 ms after the onset of the flash, does not interfere with the centered imaging beam (about 2.5 mm in diameter). However, since the alignment of the beam into the pupil was done manually, it is possible that the imaging beam was not exactly at the center of the pupil and therefore was closer to the pupil edge. Therefore, the 4% diameter change within the first 100 ms after the flash could have some effect on the imaging beam. Hence, due to the similar pattern observed in the fast IOSs (having an initial positive peak in the inner retina), it is reasonable to assume that the fast IOSs (the gray box in Fig 7.6) within the first 100 ms after the onset of the flash are mainly dominated by the signal originated from the light stimulated retina. The effect of the pupil constriction starts to dominate the IOS after ~100ms after the visible stimulation in all retinal layers (all of them suddenly start to decrease), which reaches to its minimum simultaneously with the maximum pupil constriction, which happens ~ 150 to 200 ms after the flash onset. In previous investigations done by other research groups [26], [54], [56], [79] which recorded IOSs for longer time duration, slow IOSs were also observed. The reported slow IOSs

appeared to take a long duration to reach to a positive or negative peak, which hypothesized that they were related to hemodynamic and metabolic processes stimulated by flash. In our study, because of the pupil constriction effect, observing the slow IOSs directly is impossible.

There are special drugs to immobilize the chicken's pupil muscle during the experiments which allows monitoring the potential slow IOSs. Using such drugs on the chicken's eye in my experiments caused a great decrease in the image quality acquired by OCT which interfered extensively with extracting IOSs from retina layers. Using an imaging beam with a much smaller diameter than the pupil size could potentially help to minimize the pupil effect (preventing the vignetting). However, it will decrease the lateral resolution at the retina. More experiments and a more advanced image processing code are required to extract slow IOS from the chicken retina.

7.6 Conclusion

In summary, it was demonstrated for the first time that high speed UHR-OCT is able to measure the pupillary responses to visual stimuli in living animals with very high spatial and temporal resolution. Although the current system design is limited only to ipsilateral measurements, future redesign of the imaging system could allow for recording of contralateral pupillary dynamics. By utilizing the UHR-OCT system in set of animal studies we found that red light stimuli induced the strongest pupillary contraction, that pupillary dilation following contractions was biphasic and that magnitude of the pupil constriction was affected negatively by isoflurane anesthesia. Further research needs to be undertaken to determine the physiological mechanisms driving this pupillary behaviour. Comparing the time course of the IOSs and the pupil constriction showed clear comparability between the two time courses. The strong negative peaks in the IOSs from the retinal layers were partly due to the vignetting effect of the pupil constriction.

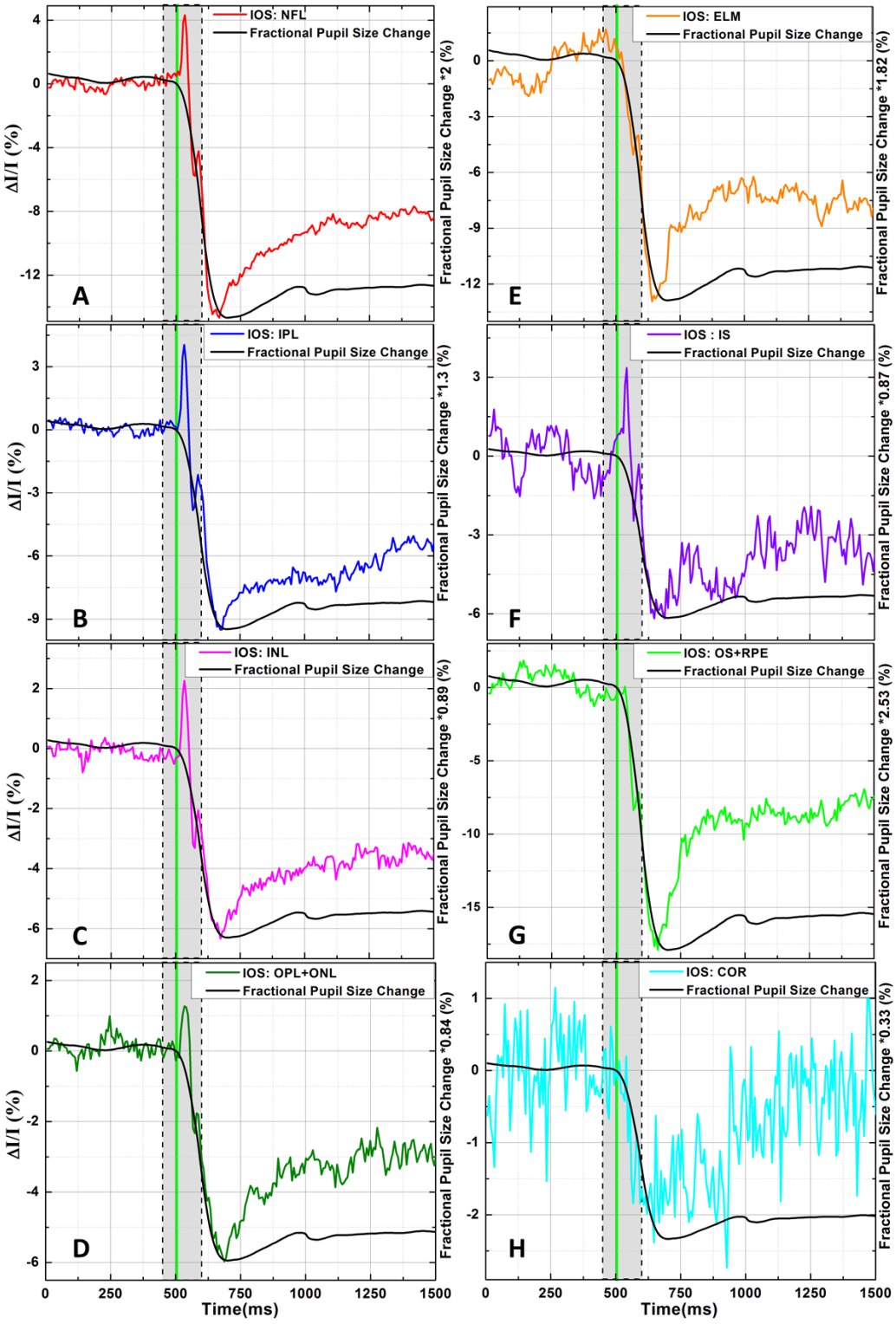

Figure 7.6 .The comparison of the time course and magnitude of the IOS in each retinal layer with the time course of the fractional pupil size change. Minimum of the fractional pupil size change for green light is normalized to the minimum of the IOSs.

Chapter 8

The effect of the Isoflurane anesthesia on the ERG components

8.1 Overview

The effect of the Isoflurane as an anesthesia agent on chicken's Electroretinogram (ERG) has been investigated. The chicken's ERG has been recorded with a commercial ERG system. Three ERG main peaks, a-wave, first and second oscillatory potentials' latency and magnitudes have been compared 10, 20, 30, and 40 minutes after the beginning of the anesthesia. Statistical analysis showed that the effect of the isoflurane is more pronounced on the inner retina layers, after 30 minutes from the beginning of the experiment.

8.2 Introduction

In previous Chapter (7), preliminary results showed that the Isoflurane gas which was used for anesthesia, could affect the size of the pupil constriction over time. Therefore, a set of experiments were designed to investigate possible effects of Isoflurane on the ERG recordings in chicken. The results of these experiments will be discussed in this chapter.

It has been shown that anesthesia can affect the normal function of the neuronal tissue. Several studies have investigated the effect of anesthesia on the ERG components. Tashiro et al [156]showed that using volatile anesthesia, i.e., methoxyflurane, halothane and enflurane on albino rabbits could significantly prolong the first oscillatory potential component of the b-wave (01). The amplitude of the a-wave and 01 decreased in a dose dependent manner, but not as severe as latency of the 01. However, the latency of the a-wave did not change [156]. Iohom et al [157], [158] showed similar results by using N_2O/sevoflurane anesthesia on human subjects. The b-wave components of the ERG underwent a significant latency. They summarized known ERG effects of several anaesthetic agents on different animals and human subjects in their paper [157]. Using Sodium Thiopental as anesthesia on a monkey and chicken, Satoh et al and Wioland et al [159], [160] showed an increase in the amplitude of the scotopic b-wave and a suppression of c-wave while, using ketamine on the same animals showed a decrease in the amplitude of the scotopic b-wave and the same effect on c-wave as

a result of anesthesia. Chynoransky et al [161] reported a prolongation and culmination of all ERG components as a result of intravenous injection of Benzodiazepines. Using Propofol and fentanyl to human subjects, Andreasson et al. [162] reported a decrease in amplitude of the b-wave and prolongation of the photopic b-wave. Yagi et al. [163] showed a prolongation of a-wave and oscillatory potentials and decrease of a-wave amplitude as a result of inhaling Enflurane in human subjects. Raita et. al. [164] used the same drug on human subjects and found a prolongation in b-wave. Reports from Wongpichedchai et. al. [165] indicated that inhalation of Halothane by human subjects did not have any effect on the photopic and scotopic oscillatory potentials. Studies on the effect of the N_2O and N_2 on the ERG acquired from rats by Wasserschaff et. al, [166] showed a smaller reduction in the amplitude of the b-wave in rats anaesthetized by N_2O rather than by N_2. Blain et. al. [167] by using Trichloroethylene as an anesthesia agent on rabbit, showed a decrease in the amplitude of the a-wave, b-wave, and oscillatory potentials. A recent study by Becker et. al. [168] on rat brain slices, using Isoflurane at low doses in the tissue, showed an enhancement in neuronal excitability (IOSs) in the hippocampus and a reduction in the neocortex. However, higher doses showed a significant reduction in IOSs in both brain regions. In summary, all studies indicated that using different anesthesia agents with different doses could differently affect the neuronal tissue.

Since Isoflurane was applied as an anesthesia agent in all experiments related to IOSs and pupil dynamics in previous chapters, the effect of Isoflurane on the ERG and IOSs needed more investigation. Here, the results of the investigation on the effect of Isoflurane on the chicken's ERG are presented.

8.3 Method

A commercial ERG system (Diagnosis LLC) was used to acquire the electrical activity of the retina to a visual stimulation under the influence of Isoflurane. The protocol and parameters of the recordings were described in previous chapters. In short, a custom designed stimulator connected to the ERG system was used to project a Maxwellian view green flash on the retina. The area of the stimulation spot was about 3.14 mm^2 and the intensity of the green flash was set to 218 $Cd/cm^2/sec$. The time resolution of the REG system was 1 ms. Three 2 weeks old White Leghorn (*Gallus domesticus*) chickens were used in this experiment. Chickens were dark adapted for two hours prior to the experiments and then anaesthetized with 3% Isoflurane gas mixed with oxygen. Animals were

put on the custom designed animal holder to keep them immobile during the experiments and to let easily adjust them according to the stimulator. A silver wire loop electrode (d = 6 mm) was used as the eye electrode on the surface of the cornea and two other electrodes were connected to the skull of the animal as ground and reference electrodes. To restrict the motion of the outer eyelid, a lid retractor was used and eye drops (Refresh tear drops) were administered frequently to hydrate the cornea. After 5 minutes of the beginning of the anesthesia, the anesthesia level was decreased to 2% and kept at this level until the end of the experiment. The recordings were conducted in Biomedical Imaging Lab at the University of Waterloo, with approval from the University of Waterloo animal ethics committee.

In about 10 minutes after the beginning of the anesthesia, the ERG recordings were started. For every chicken, after every 10 minutes until 40 minutes after the beginning of the anesthesia, three consequently ERG recordings were done. Therefore, nine recordings were acquired for each time point from three chickens. The data for each time point were averaged and statistical analysis was conducted between pairs of time points to find any significant change caused by anesthesia. Four ERG components were chosen for analysis. Figure 8.1 presents a typical ERG recording which shows the ERG components used for statistical analysis.

For the statistical analysis of the amplitude and latency of the a-wave, the first oscillatory potential peak, and the second oscillatory potential peak, a one way repeated measure ANOVA was used to test the preference difference among four time points (10 min, 20 min, 30 min and 40 min - $p < 0.05$). Holm-Bonferroni post-hoc test was used for pair comparison. The p values were corrected according to the Holm-Bonferroni correction criteria based on the number of pairs (6).

The a-wave in ERG recordings is related to the activity of the photoreceptors as a result of visible light stimulus [12]. The b-wave is related to the activity of the ON bipolar and Muller cells [12]. Oscillatory potentials are related to the negative feedback between amacrine, ganglion, and bipolar cells [12].

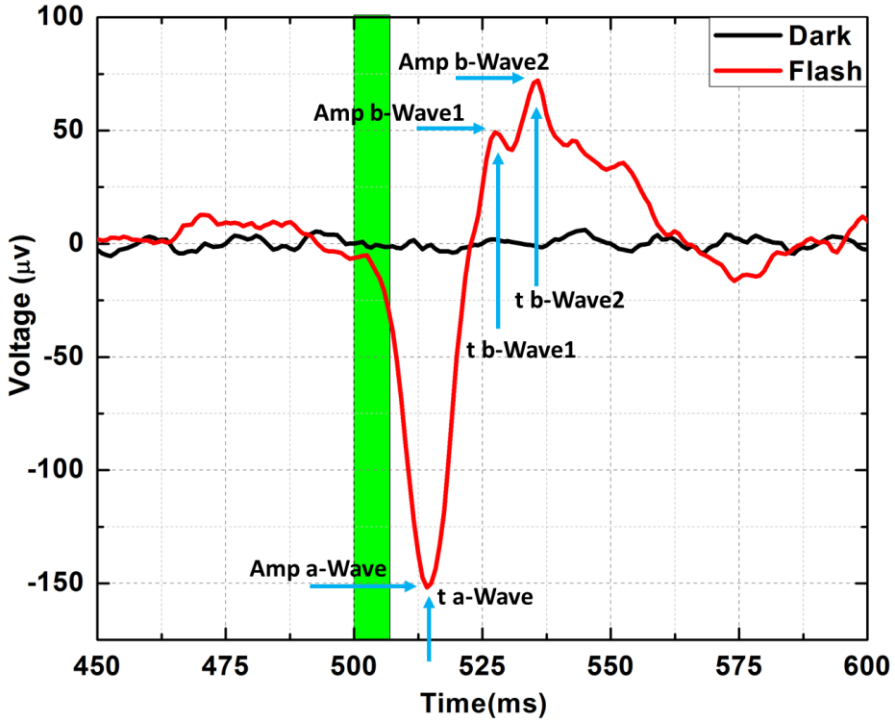

Figure 8.1: A representative ERG recording. The black line shows the un-stimulated recording, while red line shows a typical ERG recording as a result of a 7 ms green flash. Blue arrows show the ERG components which have been used for statistical analysis.

8.4 Results and Discussion

Figure 8.2 shows the average and standard error of mean (Mean±SEM) of the ERG recordings of all three chickens averaged for every time point, i.e., 10 , 20, 30, and 40 minutes after the anesthesia. The green line in the middle of the graph shows the timing and the duration of the flash. Stimulating the chicken retina with the local strong green flash resulted in an a-wave, b-wave, and oscillatory potentials in these experiments. From Fig. 8.2, it is clear that the Isoflurane has influenced the a-wave and first and second oscillatory potentials in b-wave. Figure 8.3 represents the mean, vertical and horizontal error bars (Mean±SD) of the amplitudes and latency of the three points of interest introduced in Fig.8.1, showing the variability of the measured signals in different recordings and from different chickens. The green bar on the left shows the timing and duration of the flash. Figure 8.3, shows the reduction and prolongation of the amplitudes and latencies of the a-wave and b-wave respectively.

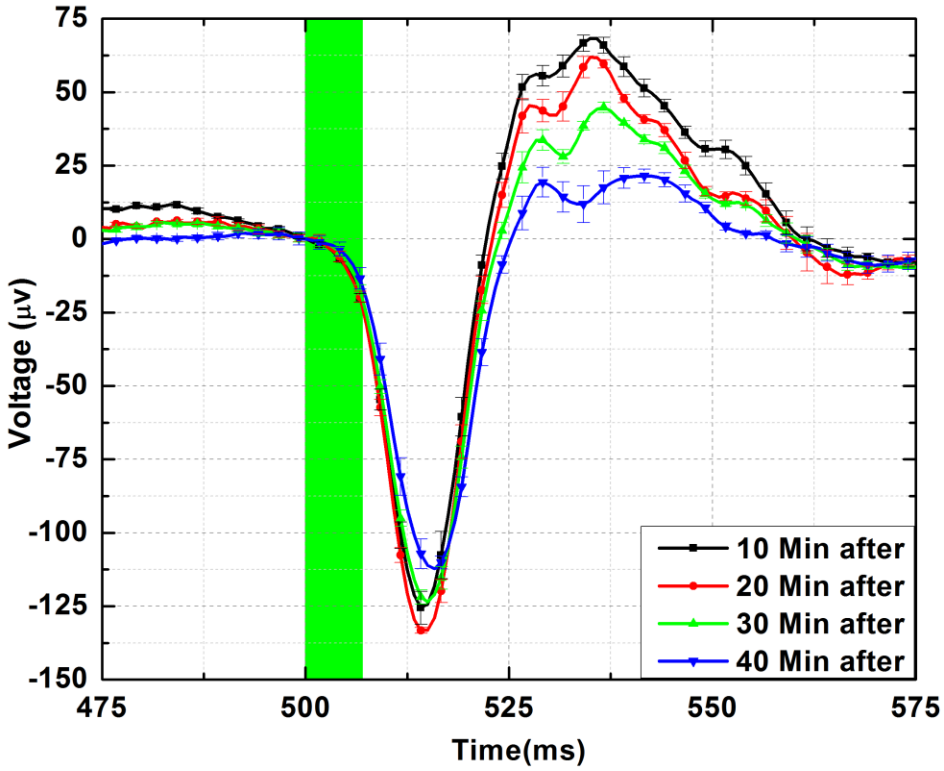

Fig.8.2: Average and SEM (Mean±SEM) of all three chickens for each time point.

A one way repeated measure ANOVA was used for statistical analysis of latency and amplitudes of a-wave, first, and second oscillatory potential peaks. For latency of the a-wave, Mauchly's test indicated that the assumption of sphericity has been violated, χ^2 (5) =15.28, p = 0.009. Greenhouse-Geisser estimate of sphericity (ε = 0.65) was used to correct the degree of freedom. The results showed that there was no significant anesthesia effect on the latency of the a-wave, F (1.95, 3.91) =3.53, p =0.13. For amplitude of the a-wave, Mauchly's test indicated that the assumption of sphericity has been violated, χ^2 (5) =24.47, p = 0.00017. Greenhouse-Geisser estimate of sphericity (ε = 0.34) was used to correct the degree of freedom. The results showed that there was no significant anesthesia effect on the amplitude of the a-wave, F (1.02, 2.04) =2.18, p =0.27. For amplitude of the first oscillatory potential, Mauchly's test indicated that the assumption of sphericity has been violated, χ^2 (5) =23.91, p = 0.00022. Greenhouse-Geisser estimate of sphericity (ε = 0.39) was used to correct the degree of freedom. The results showed that there was a significant anesthesia effect on the amplitude of the first oscillatory potential, F (1.17, 2.35) =15.53, p =0.044. Corrected Holm-

Bonferroni post-hoc pair comparison test showed that there was a significant difference between 10 & 40 min ($p = 0.005$), 20 & 40 min ($p = 0.011$), and 10 & 30 min ($p = 0.033$) pair time points. For latency of the first oscillatory potential, Mauchly's test could not be done. Greenhouse-Geisser estimate of sphericity ($\varepsilon = 0.37$) was used to correct the degree of freedom. The results showed that there was no significant anesthesia effect on the latency of the first oscillatory potential, $F(1.12, 2.24) = 1.16$, $p = 0.45$. For amplitude of the second oscillatory potential, Mauchly's test indicated that the assumption of sphericity has been violated, $\chi^2(5) = 22.80$, $p = 0.00036$. Greenhouse-Geisser estimate of sphericity ($\varepsilon = 0.54$) was used to correct the degree of freedom. The results showed that there was a significant anesthesia effect on the amplitude of the second oscillatory potential, $F(1.62, 3.24) = 25.40$, $p = 0.01$. Corrected Holm-Bonferroni post-hoc pair comparison test showed that there was a significant difference between 10 & 40 min ($p = 0.0015$), 20 & 40 min ($p = 0.002$), 10 & 30 min ($p = 0.022$), 20 & 30 min ($p = 0.035$), and 30 & 40 min ($p = 0.026$) pair time points. For latency of the second oscillatory potential, Mauchly's test could not be done. Greenhouse-Geisser estimate of sphericity ($\varepsilon = 0.39$) was used to correct the degree of freedom. The results showed that there was no significant anesthesia effect on the latency of the first oscillatory potential, $F(1.19, 2.4) = 6.92$, $p = 0.1$.

In summary, only the amplitudes of the first and the second oscillatory potentials showed significant change from the beginning of the anesthesia to the end. This result is in agreement with what other research groups have reported [156]–[158], [163]. In most of these studies, reviewed in the introduction, the amplitudes of the first and second oscillatory potentials decreased under the different anesthesia agents. Since the latency and the amplitude of the a-wave did not show a significant change over time under the Isoflurane in this study, it is reasonable to assume that the Isoflurane mainly affects the inner retina in the chicken. More experiments are needed to confirm the observed effect.

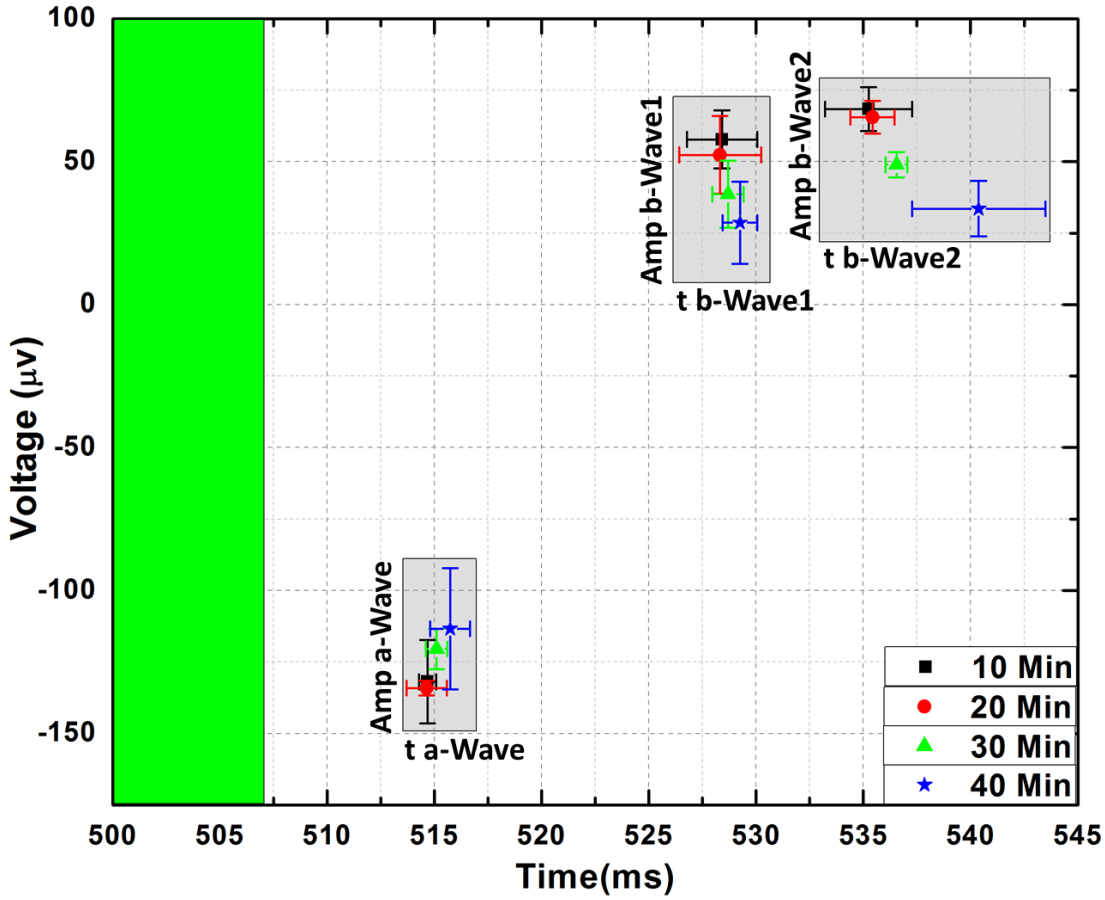

Figure 8.3: The Mean±SD of the amplitude and latencies of the a-wave, first and second oscillatory potentials.

Based on the influence of the Isoflurane on the normal neuronal activity of the retina from ERG and pupil dynamic experiments, it is reasonable to assume that Isoflurane could also affect the IOSs acquired from the chicken retina. However, since the experiments for acquiring IOSs from the chicken retina were not initially designed to monitor the effect of the anesthesia on IOSs over time (variation in Isoflurane amount based on the chicken response and different intervals between consecutive recordings), statistical analysis could not be performed and no conclusion can be made at this point. A properly designed experiment needs to be performed to investigate the possible effect of the anesthesia on the IOSs.

8.5 Conclusion

Here the effects of Isoflurane as an inhalation anesthesia gas on chicken's neuronal activity in the retina have been presented. Statistical analysis of the data showed a significant decrease in the amplitudes of the first and second oscillatory potentials over time as a result of anesthesia. It was hypothesized that the anesthesia mainly affected the inner retinal function.

Chapter 9
Summary and Discussion

9.1 Summary and Discussion

The main goal of this project was to image the IOSs from the visible light activated chicken retina with a combined OCT and ERG system. As discussed in the previous chapters, the IOSs recorded from the inner retina showed an initial increase followed by a decrease in the backreflected imaging light intensity within the first 100 ms after the onset of the stimulation. At later time-points, the effect of the pupil constriction dominates the observed signal. The effect of the visible light stimuli on the outer retina was different. A pattern similar to the one measured from inner retina was recorded from the IS of the photoreceptors. However, there was no initial increase in the intensity of backreflected light from the OS and only a decrease in the intensity of the backreflected light was observed. The total time interval during which the positive and negative peaks in IOS occurred matched with the time period during which a- and b-waves of the ERG recordings develop. Considering the time resolution of these IOSs measurements with OCT (7 ms), the timing of the negative and positive peaks of different retinal layers was about the same. The measured IOSs were reproducible within a single animal and across animals.

As discussed in chapter 7, since no drugs were available that can induce pupil dilation in chicken without significantly altering the measured IOS, stimulation of the chicken retina with visible light caused pupil constriction. The latency of the maximum pupil constriction was measured to be about 150 ms from the onset of the green color stimulus. Comparison between the timing of the IOSs and pupil constriction revealed that the measured IOSs from the chicken retina were modulated by the pupil constriction. Within the first 150 ms after the flash, the effect of the pupil constriction on the measured IOSs would depend on the location of the imaging beam compared to the edges of the pupil (possible vignetting effect) and could have a minimal effect on the observed IOSs (within the initial 50ms – 100 ms after the flash onset). In general, the pupil constriction changes the magnitude of the IOSs by decreasing the intensity of the backreflected imaging beam, which could add undesired variability to the measured IOSs.

Preliminary results from pupil constriction and ERG measurements (chapter 7 and 8 respectively) suggested that anesthesia has an effect on the magnitude of the pupil constriction and consequently on the magnitude of some of the ERG peaks. Due to the insufficient data for analysis, there were no conclusive results about the effect of the anesthesia on the IOSs (chapter 8). However, based on its effect on the ERG recordings and the pupil constriction, it can be hypothesized that anesthesia could also affect the IOS recording and add some unknown variability factor to the measured IOSs. Further investigation is required to shed light on this matter.

Another factor that contributes to the variability of the measured IOSs is the involuntary eye motion while the animal is under anesthesia. The eye movements in chicken can occur due to different factors, such as eye muscles relaxing and engaging through anesthesia, and affect the measurement results. As mentioned in chapter 5, the effect of the involuntary eye movements was removed as much as possible by post processing of the data. However, since the OCT system used for the experiments summarized here was not designed to provide an *en face* view of the retina, it was not possible to register any lateral eye movement that could potentially affect the measured IOSs.

Results from a number of studies reviewed in chapter 3, suggest that the IOSs from cones and rods are different [7], [9], [50], [96]. Furthermore, they show that the IOSs from different locations of the retina are different in polarity, timing and magnitude [26], [27]. Since the imaged area of the chicken retina in this project was very small (600 μm^2) and the measured IOSs were calculated by averaging the responses of all photoreceptors in the imaged area (maximum 8 cones and a few rods depending on the location), any lateral eye movement could have added variability between different imaging sets in chickens (Fig. 5.3 and 5.4). The combination of the effect of the pupil constriction, anesthesia, and eye movement are most likely the major reasons for the observed variability in the measured IOSs from the chicken retina. This combined effect made it difficult to isolate and eliminate the pupil constriction effect using a post processing method.

Comparison between the results of this project and the results obtained by other research groups reviewed in chapter 3, despite the use of different imaging methods, protocols and subjects, showed similar findings. Photoreceptor OS has been the focus of most of the studies on measuring the IOSs from the visible light activated retina. In many of these studies [9], [11], [26], [49], [80], [83], similar to what was found in this thesis, the polarity of the OS of the photoreceptor layer was negative.

Although, there were investigations that showed a positive polarity for the OS of photoreceptor [7], [8], [10], [50], [56], [96]. The measured IOSs in these studies were the average of the signal over the scanned area. As mentioned before, it seems that the polarity of the IOSs depends on the type of photoreceptor (rod vs. cone) and the location of the imaging (the ratio between cones and rods at that location). Therefore, depending on the location, the average would be a mixture of the signals from cones and rods which could result in positive, negative, oscillating or non-changing polarity.

Yao et. al. [89]–[91] showed both positive (increase) and negative (decrease) polarities in IOSs from photoreceptor layer at the stimulated area. Rha et. al. [83] also showed similar patterns in the polarity of the photoreceptors. Thus, it is reasonable to assume that besides taking the spatial average of the signal over the stimulated area, the 2D (en face) pattern of the signal over the entire layer should be considered. For instance, Ts'o et. al. [84], Tsunoda et. al. [26], and Yao et. al. [89]–[91] showed 2D patterns of the IOSs of visible light stimulated photoreceptor layer, which showed interesting positive/negative patterns on the surface of the photoreceptor layer. Despite the very small (600 μm2) scanned area in this study, such 2D spatio-temporal IOSs from different retinal layers were presented in Fig.6.5 and clearly showed the presence of both positive and negative polarities in individual layers. For better visualization and analysis of these patterns, a larger scanned area, higher lateral resolution (AO-OCT) and motion artifact correction are necessary.

According to the literature [7], [10], [11], [26], [80], [83], [84], [89], [91], the origins of the fast IOS recorded from the photoreceptor layer are the physiological processes accompanying the phototransduction. Ion shift, cell swelling/de-swelling, water efflux/influx, and any processes that result in the refractive index change in the photoreceptors were mentioned as possible mechanisms leading to change in the intensity of the backreflected imaging beam from the photoreceptor layer. The timing of the maximum peak of the IOS of the photoreceptor layer in this project (chapter 6) and reported by other research groups [10], [11] did not coincide with the timing of the a-wave's peak in the ERG measurements. However, it was close to the timing of the b-wave peak. These findings suggest that either the time resolution of IOSs measurements was not sufficient to capture the optical equivalent of the a-wave, or the optical methods measured the after effects of electrical signal propagation through the photoreceptors.

There are only a few studies that reported IOSs acquired from the inner retinal layers. Yao et. al. [11], [49], [59] showed increase (positive IOSs) in the intensity of the backreflected imaging beam from the inner retina as a result of the visible light stimulation. The timing of the peak of this positive IOS was about the same as the observed negative IOS from photoreceptors. Bizheva et. al. also reported a slow positive IOS from IPL. However, Theelen et. al. [169] showed a negative IOS for the inner retina. The IOSs recorded from different inner retinal layers in this project showed almost (considering the 7 ms time resolution between two data points) a simultaneous increase followed by a decrease in the intensity of the backreflected light within the initial 100 ms after the onset of the flash.

It has been suggested that the origin of the stimulus-induced reflectivity changes in the inner retina maybe caused by changes in the refractive index of the activated neuronal tissue and swelling/de-swelling in the Muller cells as a result of ongoing physiological processes in the activated inner retina [10], [60], [169]. Since there was no time delay between major peaks of the IOSs recorded from different retinal layers (Fig. 6.3), it seems that the recorded IOSs do not correspond directly to electrical activity of the stimulated neurons. If the synchronicity of the observed IOSs measured from the inner retina was not due to insufficient temporal resolution of the imaging system, it is possible that the IOSs represent the after effect of the electrical signal propagating from outer retinal to the inner retina.

Muller cells extend from the surface of the retina to the IS of the photoreceptors and there are about the same number of Muller cells in the retina as cones [170]. These Muller cells are very crucial to the normal function of the retina. Water efflux and influx, different ion species transportation (e.g. K and Na channels), and metabolism of different biochemical molecules (e.g. Glutamate removal and Dopamine/Serotonin uptake) during different neuronal cell activities are some of the examples of Muller cells' role in the retina [170]. Based on the Muller cells' length and density in the retina and the synchronicity between IOSs acquired from different retinal layers, it is reasonable to hypothesize that, Muller cells might have a major role in the observed simultaneous IOSs across the entire inner retina. More studies are needed to confirm this hypothesis.

Since only the fast IOSs have been considered in this project due to the pupil constriction effect, the findings from other studies on the slow IOSs could not directly be compared with this project's findings.

This thesis continued the footsteps of different research groups who tried to image the IOSs from the visible light activated retina. A combined UHROCT and ERG system was developed and repeatable results were recorded from the chicken retina for the first time. Avascularity and cone dominance of the chicken retina were the two major advantages of using this animal model and allowed for getting reproducible recordings from the complex physiological activity in the stimulated retina. This project was the starting point to test the capacity of the UHR-OCT system in imaging the fast IOSs from the cone dominated chicken retina. To follow this work to the next step, there are many directions. Understanding the dynamics of the IOSs originated from different retinal layers, different regions of the retina and the response to different visual stimuli can potentially help in isolating a clearer signal from the background noise. In doing so, a faster OCT system with higher lateral resolution (AO-OCT) is needed. As mentioned before, scanning larger area in the retina would help to understand better the dynamic of the IOSs and the pattern of different polarities in each individual retinal layer. A capable alignment algorithm for large b-scan alignment is also necessary in this next step. Specifically designed image processing codes could be used to reduce the noise and improve the image quality. Controlling the pupil constriction by using suitable drugs or eliminating its effect by post processing would help in investigating the slow IOSs. Furthermore, using different wavelengths of the light (from UV to red) with different intensities and durations for stimulation in dark or light adapted conditions, using different retina cell inhibitors, and using diseased models would potentially improve our understanding about the origins of the IOSs and their possible underlying physiological processes in the chicken retina. Understanding the origins of IOS in this cone dominated animal model could help to develop better imaging systems and protocols for imaging the IOSs from the human retina.

Appendix A

A combined optical coherence tomography and electroretinography system for *in-vivo*, simultaneous morphological and functional imaging of the rodent retina

A.1 Overview

A combined ultrahigh resolution optical coherence tomography (UHROCT) and an electroretinography (ERG) system is presented, for simultaneous imaging of the retinal structure and physiological response to light stimulation in the rodent eye. The 1060nm UHROCT system provides ~3µm x 5µm (axial x lateral) resolution in the rat retina and time resolution of 22µs. A custom designed light stimulator, integrated into the UHROCT imaging probe provides light stimuli with user-selected color, duration and intensity. The performance of the combined system is demonstrated *in-vivo* in healthy rats, and in a rat model of drug-induced outer retinal degeneration. Experimental results show changes in both structure and function in the healthy and degenerated retina.

A.2 Introduction

Neurodegenerative retinal diseases, such as age related macular degeneration (AMD), diabetic retinopathy, and glaucoma cause both morphological and physiological changes in the retina at different stages of their development. The dynamic relationship between structural and functional abnormalities in diseased retinas is still not well understood. Rodent (normal and transgenic mice, and rat) models of retinal diseases are well established research tools for studying the origins and stages of progression of retinal diseases [171], [172]. Technologies such as confocal scanning laser ophthalmoscopy (CSLO) and OCT that are either commercially available [173], [174] or research-grade [113], [175] are currently used for *in-vivo* morphological imaging of the rodent retina. Full field ERG recordings [176] are used for *in-vivo* assessment of impaired physiological response of the

retina to light stimulation in rodents. When multiple measurement modalities are applied sequentially to the same animal in a longitudinal study of a retinal disease, direct correlation between the changes in retinal structure and physiological response in terms of their spatial location and time evolution is very challenging. Furthermore, sequential measurements increase the overall measurement time and require relocation and repositioning of the animal, which can interfere with the anesthesia.

A.3 Method

Here we present, to our knowledge, the first combined UHROCT+ERG system, designed for simultaneous probing of retina structure and function in the rodent eye. The results presented here demonstrate the potential of the combined system to enable improved understanding of the dynamic relationship between structure, physiology and metabolism of healthy and diseased rodent retinas.

A schematic of the combined imaging system is presented in Fig.A1A. The UHROCT system is based on a fiberoptic Michelson interferometer, connected to a superluminescent diode, SLD (Superlum Ltd., λ_c = 1020 nm, $\Delta\lambda$ = 108nm). A system operating in the 1060nm spectral region is chosen, to insure that the imaging beam will not stimulate visually the retinal photoreceptors. Details about the UHROCT system core design and performance have been published previously [112], [113]. With 2.5mm imaging beam incident on the cornea, the resolution in the rat retina is 3µm x 5µm (axial x lateral). The UHROCT system sensitivity is 99dB for 1.3mW power at the rat cornea. The interference signal is detected with an InGaAs linear array CCD camera (SUI, Goodrich) with 47 kHz readout rate. The maximum permissible exposure intensity of the incident imaging beam at the cornea for the wavelength region used here is about 2 mw for 10 s continues exposure for human [113]. The higher numerical aperture of the rat eye results in a smaller imaging spot size on the retina and a higher energy density which suggests the need for more conservative measures. However, the high imaging speed (21 µs/A-scan) limits the tissue exposure to about 5 s for a total 2.25 mm^2 (1000 A-scans x 256 B-scans) on the retina.

A light stimulator designed in the shape of a ring (Fig.1B), containing 12 LEDs (red, blue and green) and covered with a diffuser is used to provide uniform, full field illumination of the rat retina. A 12mm center hole in the ring provides a clear path of the imaging beam. The stimulator is mounted co-axially to the distal end of the UHROCT imaging probe (a pair of lenses, Edmund Optics, d =

25mm, f = 35mm), to ensure full overlap between the illuminated and imaged areas in the rat retina. A commercial ERG system (Diagnosys LLC) is combined with the UHROCT system and both the

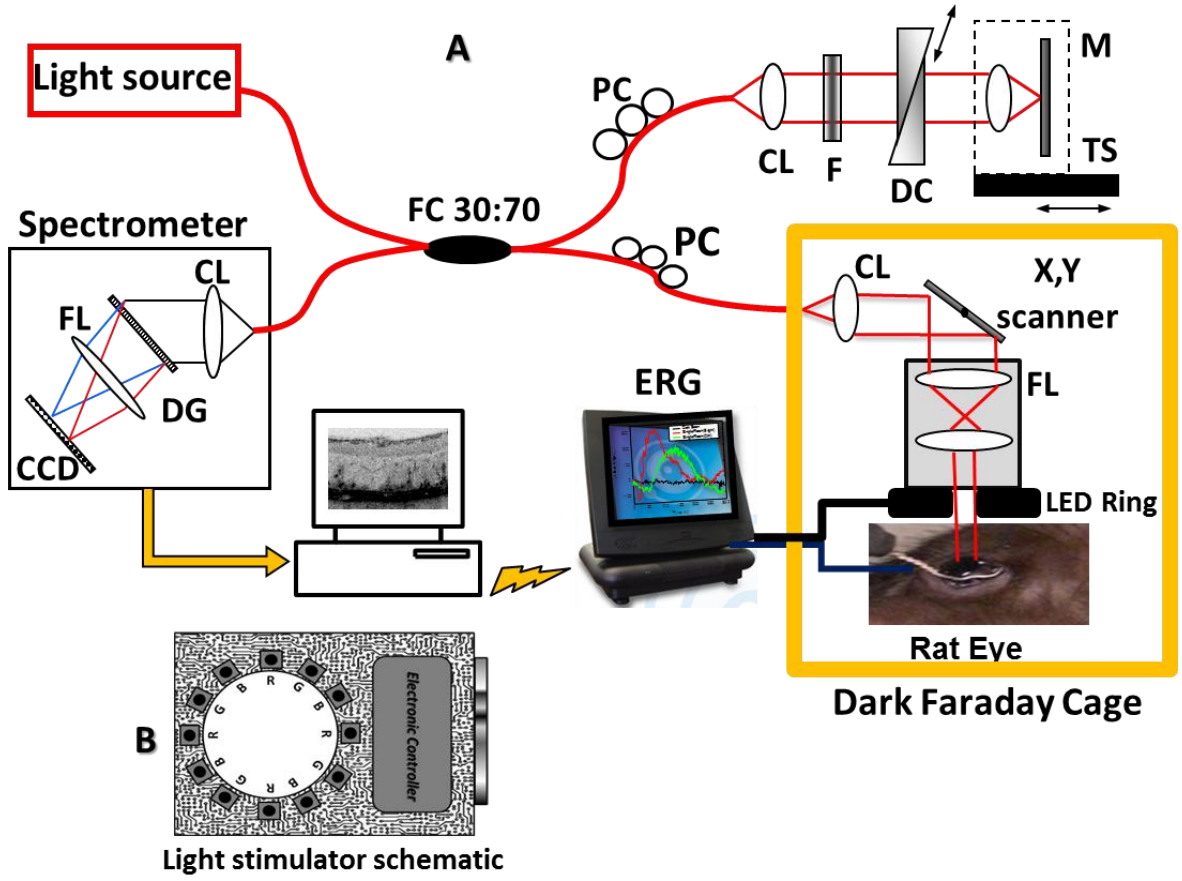

Fig.A1: (A) Schematic of the combined UHROCT and ERG system: (CL) - collimating lenses, (DC) - dispersion compensation unit, (NDF) - neutral-density filters, (FOI) - fiberoptic isolator, (M) – mirror, (PC) - polarization controllers, (SLD) – superluminescent diode and (TS) - translation stage. The spectrometer consists of a collimating lens (CL), a volumetric diffraction grating (DG), a focusing lens (FL) and a high speed InGaAs camera. (B) Schematic of the light stimulator, consisting of 12 single color LEDs (B – blue, G – green and R – red). Taken from [177] with permission.

light stimulus onset and the acquisition of the optical and electrical data are synchronized. A solid, grounded Faraday cage provides dark environment for the optical and ERG recordings and reduction of the ambient electromagnetic noise. A custom animal holder is used for permit precise alignment of the imaging beam with respect to the rodent eye.

Healthy female Long Evans rats (~8 weeks old) were used in this study, which was approved by the Animal Research Ethics review board of the University of Waterloo. The animals were anaesthetized

with intra-peritoneal injections of Ketamine (75mg/kg) and Xylazine (10mg/kg) and dark adapted for 12 hours prior to the experiments. Pupil dilation was achieved by use of 1-2 drops of Tropicamide (1% Mydriacyl) per eye. An ERG electrode in the shape of a loop (d = 6mm) was placed gently on the rat's cornea, while ground and reference electrodes were inserted in the animal's mouth and behind the ear respectively. Subsequently the rats were placed on the holder inside the dark Faraday cage. During the imaging procedure the rat corneas were hydrated by frequent administration of artificial tear drops. Outer retinal degeneration was induced by intravenous injection of $NaIO_3$ (40mg/mL), administered on Day 0 (baseline).

Three-dimensional UHROCT tomograms (1000 A-scans x 256 B-scans x 512 pixels) were acquired from the rat retina on days 0 (baseline), 3 and 7 of the study. These were followed by 2D images acquired synchronously with a single white light flash (0.9 log cds/m^2 intensity and 4ms duration) and simultaneous ERG recordings. Fixed gain of 100 was applied to the ERG data. Multiple recordings were acquired from the same eye with ~1 minute pause in between to allow for recover of the retina. The UHROCT tomograms were processed with Matlab and Amira.

A.4 Results and Discussion

UHROCT and ERG recordings were acquired simultaneously from healthy (Day 0) and damaged (Days 3 and 7 post $NaIO_3$ injection) rat retinas, and representative results from this study are summarized in Fig.A2. A cross-sectional image of a healthy rat retina acquired away from the optic disc (Fig.A2A) demonstrates the ability of the UHROCT system to visualize clearly all retinal layers and small capillaries (red arrow) in the inner and outer plexiform layers. Note that photoreceptor layer consist of 2 pairs of light and dark bands corresponding to the photoreceptor inner (IS) and outer (OS) segments respectively. Figure A2B shows the healthy retina structure in 3D (~1.5mm x 1.5mm area), while Fig. A2C shows a cross-section of the A3D image stack at a plane corresponding to the photoreceptor IS/OS junction. Figure A2C shows an en-face image of the IS/OS photoreceptor junction. Figure A2D shows a representative ERG trace acquired from the healthy rat retina (Day 0). The red line marks the timing and duration of the light flash. Figure A2E shows a representative two-dimensional tomogram of the rat retina 3 days after injection of $NaIO_3$. The tomogram shows loss of the external limiting membrane (ELM), disruption of the multilayered structure of the photoreceptor

IS and OS, which were both clearly visible on Day0 of the study, and highly reflective spots in the photoreceptor layer (yellow arrow).

Note that the inner retinal layers appear not to be affected by the $NaIO_3$. The morphological changes corresponding to partial degeneration of the outer retina are better observed in three dimensions, which show modulations at the photoreceptor layer (Fig. A2F) as well as bright and dark spots at the plane corresponding to the photoreceptor IS/OS junction (Fig. A2G). Although the UHROCT tomograms clearly show changes in the structural integrity of the outer rat retina, the ERG traces acquired on Day 3 show distinct a- and b-waves (Fig. A2H), indicating that at least some of the photoreceptors and bipolar cells are still functioning.

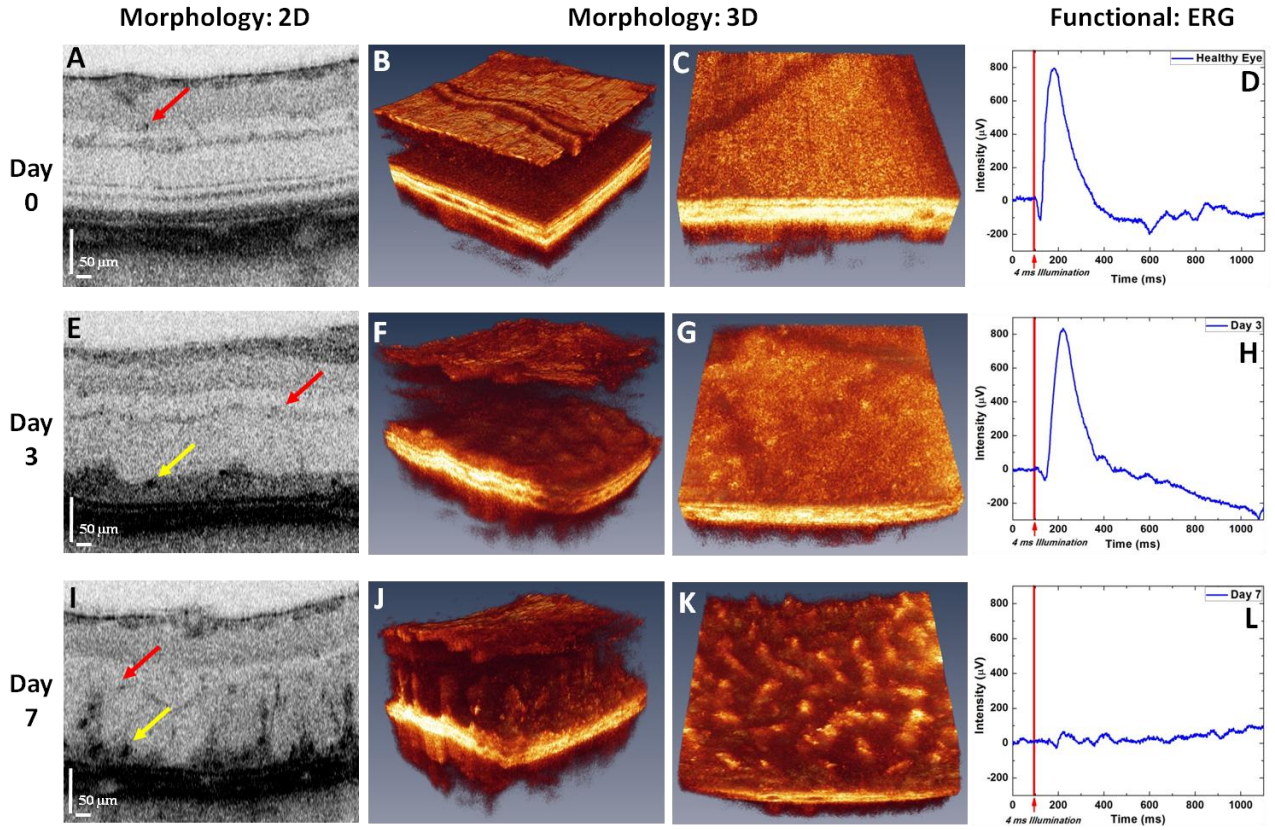

Figure A2: Summary of the UHROCT morphological and the ERG physiological data. Representative two-dimensional cross-sectional (A, E and I), three-dimensional (B, F and J) and two-dimensional en-face (C, G and K) images of ~1.5mm x 1.5mm area of the rat retina acquired on days 0, 3 and 7 of the study. Red arrows indicate capillaries in the inner- and outer plexiform layers, while the highly reflective cellular debris in the photoreceptor layer are indicated with yellow arrows. Representative ERG traces acquired on days 0 (D), 3 (H) and 7 (L) of the study. The red line indicates the timing of the light flash. Taken from [177] with permission.

Figure A2I shows a representative 2D tomogram of the rat retina 7 days after injection of $NaIO_3$. The tomogram shows almost complete loss of the photoreceptor layer, highly reflective spots (yellow arrow), as well as disruption in the structural integrity of the outer nuclear (ONL) and inner plexiform (IPL) layers. The morphological changes are better observed in three dimensions in Fig. A2J which shows columns of highly reflective material in the ONL and photoreceptor layers. These structural changes appear as bright and dark spots at the photoreceptor IS/OS junction (Fig. A2K). The corresponding ERG trace shows complete loss of the a- and b-waves (Fig. A2L), indicating that the rat retina is no longer responsive to light stimulation.

Results from Day 0 of the study show correspondence between the structural integrity and the light induced physiological response of the healthy rat retina. The magnitude and timing of the a- and b-waves in the ERG recording (Fig. A2D) are typical and similar to previously published results [178], [179]. The 2D and 3D UHROCT tomograms show fine morphological details of the rat retina similar to previously published results both at 1060nm [113] and 800nm [180]. Results from Day 3 of the study show loss of the ELM and the layered structure of the photoreceptors – the pairs of bright and dark bands, corresponding to the IS and OS are no longer visible. This suggests that the IS and OS of most of the photoreceptor cells have been disrupted on sub-cellular level. The highly reflective spots observed in the photoreceptor layer (Fig.A2E, yellow arrow) are potentially disrupted RPE or inflammatory cells. Similar changes were observed in H&E histological cross-sections in previously published studies [178], [179] of $NaIO_3$ induced outer retinal degeneration in the rat retina. The ERG recordings at Day 3 of the study show a- and b-waves, however the decreased peak magnitude, as well as the latency of the a- and b-wave peaks as compared to Day0 suggests damage to the remaining photoreceptor population. The UHROCT tomograms from Day 7 of the study show complete disintegration of the photoreceptor layer, gaps in the RPE, larger clusters of highly reflective material that extend to the inner retinal layers, as well as disruption of the structural integrity of the ONL and IPL. These observations are comparable well with H&E histological findings published previously [179]. The ERG recordings show no electrical activity in the retina, suggesting complete loss of photoreceptor functionality, which corresponds with the structural changes presented in this paper, as well as with previously published ERG studies [178], [179].

A.5 Conclusion

To the best of our knowledge, the first combined UHROCT and ERG system has been developed and designed for simultaneous probing of the rodent retina structure and functional response to light stimulation. Results obtained with the combined system *in-vivo* from healthy and degenerated rat retinas show correspondence between the structural integrity and the normal / abnormal light induced physiological response of the retina.

Appendix B

Copyright Permissions

B.1 Co-authors' Contributions and copyright permissions for chapter 4:

Chapter 4 is based on the following published paper:

Alireza Akhlagh Moayed, Sepideh Hariri, Eun Sun Song, Vivian Choh, and Kostadinka Bizheva. "In Vivo Volumetric Imaging of Chicken Retina with Ultrahigh-resolution Spectral Domain Optical Coherence Tomography." Biomedical Optics Express 2, no. 5 (2011): 1268–1274. [118]

Alireza Akhlagh Moayed: Planning the experiments, helping with building Zemax model, chicken handling and imaging, data processing, making 3D tomograms, writing and revising the manuscript.

Sepideh Hariri: Assisting with imaging and data processing, manuscript revision.

Eun Sun Song: Assisting with data processing, manuscript proofread.

Vivian Choh: Supervising chicken imaging, performing histology, giving advice about chicken retina structure, manuscript revision.

Kostadinka Bizheva: Supervising the experiments, designing and building the OCT system, manuscript revision.

B.1.1 Copyright permission from publisher:

From: pubscopyright <copyright@osa.org>

To: Alireza Akhlagh Moayed <aakhlagh@uwaterloo.ca>

Date: Wed, 15 Aug 2012 18:08:36

Subject: RE: Permission to use my paper as a part of my PhD thesis

Dear Alireza,

Thank you for contacting The Optical Society. This email is in response to both of your emailed permissions requests:

Moayed, A.A., Hariri, S., Song, E.S., Choh, V., Bizheva, K., 2011. In vivo volumetric imaging of chicken retina with ultrahigh-resolution spectral domain optical coherence tomography. Biomed Opt Express 2, 1268-1274.

Because you are the author of the source papers from which you wish to reproduce material, OSA considers your requested use of its copyrighted materials to be permissible within the author rights granted in the Copyright Transfer Agreement submitted by the requester on acceptance for publication of his/her manuscript. It is requested that a complete citation of the original material be included in any publication. This permission assumes that the material was not reproduced from another source when published in the original publication.

Please let me know if you have any questions.

Best,

Hannah

Hannah Bembia

August 15, 2012

Authorized Agent, The Optical Society

B.1.2 Copyright permission from co-authors:

On Tue, Oct 9, 2012 at 2:19 PM, Alireza Akhlagh Moayed <aakhlagh@uwaterloo.ca> wrote:

Hi

I would like to ask your permission for using the material of the following publication ,in which you are one of the co-authors, in my PhD thesis:

Moayed, A.A., Hariri, S., Song, E.S., Choh, V., Bizheva, K., 2011. In vivo volumetric imaging of chicken retina with ultrahigh-resolution spectral domain optical coherence tomography. Biomed Opt Express 2, 1268-1274.

I sincerely appreciate your kind attention to this matter.

Best regards

Alireza A.Moayed

PhD Candidate

Department of Physics and Astronomy

University of Waterloo

200 University Ave West
Waterloo, Ontario Canada N2L 3G1
(519) 888 4567 ext. 35665
aakhlagh@uwaterloo.ca

Date: Tue, 9 Oct 2012 14:30:09 -0400 [10/09/12 14:30:09 EDT]
From: Sepideh Hariri <sepidhariri@gmail.com>
To: Alireza Akhlagh Moayed <aakhlagh@uwaterloo.ca>
Subject: Re: Permission for reproduction of paper material
Permission granted.
Best regards
Sepideh Hariri
PhD Candidate
Department of Physics and Astronomy
University of Waterloo
200 University Ave West
Waterloo, Ontario Canada N2L 3G1
(519) 888 4567 ext. 35665
shariri@sciborg.uwaterloo.ca

Date: Tue, 9 Oct 2012 23:10:28 -0400 [10/09/12 23:10:28 EDT]
From: Vivian Choh <vchoh@uwaterloo.ca>
To: Alireza Akhlagh Moayed <aakhlagh@uwaterloo.ca>
Subject: Re: Permission for reproduction of paper material
You have my permission.
Vivian Choh
Associate Professor
Room 260, School of Optometry
University of Waterloo

Tel: 1 (519) 888-4567 x35005

Email: vchoh@uwaterloo.ca

From: Dida <kbizheva@uwaterloo.ca>

To: Alireza Akhlagh Moayed <aakhlagh@uwaterloo.ca>

Date: Tue, 9 Oct 2012 17:04:14 -0400

Subject: Re: Permission for reproduction of paper material

You have my permission to reprint materials from all papers where I am listed as co-author.

Dr. Kostadinka Bizheva

Associate Professor

Department of Physics and Astronomy

University of Waterloo

200 University Ave West

Waterloo, ON N2L 3G1

Canada

Phone: (519) 888 4567 x 37517 (office), x35665 (old lab), x31133 (new lab)

Cell Phone: 519 572 1774

E-mail: kbizheva@uwaterloo.ca

Following co-author did not replied to my email: Eun Sun Song

B.2 Co-authors' Contributions and copyright permissions foe chapter 5:

Chapter 5 is based on the following published paper:

Moayed, A.A., Hariri, S., Choh, V., Bizheva, K., 2011. In vivo imaging of intrinsic optical signals in chicken retina with functional optical coherence tomography. Opt.Lett. 36, 4575. [126]

Alireza Akhlagh Moayed: Planning the experiments, designing the imaging probe, acquiring the images and ERG recordings from chicken, data processing, writing and revising the manuscript.

Sepideh Hariri: Assisting in imaging, manuscript revisions.

Vivian Choh: Giving advice about chicken retina structure, manuscript revisions.

Kostadinka Bizheva: Supervising the experiments, designing and building the OCT system, manuscript revisions.

B.2.1Copyright permission from publisher:

From: pubscopyright copyright@osa.org

To: Alireza Akhlagh Moayed aakhlagh@uwaterloo.ca

Date: Wed, 15 Aug 2012 18:08:36 +0000

Subject: RE: Permission to use my paper as a part of my PhD thesis

Dear Alireza,

Thank you for contacting The Optical Society. This email is in response to both of your emailed permissions requests:

Moayed, A.A., Hariri, S., Choh, V., Bizheva, K., 2011. In vivo imaging of intrinsic optical signals in chicken retina with functional optical coherence tomography. Opt.Lett. 36, 4575.

Because you are the author of the source papers from which you wish to reproduce material, OSA considers your requested use of its copyrighted materials to be permissible within the author rights granted in the Copyright Transfer Agreement submitted by the requester on acceptance for publication of his/her manuscript. It is requested that a complete citation of the original material be included in any publication. This permission assumes that the material was not reproduced from another source when published in the original publication.

Please let me know if you have any questions.

Best,

Hannah

Hannah Bembia

August 15, 2012

Authorized Agent, The Optical Society

B.2.2 Copyright permission from co-authors:

Hi

I would like to ask your permission for using the material of the following publication, in which you are one of the co-authors, in my PhD thesis:

Moayed, A.A., Hariri, S., Choh, V., Bizheva, K., 2011. In vivo imaging of intrinsic optical signals in chicken retina with functional optical coherence tomography. Opt.Lett. 36, 4575.

I sincerely appreciate your kind attention to this matter.

Best regards

Alireza A.Moayed
PhD Candidate
Department of Physics and Astronomy
University of Waterloo
200 University Ave West
Waterloo, Ontario Canada N2L 3G1
(519) 888 4567 ext. 35665
aakhlagh@uwaterloo.ca

Date: Tue, 9 Oct 2012 14:30:09 -0400 [10/09/12 14:30:09 EDT]
From: Sepideh Hariri <sepidhariri@gmail.com>
To: Alireza Akhlagh Moayed <aakhlagh@uwaterloo.ca>
Subject: Re: Permission for reproduction of paper material

Permission granted.

Best regards

Sepideh Hariri
PhD Candidate
Department of Physics and Astronomy
University of Waterloo
200 University Ave West
Waterloo, Ontario Canada N2L 3G1
(519) 888 4567 ext. 35665
shariri@sciborg.uwaterloo.ca

Date: Tue, 9 Oct 2012 23:10:28 -0400 [10/09/12 23:10:28 EDT]
From: Vivian Choh <vchoh@uwaterloo.ca>
To: Alireza Akhlagh Moayed <aakhlagh@uwaterloo.ca>
Subject: Re: Permission for reproduction of paper material

You have my permission

Vivian Choh
Associate Professor
Room 260, School of Optometry
University of Waterloo
Tel: 1 (519) 888-4567 x35005
Email: vchoh@uwaterloo.ca

From: Dida <kbizheva@uwaterloo.ca>
To: Alireza Akhlagh Moayed <aakhlagh@uwaterloo.ca>
Date: Tue, 9 Oct 2012 17:04:14 -0400
Subject: Re: Permission for reproduction of paper material
Hello Ali,
You have my permission to reprint materials from all papers where I am listed as co-author.
Dr. Kostadinka Bizheva
Associate Professor
Department of Physics and Astronomy
University of Waterloo
200 University Ave West
Waterloo, ON N2L 3G1
Canada
Phone: (519) 888 4567 x 37517 (office), x35665 (old lab), x31133 (new lab)
Cell Phone: 519 572 1774
E-mail: kbizheva@uwaterloo.ca

B.3 Co-authors' Contributions and copyright permissions for chapter 6:

Chapter 6 is based on the following published paper:
Akhlagh Moayed, A., Hariri, S., Choh, V., Bizheva, K., 2012. Correlation of visually evoked intrinsic optical signals and electroretinograms recorded from chicken retina with a combined functional optical coherence tomography and electroretinography system. J. Biomed. Opt. 17, 016011. [131]

Alireza Akhlagh Moayed: Planning the experiments, designing the imaging probe, acquiring the images and ERG recordings from chicken, data processing, writing and revising the manuscript.
Sepideh Hariri: Assisting in imaging, manuscript revisions.
Vivian Choh: Giving advice about chicken retina structure, manuscript revisions.
Kostadinka Bizheva: Supervising the experiments, designing and building the OCT system, manuscript revisions.

B.3.1 Copyright permission from publisher:

From: Alireza Akhlagh Moayed [mailto:aakhlagh@uwaterloo.ca]
Sent: Wednesday, August 15, 2012 10:04 AM
To: authorhelp
Subject: Permission to use my papers as a part of my PhD thesis
Hi,
I am a PhD student at University of Waterloo, Canada. I would like to use my papers as a part of my PhD Thesis.
Could you please let me know how to proceed to acquire an official permission?
My paper information is:
Akhlagh Moayed, A., Hariri, S., Choh, V., Bizheva, K., 2012. Correlation of visually evoked intrinsic optical signals and electroretinograms recorded from chicken retina with a combined functional optical coherence tomography and electroretinography system. J.Biomed.Opt. 17, 016011.
Thank you in advance for your kind attention.
Best regards
Alireza A.Moayed
PhD Candidate
Department of Physics and Astronomy
University of Waterloo
200 University Ave West
Waterloo, Ontario Canada N2L 3G1
(519) 888 4567 ext. 35665

aakhlagh@uwaterloo.ca

From: Scott McNeill scottm@spie.org
To: "aakhlagh@uwaterloo.ca" aakhlagh@uwaterloo.ca
Date: Thu, 23 Aug 2012 14:31:27
Subject: RE: Permission to use my papers as a part of my PhD thesis
Dear Alireza Moayed,

Thank you for seeking permission from SPIE to reprint material from our publications. As an author of the cited works, you retain co-owner rights to the original content therein. Publisher's permission is hereby granted under the following conditions: (1) the material to be used has appeared in our publication without credit or acknowledgment to another source; and (2) you credit the original SPIE publication. Include the authors' names, title of paper, volume title, SPIE volume number, and year of publication in your credit statement.
Sincerely,
Scott McNeill for Eric Pepper,
Director of Publications SPIE
P.O. Box 10, Bellingham WA 98227-0010 USA
360/676-3290 (Pacific Time) eric@spie.org

B.3.2 Copyright permission from co-authors:

Hi
I would like to ask your permission for using the material of the following publication, in which you are one of the co-authors, in my PhD thesis:
Akhlagh Moayed, A., Hariri, S., Choh, V., Bizheva, K., 2012. Correlation of visually evoked intrinsic optical signals and electroretinograms recorded from chicken retina with a combined functional optical coherence tomography and electroretinography system. J.Biomed.Opt. 17, 016011.
I sincerely appreciate your kind attention to this matter.
Best regards
Alireza A.Moayed

PhD Candidate
Department of Physics and Astronomy
University of Waterloo
200 University Ave West
Waterloo, Ontario Canada N2L 3G1
(519) 888 4567 ext. 35665
aakhlagh@uwaterloo.ca
Date: Tue, 9 Oct 2012 14:29:33 -0400 [10/09/12 14:29:33 EDT]
From: Sepideh Hariri <sepidhariri@gmail.com>
To: Alireza Akhlagh Moayed <aakhlagh@uwaterloo.ca>
Subject: Re: Permission for reproduction of paper material
Permission granted.
Best Regards
Sepideh Hariri
PhD Candidate
Department of Physics and Astronomy
University of Waterloo
200 University Ave West
Waterloo, Ontario Canada N2L 3G1
(519) 888 4567 ext. 35665
shariri@sciborg.uwaterloo.ca

Date: Tue, 9 Oct 2012 23:10:28 -0400 [10/09/12 23:10:28 EDT]
From: Vivian Choh <vchoh@uwaterloo.ca>
To: Alireza Akhlagh Moayed <aakhlagh@uwaterloo.ca>
Subject: Re: Permission for reproduction of paper material
You have my permission
Vivian Choh
Associate Professor

Room 260, School of Optometry
University of Waterloo
Tel: 1 (519) 888-4567 x35005
Email: vchoh@uwaterloo.ca

From: Dida <kbizheva@uwaterloo.ca>
To: Alireza Akhlagh Moayed <aakhlagh@uwaterloo.ca>
Date: Tue, 9 Oct 2012 17:04:14 -0400
Subject: Re: Permission for reproduction of paper material
Hello Ali,
You have my permission to reprint materials from all papers where I am listed as co-author.
Dr. Kostadinka Bizheva
Associate Professor
Department of Physics and Astronomy
University of Waterloo
200 University Ave West
Waterloo, ON N2L 3G1
Canada
Phone: (519) 888 4567 x 37517 (office), x35665 (old lab), x31133 (new lab)
Cell Phone: 519 572 1774
E-mail: kbizheva@uwaterloo.ca

B.4 Co-authors' Contributions and copyright permissions for chapter 7:

Chapter 7 is based on the following published paper:
Moayed, A.A., Choh, V., Hariri, S., Liu, C., Wong, A., Bizheva, K., 2012. Stimulus Specific Pupil Dynamics Measured in Birds (Gallus Gallus Domesticus) in vivo with Ultrahigh Resolution Optical Coherence Tomography. IOVS. 10.1167/iovs.12-10291. [140]
Alireza Akhlagh Moayed: Planning the experiments, designing the imaging probe, acquiring the images from chicken, data processing, assisting in development of the pupil diameter measurement Matlab code, writing and revising the manuscript.

Vivian Choh: Giving advice about chicken retina structure, assisting in statistical analysis, manuscript revisions.

Sepideh Hariri: Assisting in imaging, manuscript revisions.

Chenyi Liu: Developing the Matlab code for pupil diameter measurements from pupil images, manuscript revisions.

Alexander Wong: Supervising the development of Matlab code for pupil diameter measurements from pupil images, manuscript revisions

Kostadinka Bizheva: Supervising the experiments, designing and building the OCT system, manuscript revisions.

B.4.1 Copyright permission from publisher:

From: Alireza Akhlagh Moayed

Sent: Tuesday, October 09, 2012 2:01 PM

To: Ilana R. Ostrin

Subject: permission for using paper content in PhD thesis

Hi,

I am a PhD student at University of Waterloo, Canada. I would like to use my paper material as a part of my PhD Thesis.

Could you please let me know how to proceed to acquire an official permission from your journal?

My paper information is:

Moayed, A.A., Choh, V., Hariri, S., Liu, C., Wong, A., Bizheva, K., 2012. Stimulus Specific Pupil Dynamics Measured in Birds (Gallus Gallus Domesticus) in vivo with Ultrahigh Resolution Optical Coherence Tomography. IOVS. 10.1167/iovs.12-10291

Thank you in advance for your kind attention.

Best regards

Alireza A.Moayed

PhD Candidate

Department of Physics and Astronomy

University of Waterloo

200 University Ave West

Waterloo, Ontario Canada N2L 3G1

(519) 888 4567 ext. 35665

aakhlagh@uwaterloo.ca

From: Debbie Chin dchin@arvo.org

To: '"aakhlagh@uwaterloo.ca"' aakhlagh@uwaterloo.ca

Date: Wed, 17 Oct 2012 14:52:00

Subject: RE: permission for using paper content in PhD thesis

Dear Alireza A.Moayed,

Permission is hereby granted to include the following article in your PhD thesis for the University of Waterloo:

Moayed AA, Choh V, Hariri S, Liu C, Wong A, Bizheva K. Stimulus-Specific Pupil Dynamics Measured in Birds (Gallus gallus domesticus) In Vivo with Ultrahigh Resolution Optical Coherence Tomography. Invest Ophthalmol Vis Sci. 2012;53:6863-6869.

A reprint of this material must include a full article citation and acknowledge the Association for Research in Vision and Ophthalmology as the copyright holder.

Best regards,

Debbie Chin

IOVS

Association for Research in Vision and Ophthalmology

1801 Rockville Pike, Suite 400

Rockville MD 20852 USA

Direct: +1.240.221.2926 | Main: +1.240.221.2900 | Fax: +1.240.221.0370

www.arvo.org

B.4.2 Copyright permission from co-authors:

Hi

I would like to ask your permission for using the material of the following publication, in which you are one of the co-authors, in my PhD thesis:

Moayed, A.A., Choh, V., Hariri, S., Liu, C., Wong, A., Bizheva, K., 2012. Stimulus Specific Pupil Dynamics Measured in Birds (Gallus Gallus Domesticus) in vivo with Ultrahigh Resolution Optical Coherence Tomography. IOVS.

I sincerely appreciate your kind attention to this matter.

Best regards

Alireza A.Moayed
PhD Candidate
Department of Physics and Astronomy
University of Waterloo
200 University Ave West
Waterloo, Ontario Canada N2L 3G1
(519) 888 4567 ext. 35665
aakhlagh@uwaterloo.ca

Date: Tue, 9 Oct 2012 23:21:52 -0400 [10/09/12 23:21:52 EDT]

From: Vivian Choh <vchoh@uwaterloo.ca>

To: Alireza Akhlagh Moayed <aakhlagh@uwaterloo.ca>

Subject: Re: Permission for reproduction of paper material

You have my permission

Vivian Choh
Associate Professor
Room 260, School of Optometry
University of Waterloo
Tel: 1 (519) 888-4567 x35005
Email: vchoh@uwaterloo.ca

Date: Tue, 9 Oct 2012 14:29:33 -0400 [10/09/12 14:29:33 EDT]

From: Sepideh Hariri <sepidhariri@gmail.com>

To: Alireza Akhlagh Moayed <aakhlagh@uwaterloo.ca>

Subject: Re: Permission for reproduction of paper material

Permission granted.

Best Regards

Sepideh Hariri

PhD Candidate

Department of Physics and Astronomy

University of Waterloo

200 University Ave West

Waterloo, Ontario Canada N2L 3G1

(519) 888 4567 ext. 35665

shariri@sciborg.uwaterloo.ca

Date: Wed, 10 Oct 2012 20:54:20 +0800 [10/10/12 08:54:20 EDT]

From: Chenyi <liucheny@gmail.com>

To: Alireza Akhlagh Moayed <aakhlagh@uwaterloo.ca>

Subject: Re: Permission for reproduction of paper material

Sure, Alireza, I have no problem with this.

Best,

Chenyi Liu

Dept. of Systems Design Engineering,

University of Waterloo,

Ontario, CANADA N2L 3G1

(519) 888-4567, ext. 35342

Office: E2 1303D

Date: Tue, 9 Oct 2012 14:36:50 -0400 [10/09/12 14:36:50 EDT]

From: Alex Wong <alex.s.wong@gmail.com>

To: Alireza Akhlagh Moayed <aakhlagh@uwaterloo.ca>

Subject: Re: Permission for reproduction of paper material

Hi Ali,

You have full permission.

Alex

Date: Tue, 9 Oct 2012 23:10:07 -0400 [10/09/12 23:10:07 EDT]

From: Dida <kbizheva@uwaterloo.ca>

To: Alireza Akhlagh Moayed <aakhlagh@uwaterloo.ca>

Date: Tue, 9 Oct 2012 17:04:14 -0400

Subject: Re: Permission for reproduction of paper material

Hello Ali,

You have my permission to reprint materials from all papers where I am listed as co-author.

Dr. Kostadinka Bizheva

Associate Professor

Department of Physics and Astronomy

University of Waterloo

200 University Ave West

Waterloo, ON N2L 3G1

Canada

Phone: (519) 888 4567 x 37517 (office), x35665 (old lab), x31133 (new lab)

Cell Phone: 519 572 1774

E-mail: kbizheva@uwaterloo.ca

B.5 Co-authors' Contributions and copyright permissions for appendix A:

Appendix A is based on the following published paper:

Moayed, A.A., Hariri, S., Hyun, C., Doran, B., Kraft, T.W., Boyd, S., Bizheva, K., 2010. Combined optical coherence tomography and electroretinography system for in vivo simultaneous morphological and functional imaging of the rodent retina. Journal of Biomedical Optics 15, 040506–040506–3. [177].

Alireza Akhlagh Moayed: Planning the experiments, designing the imaging probe, acquiring the images and ERG from rats, data processing, writing and revising the manuscript.

Sepideh Hariri: Assisting in imaging, manuscript revisions.

Daryl Chulho Hyun: Developing the Labview code for data acquisition, manuscript revisions.

Timothy W. Kraft: Giving advice about rat retina, rat ERG, and sodium iodine injections, manuscript revisions.

Shelly Boyd: Giving advice about sodium iodine effect on rat retina, manuscript revisions

Kostadinka Bizheva: Supervising the experiments, designing and building the OCT system, manuscript revisions.

B.5.1 Copyright permission from publisher:

From: Alireza Akhlagh Moayed [mail to: aakhlagh@uwaterloo.ca]

Sent: Wednesday, August 15, 2012 10:04 AM

To: authorhelp

Subject: Permission to use my papers as a part of my PhD thesis

Hi,

I am a PhD student at University of Waterloo, Canada. I would like to use my papers as a part of my PhD Thesis.

Could you please let me know how to proceed to acquire an official permission?

My paper information is:

Moayed, A.A., Hariri, S., Hyun, C., Doran, B., Kraft, T.W., Boyd, S., Bizheva, K., 2010. Combined optical coherence tomography and electroretinography system for in vivo simultaneous morphological and functional imaging of the rodent retina. Journal of Biomedical Optics 15, 040506-040506-3.

Thank you in advance for your kind attention.

Best regards

Alireza A. Moayed

PhD Candidate

Department of Physics and Astronomy

University of Waterloo

200 University Ave West

Waterloo, Ontario Canada N2L 3G1

(519) 888 4567 ext. 35665
aakhlagh@uwaterloo.ca

From: Scott McNeill scottm@spie.org
To: "aakhlagh@uwaterloo.ca" <aakhlagh@uwaterloo.ca>
Date: Thu, 23 Aug 2012 14:31:27 -0700
Subject: RE: Permission to use my papers as a part of my PhD thesis
Dear Alireza Moayed,
Thank you for seeking permission from SPIE to reprint material from our publications. As an author of the cited works, you retain co-owner rights to the original content therein. Publisher's permission is hereby granted under the following conditions: (1) the material to be used has appeared in our publication without credit or acknowledgment to another source; and (2) you credit the original SPIE publication. Include the authors' names, title of paper, volume title, SPIE volume number, and year of publication in your credit statement.
Sincerely,
Scott McNeill for
Eric Pepper, Director of Publications
SPIE
P.O. Box 10, Bellingham WA 98227-0010 USA
360/676-3290 (Pacific Time) eric@spie.org

B.5.2 Copyright permission from co-authors:

On Tue, Oct 9, 2012 at 2:15 PM, Alireza Akhlagh Moayed
<aakhlagh@uwaterloo.ca> wrote:
Hi,
I would like to ask your permission for using the material of the following publication ,in which you are one of the co-authors, in my PhD thesis:
Moayed, A.A., Hariri, S., Hyun, C., Doran, B., Kraft, T.W., Boyd, S., Bizheva, K., 2010. Combined optical coherence tomography and electroretinography system for in vivo simultaneous

morphological and functional imaging of the rodent retina. Journal of Biomedical Optics 15, 040506-040506-3.

I sincerely appreciate your kind attention to this matter.

Best regards

Alireza A.Moayed
PhD Candidate
Department of Physics and Astronomy
University of Waterloo
200 University Ave West
Waterloo, Ontario Canada N2L 3G1
(519) 888 4567 ext. 35665
aakhlagh@uwaterloo.ca

From: Sepideh Hariri sepidhariri@gmail.com
To: Alireza Akhlagh Moayed aakhlagh@uwaterloo.ca
Date: Tue, 9 Oct 2012 14:28:53 -0400
Subject: Re: Permission for reproduction of paper material

Hi Alireza,

You have my permission to use the paper materials in your thesis.

It has been a pleasure working with you.

Best Regards

Sepideh Hariri
PhD Candidate
Department of Physics and Astronomy
University of Waterloo
200 University Ave West
Waterloo, Ontario Canada N2L 3G1
(519) 888 4567 ext. 35665

shariri@sciborg.uwaterloo.ca

From: Daryl Chulho Hyun <darylhyun@gmail.com>

To: Alireza Akhlagh Moayed <aakhlagh@uwaterloo.ca>

Date: Tue, 9 Oct 2012 19:05:06 -0700

Subject: Re: Permission for reproduction of paper material

Hi Ali,

Yes, of course you can use the materials.

Regards,

Daryl Chulho Hyun

BSc in Honours Physics, Co-op, Applied Physics Specialization

Research Assistant II, Imaging Unit, Integrative Oncology Department

BC Cancer Research Centre, BC Cancer Agency

Cell Phone: 1 778 873 0469

E-mail: darylhyun@gmail.com or dhyun@bccrc.ca

From: Timothy Kraft <twkraft@uab.edu>

To: Alireza Akhlagh Moayed <aakhlagh@uwaterloo.ca>

Date: Tue, 9 Oct 2012 13:25:50

Subject: Re: Permission for reproduction of paper material

You have my permission, and enthusiastic support.

Good Luck

Timothy W. Kraft, Ph.D.

Associate Professor of Vision Sciences & Neurobiology

UAB School of Optometry VH346 1720 2nd Ave S Birmingham, AL 35294-4390

(205) 975-2885

Fax (205) 934-5725

E-mail twkraft@uab.edu

Subject: permission to reproduce images

Date: Thu, 25 Oct 2012 18:37:17

From: Shelley Boyd <Boyds@smh.ca>

To: 'kbizheva@uwaterloo.ca' <kbizheva@uwaterloo.ca>

Hi Dida,

Please give my congratulations to Sepideh and Ali for their successful PhD defenses!

This email officially confirms that both Sepideh Haririr and Alireza Moayod have permission to reproduce images and text from our publications in their theses.

If you require any additional documentation, please let me know.

Best wishes,

Shelley

From: Dida <kbizheva@uwaterloo.ca>

To: Alireza Akhlagh Moayed <aakhlagh@uwaterloo.ca>

Date: Tue, 9 Oct 2012 17:04:14 -0400

Subject: Re: Permission for reproduction of paper material

Hello Ali,

You have my permission to reprint materials from all papers where I am listed as co-author.

Dr. Kostadinka Bizheva

Associate Professor

Department of Physics and Astronomy

University of Waterloo

200 University Ave West

Waterloo, ON N2L 3G1

Canada

Phone: (519) 888 4567 x 37517 (office), x35665 (old lab), x31133 (new lab)

Cell Phone: 519 572 1774

E-mail: kbizheva@uwaterloo.ca

The following co-author did not respond to my email: Bruce Doran.

Bibliography

[1] Nathan Congdon, Benita O'Colmain, Caroline C. W. Klaver, Ronald Klein, Beatriz Mun˜ oz, David S. Friedman, John Kempen, Hugh R. Taylor, Paul Mitchell, and Leslie Hyman, "Causes and Prevalence of Visual Impairment Among Adults in the UnitedStates," *Archives of Ophthalmology*, vol. 122, no. 4, pp. 477–485., 2004.

[2] S. Resnikoff, D. Pascolini, D. Etya'ale, I. Kocur, R. Pararajasegaram, G. P. Pokharel, and S. P. Mariotti, "Global data on visual impairment in the year 2002," *Bulletin of the World Health Organization*, vol. 82, no. 11, pp. 844–851, Nov. 2004.

[3] N. G. Congdon, D. S. Friedman, and T. Lietman, "Important Causes of Visual Impairment in the World Today," *JAMA*, vol. 290, no. 15, pp. 2057–2060, Oct. 2003.

[4] A. Binns and T. H. Margrain, "Evaluation of retinal function using the Dynamic Focal Cone ERG," *Ophthalmic Physiol Opt*, vol. 25, no. 6, pp. 492–500, Nov. 2005.

[5] G. Hanazono, K. Tsunoda, Y. Kazato, K. Tsubota, and M. Tanifuji, "Evaluating Neural Activity of Retinal Ganglion Cells by Flash-Evoked Intrinsic Signal Imaging in Macaque Retina," *Investigative Ophthalmology & Visual Science*, vol. 49, no. 10, pp. 4655–4663, May 2008.

[6] P. N. Dimitrov, R. H. Guymer, A. J. Zele, A. J. Anderson, and A. J. Vingrys, "Measuring rod and cone dynamics in age-related maculopathy," *Invest. Ophthalmol. Vis. Sci.*, vol. 49, no. 1, pp. 55–65, Jan. 2008.

[7] V. J. Srinivasan, Y. Chen, J. S. Duker, and J. G. Fujimoto, "In vivo functional imaging of intrinsic scattering changes in the human retina with high- speed ultrahigh resolution OCT," *Optics express*, vol. 17, no. 5, p. 3861, 2009.

[8] A. R. Tumlinson, B. Hermann, B. Hofer, B. Povazay, T. H. Margrain, A. M. Binns, and W. Drexler, "Techniques for extraction of depth-resolved in vivo human retinal intrinsic optical signals with optical coherence tomography," *Jpn. J. Ophthalmol.*, vol. 53, no. 4, pp. 315–326, Jul. 2009.

[9] T. Schmoll, C. Kolbitsch, and R. A. Leitgeb, "In vivo functional retinal optical coherence tomography," *Journal of Biomedical Optics*, vol. 15, no. 4, pp. 041513–041513–8, Jul. 2010.

[10] K. Bizheva, R. Pflug, B. Hermann, B. Považay, H. Sattmann, P. Qiu, E. Anger, H. Reitsamer, S. Popov, J. R. Taylor, and others, "Optophysiology: depth-resolved probing of retinal physiology with functional ultrahigh-resolution optical coherence tomography," *Proceedings of the National Academy of Sciences of the United States of America*, vol. 103, no. 13, pp. 5066–5071, 2006.

[11] X. C. Yao, "Intrinsic optical signal imaging of retinal activation," *Japanese journal of ophthalmology*, vol. 53, no. 4, pp. 327–333, 2009.

[12] J. R. Heckenlively and G. B. Arden, *Principles And Practice of Clinical Electrophysiology of Vision*. MIT Press, 2006.

[13] A. Grinvald, E. Lieke, R. D. Frostig, C. D. Gilbert, and T. N. Wiesel, "Functional architecture of cortex revealed by optical imaging of intrinsic signals," *Nature*, vol. 324, no. 6095, pp. 361–364, Dec. 1986.

[14] B. Chance, Q. Luo, S. Nioka, D. C. Alsop, and J. A. Detre, "Optical investigations of physiology: a study of intrinsic and extrinsic biomedical contrast," *Philos. Trans. R. Soc. Lond., B, Biol. Sci.*, vol. 352, no. 1354, pp. 707–716, Jun. 1997.

[15] D. M. Rector, K. M. Carter, P. L. Volegov, and J. S. George, "Spatio-temporal mapping of rat whisker barrels with fast scattered light signals," *Neuroimage*, vol. 26, no. 2, pp. 619–627, Jun. 2005.

[16] M. M. Haglund, G. A. Ojemann, and D. W. Hochman, "Optical imaging of epileptiform and functional activity in human cerebral cortex," *Nature*, vol. 358, no. 6388, pp. 668–671, Aug. 1992.

[17] Y. Hoshi, I. Oda, Y. Wada, Y. Ito, Yutaka Yamashita, M. Oda, K. Ohta, Y. Yamada, and Mamoru Tamura, "Visuospatial imagery is a fruitful strategy for the digit span backward task: a study with near-infrared optical tomography," *Brain Res Cogn Brain Res*, vol. 9, no. 3, pp. 339–342, Jun. 2000.

[18] G. Strangman, J. P. Culver, J. H. Thompson, and D. A. Boas, "A quantitative comparison of simultaneous BOLD fMRI and NIRS recordings during functional brain activation," *Neuroimage*, vol. 17, no. 2, pp. 719–731, Oct. 2002.

[19] N. Pouratian, S. A. Sheth, N. A. Martin, and A. W. Toga, “Shedding light on brain mapping: advances in human optical imaging,” *Trends Neurosci.*, vol. 26, no. 5, pp. 277–282, May 2003.

[20] D. Rector and R. Harper, “Imaging of hippocampal neural activity in freely behaving animals,” *Behav. Brain Res.*, vol. 42, no. 2, pp. 143–149, Feb. 1991.

[21] S. Chen, P. Li, W. Luo, H. Gong, S. Zeng, and Q. Luo, “Time-varying spreading depression waves in rat cortex revealed by optical intrinsic signal imaging,” *Neurosci. Lett.*, vol. 396, no. 2, pp. 132–136, Mar. 2006.

[22] L. B. Cohen, R. D. Keynes, and B. Hille, “Light scattering and birefringence changes during nerve activity,” *Nature*, vol. 218, no. 5140, pp. 438–441, May 1968.

[23] L. B. Cohen, “Changes in neuron structure during action potential propagation and synaptic transmission,” *Physiol. Rev.*, vol. 53, no. 2, pp. 373–418, Apr. 1973.

[24] R. A. Stepnoski, A. LaPorta, F. Raccuia-Behling, G. E. Blonder, R. E. Slusher, and D. Kleinfeld, “Noninvasive detection of changes in membrane potential in cultured neurons by light scattering,” *Proceedings of the National Academy of Sciences*, vol. 88, no. 21, p. 9382, 1991.

[25] Q.-X. Zhang, Y. Zhang, R.-W. Lu, Y.-C. Li, S. J. Pittler, T. W. Kraft, and X.-C. Yao, “Comparative intrinsic optical signal imaging of wild-type and mutant mouse retinas,” *Opt Express*, vol. 20, no. 7, pp. 7646–7654, Mar. 2012.

[26] K. Tsunoda, G. Hanazono, K. Inomata, Y. Kazato, W. Suzuki, and M. Tanifuji, “Origins of retinal intrinsic signals: a series of experiments on retinas of macaque monkeys,” *Japanese journal of ophthalmology*, vol. 53, no. 4, pp. 297–314, 2009.

[27] D. Ts’o, J. Schallek, Y. Kwon, R. Kardon, M. Abramoff, and P. Soliz, “Noninvasive functional imaging of the retina reveals outer retinal and hemodynamic intrinsic optical signal origins,” *Japanese journal of ophthalmology*, vol. 53, no. 4, pp. 334–344, 2009.

[28] B. Bouma, *Handbook of Optical Coherence Tomography*. Taylor & Francis, 2001.

[29] *Optical coherence tomography technology and applications*. Berlin ; New York: Springer, 2008.

[30] D. Huang, E. A. Swanson, C. P. Lin, J. S. Schuman, W. G. Stinson, W. Chang, M. R. Hee, T. Flotte, K. Gregory, C. A. Puliafito, and A. Et, "Optical coherence tomography," *Science*, vol. 254, no. 5035, pp. 1178–1181, Nov. 1991.

[31] M. Wojtkowski, "High-speed optical coherence tomography: basics and applications," *Appl.Opt.*, vol. 49, no. 16, p. D30, 2010.

[32] J. W. Goodman, *Statistical Optics*, 1st ed. Wiley-Interscience, 2000.

[33] A. F. Fercher, C. K. Hitzenberger, G. Kamp, and S. Y. El-Zaiat, "Measurement of intraocular distances by backscattering spectral interferometry," *Optics Communications*, vol. 117, no. 1–2, pp. 43–48, May 1995.

[34] A. F. Fercher, W. Drexler, C. K. Hitzenberger, and T. Lasser, "Optical coherence tomography - principles and applications," *Reports on Progress in Physics*, vol. 66, no. 2, pp. 239–303, Feb. 2003.

[35] M. Wojtkowski, R. Leitgeb, A. Kowalczyk, T. Bajraszewski, and A. F. Fercher, "In vivo human retinal imaging by Fourier domain optical coherence tomography," *J Biomed Opt*, vol. 7, no. 3, pp. 457–463, Jul. 2002.

[36] G. Häusler and M. W. Lindner, "'Coherence Radar' and 'Spectral Radar'—New Tools for Dermatological Diagnosis," *Journal of Biomedical Optics*, vol. 3, no. 1, pp. 21–31, Jan. 1998.

[37] S. R. Chinn, E. A. Swanson, and J. G. Fujimoto, "Optical coherence tomography using a frequency-tunable optical source," *Opt. Lett.*, vol. 22, no. 5, pp. 340–342, Mar. 1997.

[38] M. Choma, M. Sarunic, C. Yang, and J. Izatt, "Sensitivity advantage of swept source and Fourier domain optical coherence tomography," *Opt. Express*, vol. 11, no. 18, pp. 2183–2189, 2003.

[39] R. Leitgeb, C. Hitzenberger, and A. Fercher, "Performance of fourier domain vs. time domain optical coherence tomography," *Opt. Express*, vol. 11, no. 8, pp. 889–894, Apr. 2003.

[40] A. Konstantopoulos, P. Hossain, and D. F. Anderson, “Recent advances in ophthalmic anterior segment imaging: a new era for ophthalmic diagnosis?,” *Br J Ophthalmol*, vol. 91, no. 4, pp. 551–557, Apr. 2007.

[41] J. L. B. Ramos, Y. Li, and D. Huang, “Clinical and research applications of anterior segment optical coherence tomography - a review,” *Clin. Experiment. Ophthalmol.*, vol. 37, no. 1, pp. 81–89, Jan. 2009.

[42] A. S. Wang J, V. Perez, C. Karp, S. Yoo, M. Shen, L. Cui, V. Hurmeric, C. Du, D. Zhu, Q. Chen, and Li. M., “Ultra-high resolution optical coherence tomography for imaging the anterior segment of the eye,” vol. 42 Suppl, pp. S15–27, 2011.

[43] M. Wojtkowski, B. Kaluzny, and R. J. Zawadzki, “New directions in ophthalmic optical coherence tomography,” *Optom Vis Sci*, vol. 89, no. 5, pp. 524–542, May 2012.

[44] W. Drexler and J. G. Fujimoto, “State-of-the-art retinal optical coherence tomography,” *Prog.Retin.Eye Res.*, vol. 27, no. 1, pp. 45–88, 2008.

[45] W. Choi, B. Baumann, J. J. Liu, A. C. Clermont, E. P. Feener, J. S. Duker, and J. G. Fujimoto, “Measurement of pulsatile total blood flow in the human and rat retina with ultrahigh speed spectral/Fourier domain OCT,” *Biomedical Optics Express*, vol. 3, no. 5, p. 1047, 2012.

[46] C. Fan and G. Yao, “Mapping local retardance in birefringent samples using polarization sensitive optical coherence tomography,” *Opt.Lett.*, vol. 37, no. 9, p. 1415, 2012.

[47] M. Pircher, C. K. Hitzenberger, and U. Schmidt-Erfurth, “Polarization sensitive optical coherence tomography in the human eye,” *Prog.Retin.Eye Res.*, vol. 30, no. 6, pp. 431–451, 2011.

[48] J. F. de Boer, T. E. Milner, M. J. van Gemert, and J. S. Nelson, “Two-dimensional birefringence imaging in biological tissue by polarization-sensitive optical coherence tomography,” *Opt Lett*, vol. 22, no. 12, pp. 934–936, Jun. 1997.

[49] X. C. Yao, A. Yamauchi, B. Perry, and J. S. George, “Rapid optical coherence tomography and recording functional scattering changes from activated frog retina,” *Applied optics*, vol. 44, no. 11, pp. 2019–2023, 2005.

[50] V. J. Srinivasan, M. Wojtkowski, J. G. Fujimoto, and J. S. Duker, “In vivo measurement of retinal physiology with high-speed ultrahigh-resolution optical coherence tomography,” *Optics letters*, vol. 31, no. 15, pp. 2308–2310, 2006.

[51] B. Cense, W. Gao, J. M. Brown, S. M. Jones, R. S. Jonnal, M. Mujat, B. H. Park, J. F. De Boer, and D. T. Miller, “Retinal imaging with polarization- sensitive optical coherence tomography and adaptive optics,” *Optics express*, vol. 17, no. 24, p. 21634, 2009.

[52] R. A. Leitgeb and T. Schmoll, “In vivo functional retinal optical coherence tomography fOCT,” 2009, p. 71631J–71631J–10.

[53] R. S. Jonnal, O. P. Kocaoglu, Q. Wang, S. Lee, and D. T. Miller, “Phase-sensitive imaging of the outer retina using optical coherence tomography and adaptive optics,” *Biomedical Optics Express*, vol. 3, no. 1, pp. 104–124, 2012.

[54] M. D. Abràmoff, Y. H. Kwon, D. Ts’o, P. Soliz, B. Zimmerman, J. Pokorny, and R. Kardon, “Visual Stimulus–Induced Changes in Human Near-Infrared Fundus Reflectance,” *Investigative ophthalmology & visual science*, vol. 47, no. 2, pp. 715–721, 2006.

[55] D. A. Nelson, S. Krupsky, A. Pollack, E. Aloni, M. Belkin, I. Vanzetta, M. Rosner, and A. Grinvald, “Special report: Noninvasive multi-parameter functional optical imaging of the eye,” *Ophthalmic Surg Lasers Imaging*, vol. 36, no. 1, pp. 57–66, Feb. 2005.

[56] K. Grieve and A. Roorda, “Intrinsic signals from human cone photoreceptors,” *Investigative ophthalmology & visual science*, vol. 49, no. 2, pp. 713–719, 2008.

[57] X. C. Yao and J. S. George, “Near-infrared imaging of fast intrinsic optical responses in visible light-activated amphibian retina,” *Journal of biomedical optics*, vol. 11, p. 064030, 2006.

[58] Y.-B. Zhao and X.-C. Yao, “Intrinsic optical imaging of stimulus-modulated physiological responses in amphibian retina,” *Opt. Lett.*, vol. 33, no. 4, pp. 342–344, Feb. 2008.

[59] X. C. Yao and Y. B. Zhao, “Optical dissection of stimulus-evoked retinal activation,” *Optics express*, vol. 16, no. 17, pp. 12446–12459, 2008.

[60] Y. C. Li, C. Strang, F. R. Amthor, L. Liu, Y. G. Li, Q. X. Zhang, K. Keyser, and X. C. Yao, “Parallel optical monitoring of visual signal propagation from the photoreceptors to the inner retina layers,” *Optics letters*, vol. 35, no. 11, pp. 1810–1812, 2010.

[61] X.-C. Yao, A. Foust, D. M. Rector, B. Barrowes, and J. S. George, “Cross-polarized reflected light measurement of fast optical responses associated with neural activation,” *Biophys. J.*, vol. 88, no. 6, pp. 4170–4177, Jun. 2005.

[62] X.-C. Yao, D. M. Rector, and J. S. George, “Optical lever recording of displacements from activated lobster nerve bundles and Nitella internodes,” *Appl Opt*, vol. 42, no. 16, pp. 2972–2978, Jun. 2003.

[63] M. Meister, J. Pine, and D. A. Baylor, “Multi-neuronal signals from the retina: acquisition and analysis,” *J. Neurosci. Methods*, vol. 51, no. 1, pp. 95–106, Jan. 1994.

[64] H. Kühn, N. Bennett, M. Michel-Villaz, and M. Chabre, “Interactions Between Photoexcited Rhodopsin and GTP-Binding Protein: Kinetic and Stoichiometric Analyses from Light-Scattering Changes,” *PNAS*, vol. 78, no. 11, pp. 6873–6877, Nov. 1981.

[65] P. J. DeLint, T. T. Berendschot, J. van de Kraats, and D. van Norren, “Slow optical changes in human photoreceptors induced by light,” *Invest. Ophthalmol. Vis. Sci.*, vol. 41, no. 1, pp. 282–289, Jan. 2000.

[66] B. Huang and C. J. Karwoski, “Light-evoked expansion of subretinal space volume in the retina of the frog,” *J. Neurosci.*, vol. 12, no. 11, pp. 4243–4252, Nov. 1992.

[67] J. D. Li, R. P. Gallemore, A. Dmitriev, and R. H. Steinberg, “Light-Dependent Hydration of the Space Surrounding Photoreceptors in Chick Retina.,” *IOVS*, vol. 35, no. 6, pp. 2700–2711, May 1994.

[68] W. Cao, V. Govardovskii, J. D. Li, and R. H. Steinberg, “Systemic hypoxia dehydrates the space surrounding photoreceptors in the cat retina,” *Invest. Ophthalmol. Vis. Sci.*, vol. 37, no. 4, pp. 586–596, Mar. 1996.

[69] W. S. Stiles and B. H. Crawford, “The Luminous Efficiency of Rays Entering the Eye Pupil at Different Points,” *Royal Society of London Proceedings Series B*, vol. 112, pp. 428–450, Mar. 1933.

[70] J.-M. Gorrand, “Directional effects of the retina appearing in the aerial image,” *Journal of Optics*, vol. 16, no. 6, pp. 279–287, Nov. 1985.

[71] G. J. van Blokland, “Directionality and alignment of the foveal receptors, assessed with light scattered from the human fundus in vivo,” *Vision Res.*, vol. 26, no. 3, pp. 495–500, 1986.

[72] J. Gorrand and F. Delori, “A method for assessing the photoreceptor directionality,” *Invest.Ophthalmol.Vis.Sci.Suppl*, vol. 31, p. 425, 1990.

[73] J. M. Gorrand and F. Delori, “A reflectometric technique for assessing photoreceptor alignment,” *Vision Res.*, vol. 35, no. 7, pp. 999–1010, Apr. 1995.

[74] S. A. Burns, S. Wu, A. E. Elsner, and F. C. Delori, “Optical imaging of photoreceptor alignment,” *Invest Ophthalmol Vis Sci*, vol. 35, p. 1572, 1994.

[75] S. A. Burns, S. Wu, F. Delori, and A. E. Elsner, “Direct measurement of human-conephotoreceptor alignment,” *J. Opt. Soc. Am. A*, vol. 12, no. 10, pp. 2329–2338, Oct. 1995.

[76] P. L. Walraven, “Recovery from the increase of the Stiles-Crawford effect after bleaching,” *Nature*, vol. 210, no. 5033, pp. 311–312, Apr. 1966.

[77] P. J. Delint, T. T. Berendschot, and D. van Norren, “Local photoreceptor alignment measured with a scanning laser ophthalmoscope,” *Vision Res.*, vol. 37, no. 2, pp. 243–248, Jan. 1997.

[78] A. W. Snyder and C. Pask, “The Stiles-Crawford effect--explanation and consequences,” *Vision Res.*, vol. 13, no. 6, pp. 1115–1137, Jun. 1973.

[79] C. E. Riva, E. Logean, and B. Falsini, “Visually evoked hemodynamical response and assessment of neurovascular coupling in the optic nerve and retina,” *Progress in retinal and eye research*, vol. 24, no. 2, pp. 183–215, 2005.

[80] R. S. Jonnal, J. Rha, Y. Zhang, B. Cense, W. Gao, and D. T. Miller, "In vivo functional imaging of human cone photoreceptors," *Optics Express*, vol. 15, no. 24, p. 16141, 2007.

[81] E. N. Pugh Jr and T. D. Lamb, "Amplification and kinetics of the activation steps in phototransduction," *Biochim. Biophys. Acta*, vol. 1141, no. 2–3, pp. 111–149, Mar. 1993.

[82] S. T. Menon, M. Han, and T. P. Sakmar, "Rhodopsin: Structural Basis of Molecular Physiology," *Physiol Rev*, vol. 81, no. 4, pp. 1659–1688, Jan. 2001.

[83] J. Rha, B. Schroeder, P. Godara, and J. Carroll, "Variable optical activation of human cone photoreceptors visualized using a short coherence light source," *Optics letters*, vol. 34, no. 24, pp. 3782–3784, 2009.

[84] J. Schallek, H. Li, R. Kardon, Y. Kwon, M. Abramoff, P. Soliz, and D. Ts'o, "Stimulus-evoked intrinsic optical signals in the retina: spatial and temporal characteristics," *Invest. Ophthalmol. Vis. Sci.*, vol. 50, no. 10, pp. 4865–4872, Oct. 2009.

[85] J. Schallek, R. Kardon, Y. Kwon, M. Abramoff, P. Soliz, and D. Ts'o, "Stimulus-evoked intrinsic optical signals in the retina: pharmacologic dissection reveals outer retinal origins," *Investigative ophthalmology & visual science*, vol. 50, no. 10, pp. 4873–4880, 2009.

[86] J. B. Schallek, G. J. McLellan, S. Viswanathan, and D. Y. Ts'o, "Retinal intrinsic optical signals in a cat model of primary congenital glaucoma," *Invest. Ophthalmol. Vis. Sci.*, vol. 53, no. 4, pp. 1971–1981, Apr. 2012.

[87] G. Hanazono, K. Tsunoda, K. Shinoda, K. Tsubota, Y. Miyake, and M. Tanifuji, "Intrinsic signal imaging in macaque retina reveals different types of flash-induced light reflectance changes of different origins," *Investigative ophthalmology & visual science*, vol. 48, no. 6, pp. 2903–2912, 2007.

[88] K. Inomata, K. Tsunoda, G. Hanazono, Y. Kazato, K. Shinoda, M. Yuzawa, M. Tanifuji, and Y. Miyake, "Distribution of Retinal Responses Evoked by Transscleral Electrical Stimulation Detected by Intrinsic Signal Imaging in Macaque Monkeys," *IOVS*, vol. 49, no. 5, pp. 2193–2200, May 2008.

[89] X.-C. Yao, L. Liu, and Y.-G. Li, “Reflected light imaging of ON and OFF responses in frog retina,” 2009, p. 71613I–71613I–8.

[90] Y. G. Li, L. Liu, F. Amthor, and X. C. Yao, “High-speed line-scan confocal imaging of stimulus-evoked intrinsic optical signals in the retina,” *Optics letters*, vol. 35, no. 3, pp. 426–428, 2010.

[91] Q. X. Zhang, R. W. Lu, Y. G. Li, and X. C. Yao, “In vivo confocal imaging of fast intrinsic optical signals correlated with frog retinal activation,” *Optics letters*, vol. 36, no. 23, pp. 4692–4694, 2011.

[92] B. R. Biedermann, W. Wieser, C. M. Eigenwillig, G. Palte, D. C. Adler, V. J. Srinivasan, J. G. Fujimoto, and R. Huber, “Real time en face Fourier-domain optical coherence tomography with direct hardware frequency demodulation,” *Opt. Lett.*, vol. 33, no. 21, pp. 2556–2558, Nov. 2008.

[93] B. Potsaid, I. Gorczynska, V. J. Srinivasan, Y. Chen, J. Jiang, A. Cable, and J. G. Fujimoto, “Ultrahigh speed Spectral / Fourier domain OCT ophthalmic imaging at 70,000 to 312,500 axial scans per second,” *Opt Express*, vol. 16, no. 19, pp. 15149–15169, Sep. 2008.

[94] B. Potsaid, B. Baumann, D. Huang, S. Barry, A. E. Cable, J. S. Schuman, J. S. Duker, and J. G. Fujimoto, “Ultrahigh speed 1050nm swept source / Fourier domain OCT retinal and anterior segment imaging at 100,000 to 400,000 axial scans per second,” *Opt. Express*, vol. 18, no. 19, pp. 20029–20048, 2010.

[95] K. Bizheva, A. Unterhuber, B. Povazay, B. Hermann, H. Sattmann, W. Drexler, H. Reitsamer, M. Preusser, H. Budka, M. Seefeldt, R. Menzel, A. Stingl, and T. Le, “Feasibility of ultrahigh resolution optical coherence tomography for imaging brain tissue morphology and function,” in *Biomedical Topical Meeting*, 2004, p. ThE2.

[96] T. Theelen, C. B. Hoyng, B. J. Klevering, and B. Cense, “Functional imaging of inherited retinal disease with a commercial optical coherence tomography device,” in *Proceedings of SPIE*, 2011, vol. 8091, p. 80911O.

[97] J. Wallman, J. Turkel, and J. Trachtman, “Extreme myopia produced by modest change in early visual experience,” *Science*, vol. 201, no. 4362, pp. 1249–1251, Sep. 1978.

[98] E. L. Irving, M. G. Callender, and J. G. Sivak, “Inducing myopia, hyperopia, and astigmatism in chicks,” *Optom Vis Sci*, vol. 68, no. 5, pp. 364–368, May 1991.

[99] C. Wildsoet and J. Wallman, “Choroidal and scleral mechanisms of compensation for spectacle lenses in chicks,” *Vision Res.*, vol. 35, no. 9, pp. 1175–1194, May 1995.

[100] D. Mustafi, A. H. Engel, and K. Palczewski, “Structure of cone photoreceptors,” *Progress in Retinal and Eye Research*, vol. 28, no. 4, pp. 289–302, Jul. 2009.

[101] J. C. Blanks and L. V. Johnson, “Specific Binding of Peanut Lectin to a Class of Retinal Photoreceptor Cells. A Species Comparison.,” *IOVS*, vol. 25, no. 5, pp. 546–557, May 1984.

[102] V. B. Morris, “An afoveate area centralis in the chick retina,” *J. Comp. Neurol.*, vol. 210, no. 2, pp. 198–203, Sep. 1982.

[103] J. D. Pettigrew, J. Wallman, and C. F. Wildsoet, “Saccadic oscillations facilitate ocular perfusion from the avian pecten,” , *Published online: 25 January 1990; | doi:10.1038/343362a0*, vol. 343, no. 6256, pp. 362–363, Jan. 1990.

[104] Y. Zhang, J. Xu, M. Garcia, A. Roorda, and C. Wildsoet, “In vivo imaging the photoreceptors in the chicken eye with adaptive optics scanning laser ophthalmoscope,” *J Vis*, vol. 9, no. 14, pp. 79–79, Dec. 2009.

[105] K. Headington, S. S. Choi, D. Nickla, and N. Doble, “Single cell imaging of the chick retina with adaptive optics,” *Curr. Eye Res.*, vol. 36, no. 10, pp. 947–957, Oct. 2011.

[106] M. L. Kisilak, J. J. Hunter, E. L. Irving, and M. C. W. Campbell, “In vivo imaging of photoreceptors in the alert chicken,” 2007.

[107] Y. Zhang and A. Roorda, “Evaluating the lateral resolution of the adaptive optics scanning laser ophthalmoscope,” *J. Biomed. Opt*, vol. 11, no. 1, pp. 014002–014002, Jan. 2006.

[108] K. Venkateswaran, A. Roorda, and F. Romero-Borja, “Theoretical modeling and evaluation of the axial resolution of the adaptive optics scanning laser ophthalmoscope,” *J. Biomed. Opt*, vol. 9, no. 1, pp. 132–138, Jan. 2004.

[109] A. F. Fercher, “Optical coherence tomography,” *Journal of Biomedical Optics*, vol. 1, no. 2, pp. 157–173, Apr. 1996.

[110] Y. Huang, A. V. Cideciyan, G. I. Papastergiou, E. Banin, S. L. Semple-Rowland, A. H. Milam, and S. G. Jacobson, “Relation of optical coherence tomography to microanatomy in normal and rd chickens,” *Invest. Ophthalmol. Vis. Sci.*, vol. 39, no. 12, pp. 2405–2416, Nov. 1998.

[111] M. Ruggeri, J. C. Major Jr, C. McKeown, R. W. Knighton, C. A. Puliafito, and S. Jiao, “Retinal structure of birds of prey revealed by ultra-high resolution spectral-domain optical coherence tomography,” *Invest. Ophthalmol. Vis. Sci.*, vol. 51, no. 11, pp. 5789–5795, Nov. 2010.

[112] P. Puvanathasan, P. Forbes, Z. Ren, D. Malchow, S. Boyd, and K. Bizheva, “High-speed, high-resolution Fourier-domain optical coherence tomography system for retinal imaging in the 1060 nm wavelength region,” *Opt Lett*, vol. 33, no. 21, pp. 2479–2481, Nov. 2008.

[113] S. Hariri, A. A. Moayed, A. Dracopoulos, C. Hyun, S. Boyd, and K. Bizheva, “Limiting factors to the OCT axial resolution for in-vivo imaging of human and rodent retina in the 1060 nm wavelength range,” *Opt Express*, vol. 17, no. 26, pp. 24304–24316, Dec. 2009.

[114] E. L. Irving, J. G. Sivak, T. A. Curry, and M. G. Callender, “Chick eye optics: zero to fourteen days,” *J. Comp. Physiol. A*, vol. 179, no. 2, pp. 185–194, Aug. 1996.

[115] M. L. Kisilak, K. Bunghardt, J. J. Hunter, E. L. Irving, and M. C. W. Campbell, “Longitudinal In Vivo Imaging of Cones in the Alert Chicken,” *Optometry and Vision Science*, vol. 89, no. 5, pp. 644–651, May 2012.

[116] M. Wojtkowski, V. Srinivasan, T. Ko, J. Fujimoto, A. Kowalczyk, and J. Duker, “Ultrahigh-resolution, high-speed, Fourier domain optical coherence tomography and

methods for dispersion compensation," *Opt Express*, vol. 12, no. 11, pp. 2404–2422, May 2004.

[117] A. Mishra, A. Wong, K. Bizheva, and D. A. Clausi, "Intra-retinal layer segmentation in optical coherence tomography images," *Opt. Express*, vol. 17, no. 26, pp. 23719–23728, Dec. 2009.

[118] A. A. Moayed, S. Hariri, E. S. Song, V. Choh, and K. Bizheva, "In vivo volumetric imaging of chicken retina with ultrahigh-resolution spectral domain optical coherence tomography," *Biomed Opt Express*, vol. 2, no. 5, pp. 1268–1274, 2011.

[119] C. Straznicky and M. Chehade, "The formation of the area centralis of the retinal ganglion cell layer in the chick," *Development*, vol. 100, no. 3, pp. 411–420, Jul. 1987.

[120] D. Ehrlich, "Regional specialization of the chick retina as revealed by the size and density of neurons in the ganglion cell layer," *The Journal of Comparative Neurology*, vol. 195, no. 4, pp. 643–657, 1981.

[121] D. B. Meyer, "The topographical distribution of rods and cones in the adult chicken retina," *Experimental Eye Research*, vol. 17, no. 4, pp. 347–355.

[122] I. G. Morgan, "Intraocular colchicine selectively destroys immature ganglion cells in chicken retina," *Neurosci. Lett.*, vol. 24, no. 3, pp. 255–260, Jul. 1981.

[123] V. Choh, J. Banh, and C. f. Wildsoet, "Thickness and Histological Changes in Optic Nerve-Sectioned Chick Retina," *Invest. Ophthalmol. Vis. Sci.*, vol. 45, no. 5, p. 47, May 2004.

[124] A. Grinvald, R. D. Frostig, E. Lieke, and R. Hildesheim, "Optical imaging of neuronal activity.," *Physiol Rev*, vol. 68, no. 4, pp. 1285–1366, Oct. 1988.

[125] A. Villringer and B. Chance, "Non-invasive optical spectroscopy and imaging of human brain function," *Trends in Neurosciences*, vol. 20, no. 10, pp. 435–442, Oct. 1997.

[126] A. A. Moayed, S. Hariri, V. Choh, and K. Bizheva, "In vivo imaging of intrinsic optical signals in chicken retina with functional optical coherence tomography," *Opt.Lett.*, vol. 36, no. 23, p. 4575, 2011.

[127] A. A. Paupoo, O. A. Mahroo, C. Friedburg, and T. D. Lamb, “Human cone photoreceptor responses measured by the electroretinogram [correction of electoretinogram] a-wave during and after exposure to intense illumination,” *J. Physiol. (Lond.)*, vol. 529 Pt 2, pp. 469–482, Dec. 2000.

[128] O. A. R. Mahroo and T. D. Lamb, “Recovery of the human photopic electroretinogram after bleaching exposures: estimation of pigment regeneration kinetics,” *J. Physiol. (Lond.)*, vol. 554, no. Pt 2, pp. 417–437, Jan. 2004.

[129] M. A. Duarte, A. C. G. Almeida, A. F. C. Infantosi, and J. W. M. Bassani, “Functional imaging of the retinal layers by laser scattering: an approach for the study of Leao’s spreading depression in intact tissue,” *Journal of Neuroscience Methods*, vol. 123, no. 2, pp. 139–151, 2003.

[130] K. Tsunoda, Y. Oguchi, G. Hanazono, and M. Tanifuji, “Mapping cone-and rod-induced retinal responsiveness in macaque retina by optical imaging,” *Investigative ophthalmology & visual science*, vol. 45, no. 10, pp. 3820–3826, 2004.

[131] A. Akhlagh Moayed, S. Hariri, V. Choh, and K. Bizheva, “Correlation of visually evoked intrinsic optical signals and electroretinograms recorded from chicken retina with a combined functional optical coherence tomography and electroretinography system,” *J.Biomed.Opt.*, vol. 17, no. 1, p. 016011, 2012.

[132] J. Rymer, V. Choh, S. Bharadwaj, V. Padmanabhan, L. Modilevsky, E. Jovanovich, B. Yeh, Z. Zhang, H. Guan, W. Payne, and C. F. Wildsoet, “The albino chick as a model for studying ocular developmental anomalies, including refractive errors, associated with albinism,” *Exp. Eye Res.*, vol. 85, no. 4, pp. 431–442, Oct. 2007.

[133] J. M. McGoogan and V. M. Cassone, “Circadian regulation of chick electroretinogram: effects of pinealectomy and exogenous melatonin,” *Am. J. Physiol.*, vol. 277, no. 5 Pt 2, pp. R1418–1427, Nov. 1999.

[134] J. L. Barbur, N. B. Prescott, R. H. Douglas, J. R. Jarvis, and C. M. Wathes, “A comparative study of stimulus- specific pupil responses in the domestic fowl (Gallus gallus domesticus) and the human,” *Vision Res.*, vol. 42, no. 2, pp. 249–255, 2002.

[135] Z. Zhi, Y. Jung, Y. Jia, L. An, and R. K. Wang, “Highly sensitive imaging of renal microcirculation in vivo using ultrahigh sensitive optical microangiography,” *Biomedical optics express*, vol. 2, no. 5, p. 1059, 2011.

[136] T. Li and H. C. Howland, “A true neuronal consensual pupillary reflex in chicks,” *Vision Res.*, vol. 39, no. 5, pp. 897–900, 1999.

[137] D. C. Tu, M. L. Batten, K. Palczewski, and R. N. Van Gelder, “Nonvisual photoreception in the chick iris,” *Science (New York, N.Y.)*, vol. 306, no. 5693, p. 129, 2004.

[138] O. E. Lind, A. Kelber, and R. H. H. Kröger, “Multifocal optical systems and pupil dynamics in birds,” *J.Exp.Biol.*, vol. 211, p. 2752, 2008.

[139] D. Valdez, P. Nieto, E. Garbarino-Pico, L. Avalle, H. Diaz-Fajreldines, C. Schurrer, K. Cheng, and M. Guido, “A nonmammalian vertebrate model of blindness reveals functional photoreceptors in the inner retina,” *FASEB JOURNAL*, vol. 23, no. 4, pp. 1186–1195, 2009.

[140] A. A. Moayed, V. Choh, S. Hariri, C. Liu, A. Wong, and K. Bizheva, “Stimulus Specific Pupil Dynamics Measured in Birds (Gallus Gallus Domesticus) in vivo with Ultrahigh Resolution Optical Coherence Tomography,” *IOVS*, Aug. 2012.

[141] R. Kardon, S. C. Anderson, T. G. Damarjian, E. M. Grace, E. Stone, and A. Kawasaki, “Chromatic pupil responses: preferential activation of the melanopsin-mediated versus outer photoreceptor-mediated pupil light reflex,” *Ophthalmology*, vol. 116, no. 8, pp. 1564–1573, Aug. 2009.

[142] T. Xue, M. T. H. Do, A. Riccio, Z. Jiang, J. Hsieh, H. C. Wang, S. L. Merbs, D. S. Welsbie, T. Yoshioka, P. Weissgerber, S. Stolz, V. Flockerzi, M. Freichel, M. I. Simon, D. E. Clapham, and K.-W. Yau, “Melanopsin signalling in mammalian iris and retina,” *Nature*, vol. 479, no. 7371, pp. 67–73, Nov. 2011.

[143] A. Ham and D. Osorio, “Colour preferences and colour vision in poultry chicks,” *Proceedings of the Royal Society B: Biological Sciences*, vol. 274, no. 1621, pp. 1941–1948, 2007.

[144] N. Wioland and N. Bonaventure, “Colour coding in the chicken ERG,” *Vision Res.*, vol. 21, no. 11, pp. 1621–1624, 1981.

[145] J. K. Bowmaker, L. A. Heath, S. E. Wilkie, and D. M. Hunt, “Visual pigments and oil droplets from six classes of photoreceptor in the retinas of birds,” *Vision Res.*, vol. 37, no. 16, pp. 2183–2194, Aug. 1997.

[146] D. Osorio, M. Vorobyev, and C. D. Jones, “Colour vision of domestic chicks,” *J. Exp. Biol.*, vol. 202, no. Pt 21, pp. 2951–2959, Nov. 1999.

[147] T. Yoshizawa, “The road to color vision: structure, evolution and function of chicken and gecko visual pigments,” *Photochem. Photobiol.*, vol. 56, no. 6, pp. 859–867, Dec. 1992.

[148] V. I. Govardovskiĭ and L. V. Zueva, “Visual pigments of chicken and pigeon,” *Vision Res.*, vol. 17, no. 4, pp. 537–543, 1977.

[149] O. Lind and A. Kelber, “Avian colour vision: effects of variation in receptor sensitivity and noise data on model predictions as compared to behavioural results,” *Vision Res.*, vol. 49, no. 15, pp. 1939–1947, Jul. 2009.

[150] M. J. Bailey and V. M. Cassone, “Melanopsin expression in the chick retina and pineal gland,” *Brain Res. Mol. Brain Res.*, vol. 134, no. 2, pp. 345–348, Apr. 2005.

[151] S. Tomonari, A. Takagi, S. Akamatsu, S. Noji, and H. Ohuchi, “A non-canonical photopigment, melanopsin, is expressed in the differentiating ganglion, horizontal, and bipolar cells of the chicken retina,” *Dev. Dyn.*, vol. 234, no. 3, pp. 783–790, Nov. 2005.

[152] T. Neumann, C. Ziegler, and A. Blau, “Multielectrode array recordings reveal physiological diversity of intrinsically photosensitive retinal ganglion cells in the chick embryo,” *Brain Res.*, vol. 1207, pp. 120–127, May 2008.

[153] H. Ishikawa, A. Onodera, K. Asakawa, S. Nakadomari, and K. Shimizu, “Effects of selective-wavelength block filters on pupillary light reflex under red and blue light stimuli,” *Jpn. J. Ophthalmol.*, vol. 56, no. 2, pp. 181–186, Mar. 2012.

[154] A. Kawasaki and R. H. Kardon, “Intrinsically Photosensitive Retinal Ganglion Cells,” *Journal of Neuro-Ophthalmology*, vol. 27, no. 3, pp. 195–204, Sep. 2007.

[155] G. Pilar, R. Nuñez, I. S. Mclennan, and S. D. Meriney, “Muscarinic and nicotinic synaptic activation of the developing chicken iris,” *The Journal of neuroscience : the official journal of the Society for Neuroscience*, vol. 7, no. 12, p. 3813, 1987.

[156] C. Tashiro, R. Muranishi, I. Gomyo, T. Mashimo, K. Tomi, and I. Yoshiya, “Electroretinogram as a possible monitor of anesthetic depth,” *Graefe’s archive for clinical and experimental ophthalmology*, vol. 224, no. 5, pp. 473–476, 1986.

[157] G. Iohom, A. Whyte, T. Flynn, G. O’Connor, and G. Shorten, “Postoperative changes in the full-field electroretinogram following sevoflurane anaesthesia,” *European journal of anaesthesiology*, vol. 21, no. 4, pp. 272–278, 2004.

[158] G. Iohom, C. Gardiner, A. Whyte, G. O’Connor, and G. Shorten, “Abnormalities of contrast sensitivity and electroretinogram following sevoflurane anaesthesia,” *European journal of anaesthesiology*, vol. 21, no. 08, pp. 646–652, 2004.

[159] H. Satoh, N. Fukuda, H. Kuriki, Y. Maki, M. Nomura, Y. Saji, and Y. Nagawa, “[A procedure for recording electroretinogram (ERG) in conscious monkeys, and effects of some drugs (author’s transl)],” *Nippon Yakurigaku Zasshi*, vol. 76, no. 7, pp. 581–594, Oct. 1980.

[160] N. Wioland and N. Bonaventure, “Photopic c-wave in the chicken ERG: sensitivity to sodium azide, epinephrine, sodium iodate, barbiturates, and other general anesthetics,” *Doc Ophthalmol*, vol. 60, no. 4, pp. 407–412, Oct. 1985.

[161] M. Chynoranský, “[The effect of diazepam on the electroretinogram],” *Bratisl Lek Listy*, vol. 91, no. 7, pp. 527–532, Jul. 1990.

[162] S. Andréasson, K. Tornqvist, and B. Ehinger, “Full-field electroretinograms during general anesthesia in normal children compared to examination with topical anesthesia,” *Acta Ophthalmol (Copenh)*, vol. 71, no. 4, pp. 491–495, Aug. 1993.

[163] M. Yagi, C. Tashiro, and I. Yoshiya, “[Changes in the electroretinogram during enflurane anesthesia],” *Masui*, vol. 38, no. 11, pp. 1438–1443, Nov. 1989.

[164] C. Raitta, U. Karhunen, and A. M. Seppäläinen, “Changes in the electroretinogram and visual evoked potentials during general anaesthesia using enflurane,” *Graefes Arch. Clin. Exp. Ophthalmol.*, vol. 218, no. 6, pp. 294–296, 1982.

[165] S. Wongpichedchai, R. M. Hansen, B. Koka, V. M. Gudas, and A. B. Fulton, “Effects of halothane on children’s electroretinograms,” *Ophthalmology*, vol. 99, no. 8, pp. 1309–1312, Aug. 1992.

[166] M. Wasserschaff and J. G. Schmidt, “Electroretinographic responses to the addition of nitrous oxide to halothane in rats,” *Doc Ophthalmol*, vol. 64, no. 4, pp. 347–354, 1986.

[167] L. Blain, P. Lachapelle, and S. Molotchnikoff, “The effect of acute trichloroethylene exposure on electroretinogram components,” *Neurotoxicol Teratol*, vol. 12, no. 6, pp. 633–636, Dec. 1990.

[168] K. Becker, M. Eder, A. Ranft, L. von Meyer, W. Zieglgänsberger, E. Kochs, and H.-U. Dodt, “Low Dose Isoflurane Exerts Opposing Effects on Neuronal Network Excitability in Neocortex and Hippocampus,” *PLoS ONE*, vol. 7, no. 6, p. e39346, Jun. 2012.

[169] T. T, H. CB, K. BJ, and C. B, “Functional imaging of inherited retinal disease with a commercial optical coherence tomography device,” in *Optical Coherence Tomography and Coherence Techniques V*, 2011, vol. 8091, p. 80911O.

[170] A. Reichenbach and A. Bringmann, *Müller Cells in the Healthy and Diseased Retina*. Springer, 2010.

[171] J. Barnett, S. Yanni, and J. Penn, “The development of the rat model of retinopathy of prematurity,” *Documenta Ophthalmologica*, vol. 120, no. 1, pp. 3–12, 2010.

[172] C. J. Zeiss, “Animals as models of age-related macular degeneration: an imperfect measure of the truth,” *Vet. Pathol.*, vol. 47, no. 3, pp. 396–413, May 2010.

[173] C. K. S. Leung, J. D. Lindsey, L. Chen, Q. Liu, and R. N. Weinreb, “Longitudinal profile of retinal ganglion cell damage assessed with blue-light confocal scanning laser ophthalmoscopy after ischaemic reperfusion injury,” *Br J Ophthalmol*, vol. 93, no. 7, pp. 964–968, Jul. 2009.

[174] M. D. Fischer, G. Huber, S. C. Beck, N. Tanimoto, R. Muehlfriedel, E. Fahl, C. Grimm, A. Wenzel, C. E. Remé, S. A. van de Pavert, J. Wijnholds, M. Pacal, R. Bremner, and M. W. Seeliger, “Noninvasive, In Vivo Assessment of Mouse Retinal

Structure Using Optical Coherence Tomography," *PLoS ONE*, vol. 4, no. 10, p. e7507, Oct. 2009.

[175] M. D. Fischer, G. Huber, Y. Feng, N. Tanimoto, R. Mühlfriedel, S. C. Beck, E. Tröger, C. Kernstock, M. N. Preising, B. Lorenz, H. P. Hammes, and M. W. Seeliger, "In vivo assessment of retinal vascular wall dimensions," *Invest. Ophthalmol. Vis. Sci.*, vol. 51, no. 10, pp. 5254–5259, Oct. 2010.

[176] B. Xie, S. Nakanishi, Q. Guo, F. Xia, G. Yan, J. An, L. Li, T. Serikawa, T. Kuramoto, and Z. Zhang, "A novel middle-wavelength opsin (M-opsin) null-mutation in the retinal cone dysfunction rat," *Exp. Eye Res.*, vol. 91, no. 1, pp. 26–33, Jul. 2010.

[177] A. A. Moayed, S. Hariri, C. Hyun, B. Doran, T. W. Kraft, S. Boyd, and K. Bizheva, "Combined optical coherence tomography and electroretinography system for in vivo simultaneous morphological and functional imaging of the rodent retina," *Journal of Biomedical Optics*, vol. 15, no. 4, pp. 040506–040506–3, Aug. 2010.

[178] H. Yamashita, K. Yamasaki, K. Sugihara, H. Miyata, S. Tsutsumi, and Y. Iwaki, "Full-field electroretinography obtained using a contact lens electrode with built-in high-intensity white-light-emitting diodes can be utilized in toxicological assessments in rats," *Ophthalmic Res.*, vol. 42, no. 1, pp. 15–20, 2009.

[179] K. Ohtaka, S. Machida, T. Ohzeki, M. Tanaka, D. Kurosaka, T. Masuda, and T. Ishii, "Protective effect of hepatocyte growth factor against degeneration of the retinal pigment epithelium and photoreceptor in sodium iodate-injected rats," *Curr. Eye Res.*, vol. 31, no. 4, pp. 347–355, Apr. 2006.

[180] V. J. Srinivasan, T. H. Ko, M. Wojtkowski, M. Carvalho, A. Clermont, S.-E. Bursell, Q. H. Song, J. Lem, J. S. Duker, J. S. Schuman, and J. G. Fujimoto, "Noninvasive volumetric imaging and morphometry of the rodent retina with high-speed, ultrahigh-resolution optical coherence tomography," *Invest. Ophthalmol. Vis. Sci.*, vol. 47, no. 12, pp. 5522–5528, Dec. 2006.